

The Nanoparticle Corona in the Deep Lung: Pulmonary Surfactant Adsorption and its Role in Nano-Bio Interactions

DISSERTATION

zur Erlangung des Grades des Doktors der Naturwissenschaften

der Naturwissenschaftlich-Technischen Fakultät III

Chemie, Pharmazie, Bio- und Werkstoffwissenschaften

der Universität des Saarlandes

von

Simon Sebastian Räsch

Saarbrücken

2016

Tag des Kolloquiums:	28.07.2016
Dekan:	Prof. Dr. Dirk Bähre
Vorsitzender:	Prof. Dr. Rolf Müller
Berichterstatter:	Prof. Dr. Claus-Michael Lehr
	Prof. Dr. Robert Bals
Akad. Mitarbeiter:	Dr. Stefan Boettcher

“It's still magic even if you know how it's done.”

— Terry Pratchett, *A Hat Full of Sky*

ZUSAMMENFASSUNG

Nanopartikel (NP) eignen sich dazu, Wirkstoffe verzögert freizusetzen oder gezielt zum Wirkort zu bringen. Sie sind daher von Interesse für die Applikation von Wirkstoffen über den Respirationstrakt zur Behandlung akuter und chronischer Krankheiten der Lunge, aber auch systemischer Erkrankungen. In den Alveolen treffen NP zuerst auf eine nicht-zelluläre Barriere, den Pulmonalen Surfactant (PS). Dieser ist ein Lipid-Protein Gemisch, welches nach Impaktion der NP auf deren Oberfläche adsorbiert. Diese „Corona“ aus Biomolekülen moduliert die biologische Identität der NP und bestimmt deren weitere Interaktionen mit Zellen. Während es relativ gut untersucht ist, wie NP mit Plasmaproteinen wechselwirken, ist noch wenig über die Adsorption von PS auf NP bekannt. Im Rahmen dieser Dissertation wurde PS aus Schweinelungen gewonnen (pPS) und dessen Interaktionen mit NP untersucht. Verschiedene Größenmessungen belegten die Ausbildung einer Corona, und auf NP verschiedener Hydrophobizität konnte die Zusammensetzung der Lipide und Proteine quantitativ bestimmt werden. Surfactant-spezifische Proteine sind entscheidend für die Ausbildung der Corona und vermitteln eine Lipidbindung auch auf hydrophile NP. Die Aufnahme von NP durch Alveolarmakrophagen konnte *in vitro* durch die PS-Corona modifiziert werden. Mit dieser Arbeit konnte der Einfluss des lange ignorierten Faktors ‚Pulmonaler Surfactant auf die Nano-Bio-Interaktionen in der tiefen Lunge‘ gezeigt werden.

ABSTRACT

Nanoparticles (NPs) for drug delivery to the respiratory tract are of considerable interest, for the treatment of chronic and acute pulmonary and systemic disorders, promising the potential for sustained release and targeted delivery. Although the targets for these formulations are usually cells, the NPs, once inhaled, first encounter a non-cellular barrier in the deep lung: the pulmonary surfactant (PS). This is a lipid-protein mixture which covers the alveoli and enables gas exchange as a result of its surface tension lowering function. While the interaction of NPs with plasma proteins is routinely elucidated, the adsorption of lung lipids and proteins onto NPs is rather disregarded; yet, such characterization is crucial for understanding the fate of the particles, as the PS corona displays the biological identity of NPs. In this work, native PS was obtained from porcine lungs (pPS). The interaction with NPs in terms of corona formation and macrophage uptake was studied. Corona composition with respect to lipids and proteins was determined to a high degree of accuracy. Evaluation of this data suggested that surfactant associated proteins have a mediating effect on lipid binding to the NPs. *In vitro* experiments with a cell line of alveolar macrophages showed that the uptake of NPs with a pPS corona is unique, making PS indispensable for such experiments. This dissertation sheds new light on the ignored factor 'pulmonary surfactant in nano-bio interactions'.

TABLE OF CONTENTS

1. INTRODUCTION.....	1
1.1 The Respiratory System.....	2
1.1.1 Morphology of the Lung.....	3
1.2 The Pulmonary Surfactant	5
1.2.1 Lipids	5
1.2.2 Proteins.....	6
1.2.3 Secretion and Structural Organization	9
1.2.4 Pathophysiology of the Pulmonary Surfactant	10
1.3 Inhalation of Particles	12
1.3.1 Size of Particles Intended for Pulmonary Drug Delivery	13
1.3.2 Particle Clearance and Cell Interactions	14
1.4 The Nanoparticle Corona.....	15
1.4.1 The Nanoparticle Corona in Blood Plasma	17
1.4.2 The Nanoparticle Corona in the Lungs	18
1.5 Aims of this Thesis.....	19
2. PREPARATION AND CHARACTERIZATION OF A PORCINE NATIVE PULMONARY SURFACTANT	21
2.1 Introduction	22
2.2 Reagents and Methods.....	24
2.2.1 Reagents.....	24
2.2.2 Broncho Alveolar Lavage of Porcine Lungs	24
2.2.3 Preparation of Concentrated Native Pulmonary Surfactant.....	24
2.2.4 Total Protein Quantification	25
2.2.5 Total Phospholipid Quantification (Phosphorous Assay)	25
2.2.6 Dynamic Light Scattering	26
2.2.7 LC-MS Analysis of Phospholipids.....	26
2.2.8 Cholesterol Quantification.....	26
2.2.9 Thin Layer Chromatography	27
2.2.10 SDS-PAGE and Western Blotting	27
2.2.11 Label-free Shotgun Proteomics.....	28
2.3 Excursus: Establishment of an HPLC-MS Method for Phospholipid Quantification	29
2.3.1 Sample Preparation.....	29
2.3.2 Identification of Distinct Headgroup Fragments.....	31
2.3.3 Normal Phase <i>vs.</i> Reversed Phase.....	33
2.3.4 Separation of Phospholipid Classes	33

2.3.5	Data Acquisition and Processing.....	34
2.3.6	Validation	36
2.4	Results and Characterization of pPS.....	38
2.4.1	Phase Transition Temperature.....	39
2.4.2	Lipid Composition.....	40
2.4.3	Protein-Lipid Interactions.....	42
2.4.4	Protein Composition	44
2.5	Summary and Conclusion	46
3.	THE NANOPARTICLE CORONA IN PULMONARY SURFACTANT	48
3.1	Introduction	49
3.2	Reagents and Methods.....	51
3.2.1	Reagents.....	51
3.2.2	Preparation of magPLGA and magEu Nanoparticles.....	51
3.2.3	Electron Microscopy	51
3.2.4	Dynamic Light Scattering	51
3.2.5	Nanoparticle Tracking Analysis	52
3.2.6	Adsorption Experiments.....	52
3.2.7	Asymmetric Flow Field Flow Fractionation	53
3.2.8	Differential Centrifugal Sedimentation.....	53
3.3	Excursus: Preparation of Magnetite-Loaded Nanoparticles	54
3.3.1	Preparation Method.....	54
3.3.2	Characterization.....	55
3.4	Results and Discussion	57
3.4.1	Dynamic Light Scattering of Nanoparticles in the Presence of Porcine Pulmonary Surfactant	57
3.4.2	Nanoparticle Tracking Analysis	58
3.4.3	Asymmetrical Flow Field Flow Fractionation	61
3.4.4	Differential Centrifugal Sedimentation.....	62
3.5	Summary and Conclusion	66
4.	THE MOLECULAR COMPOSITION OF THE PULMONARY SURFACTANT CORONA	68
4.1	Introduction	69
4.2	Reagents and Methods.....	71
4.2.1	Reagents.....	71
4.2.2	Nanoparticles.....	71
4.2.3	Adsorption Experiments.....	72
4.2.4	Separation of NPs from Pulmonary Surfactant.....	72
4.2.5	SDS-PAGE.....	73
4.2.6	Thin Layer Chromatography.....	73

4.2.7	Label-free Shotgun Proteomics.....	73
4.2.8	Lipid Determination	73
4.2.9	Statistical Analysis	73
4.3	Results and Discussion	75
4.3.1	Analyzing the Surfactant Corona.....	75
4.3.2	Lipid Corona.....	77
4.3.3	Lipid Corona Formation of an Artificial Surfactant Preparation and the Influence of Plasma Proteins.....	79
4.3.4	The Protein Corona.....	80
4.4	Summary and Conclusions.....	88
5.	IMPACT OF THE PULMONARY SURFACTANT CORONA ON NANOPARTICLE-MACROPHAGE INTERACTIONS	90
5.1	Introduction	91
5.2	Reagents and Methods.....	93
5.2.1	Reagents.....	93
5.2.2	MH-S Cultivation.....	93
5.2.3	Pre-Incubation and Incubation of Nanoparticles	93
5.2.4	Cell Viability Assay.....	94
5.2.5	Nanoparticle Uptake / Association by Flow Cytometry.....	94
5.3	Results and Discussion	95
5.3.1	Nanoparticle Cytotoxicity is modified by Surfactant Adsorption.....	95
5.3.2	Modification of Nanoparticle Uptake by Lung Macrophages after Corona Formation	96
5.3.3	NP Corona does Not form Instantaneously <i>In Situ</i>	98
5.3.4	Cell Association <i>vs.</i> Uptake	99
5.4	Summary and Conclusions.....	101
6.	SUMMARY AND OUTLOOK.....	102
7.	BIBLIOGRAPHY.....	105
8.	LIST OF.....	116
8.1	Abbreviations	117
8.2	Figures	118
8.3	Tables	119
9.	DANKSAGUNG / ACKNOWLEDGMENTS	121

1. INTRODUCTION

1.1 The Respiratory System

Of the many evolutionary feats notable in living beings, one of the most astonishing is the respiratory system. The lungs, which are found in all mammals as well as many vertebrates, are vital for life as we know it. The main function of the lungs is of course the exchange of oxygen (O_2) against carbon dioxide (CO_2). Together with the essential provision of O_2 to the mitochondrial chain in order to produce ATP, the molecular unit of energy transfer, respiration also regulates blood pH and body temperature. To achieve sufficient gas exchange between the inhaled air and the circulatory system, the lung bears an internal surface area of about 100 m^2 , making it by far the largest entry portal of the human body [1]. In order to increase the lung surface, the respiratory tract is built like an inverted tree with the trachea, bronchioles, and alveoli equaling the trunk, branches, and leaves respectively. As shown in Figure 1-1, this set-up still requires around 23 generations of junctions, progressively decreasing in diameter from about 1.8 cm for the trachea, to the bronchi, bronchioles and alveolar ducts, and finally to the approximately 480 million alveolar sacs, which measure only about $200\text{ }\mu\text{m}$ in diameter [2]. Together with the decrease in diameter the surface area increases exponentially, giving the alveoli the capacity to contain 96% of the inhaled air [3].

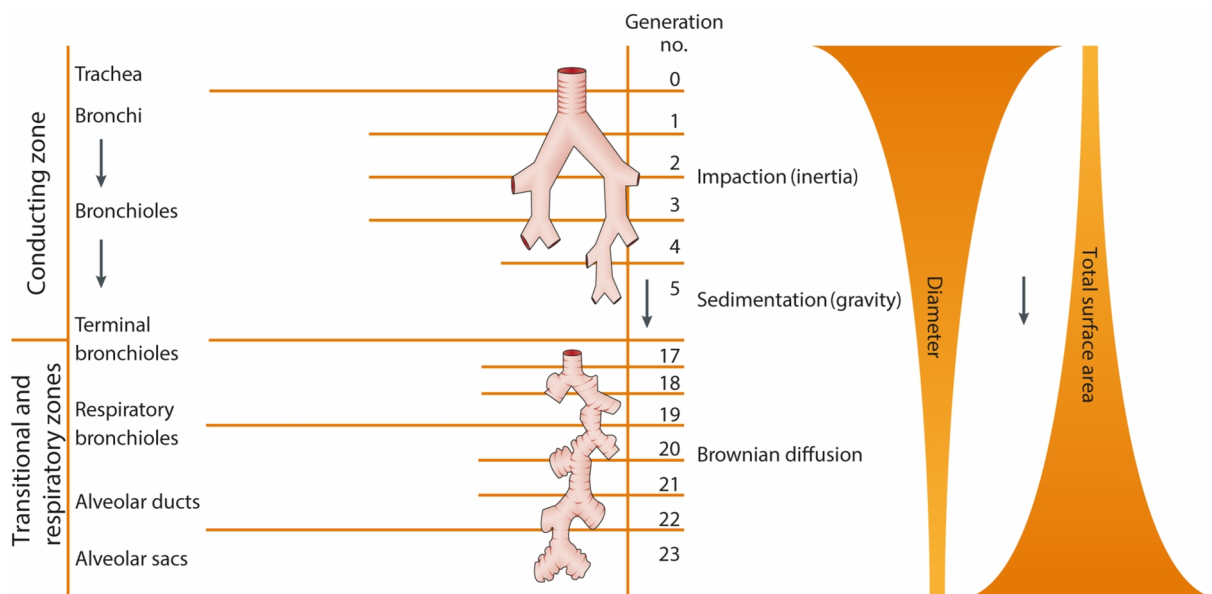


Figure 1-1: Generations of the respiratory tree. Adapted with permission from Macmillan Publishers Ltd: Nature Reviews Drug Discovery [4], copyright 2007.

1.1.1 Morphology of the Lung

The function of the upper airways, *i.e.* the trachea, bronchi, and bronchioles, is to distribute (following filtration) large amounts of air to the respiratory zone. In this area no gas exchange is taking place. The epithelium therefore consists of a relatively thick layer of goblet cells, which produce mucus (a viscous hydrogel that in turn forms a layer coating the epithelium), and ciliated cells, which efficiently transport the mucus towards the pharynx where it can be expectorated together with pollutants and pathogens that might have impacted in the airways from the air stream. The mucus layer has a variable thickness (10-30 μm in the trachea, 2-5 μm in the bronchi [5]), and is composed of glycosylated proteins organized into a porous ultrastructure in which particles can be trapped [6]. The epithelium becomes progressively thinner along the respiratory tree, reaching its minimum thickness in the respiratory zone. In the alveolar sacs (see Figure 1-2) where the gas exchange is taking place, the epithelium can be as thin as 25 nm. This region of the epithelium is not covered by mucus, but rather by a liquid film, the alveolar lining fluid (ALF) which has an average thickness of 200 nm [7]. There are three cell types which are typically found in the alveoli. The alveolar type-1 epithelial cells (AT-1) are the major constituent of the epithelial layer and are extremely squamous in nature ($\sim 5200 \mu\text{m}^2$), facilitating gas diffusion. AT-1 cells are differentiated from alveolar type-2 epithelial cells (AT-2), which are more cuboidal in shape and have a secretory function. Although AT-2 outnumber AT-1 cells by approximately 2:1, on average only about 40 AT-1 cells (in comparison to 77 AT-2 cells) are needed to build 95% of an alveolus with an inner surface area of $2.2 \cdot 10^5 \mu\text{m}^2$ [8, 9]. This unique epithelium can withstand the extreme pressure and size changes that occur during in- and exhalation, but is relatively sensitive to inhaled toxic chemicals, injuries caused by a sepsis or even O_2 intoxication. Without the ability to physically remove any pollutants, as is possible in the conducting airways, the deep lung counteracts any intruding pathogens and pollutants with large quantities of alveolar macrophages (AM; $\sim 9\%$ of total lung cells, in comparison with only 8% being AT-1 cells [8]). AMs are highly proliferating in smokers, resulting in even higher numbers (two-fold to ten-fold) [10].

Besides the hazards of inhaled particles, at the end of exhalation the alveoli hold only a minimal amount of air, and as such are at risk of atelectasis, a serious medical condition defined by the collapse and conglutination of the alveolar walls [11]. To circumvent alveoli collapse, the surface tension of the ALF is lowered by a surface active agent, the pulmonary surfactant (PS), a lipid-protein mixture that is secreted by AT-2 cells.

In conclusion, the blood within the pulmonary circulation is separated from the inhaled air by only a thin epithelial layer (covered with pulmonary surfactant and cleansed by alveolar macrophages), a basal membrane, and the endothelium of the blood vessels. This very thin setup of the air-blood barrier facilitates gas exchange by passive diffusion.

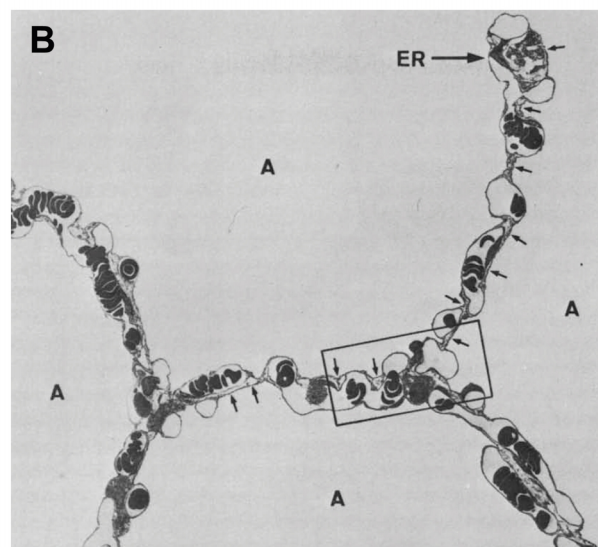
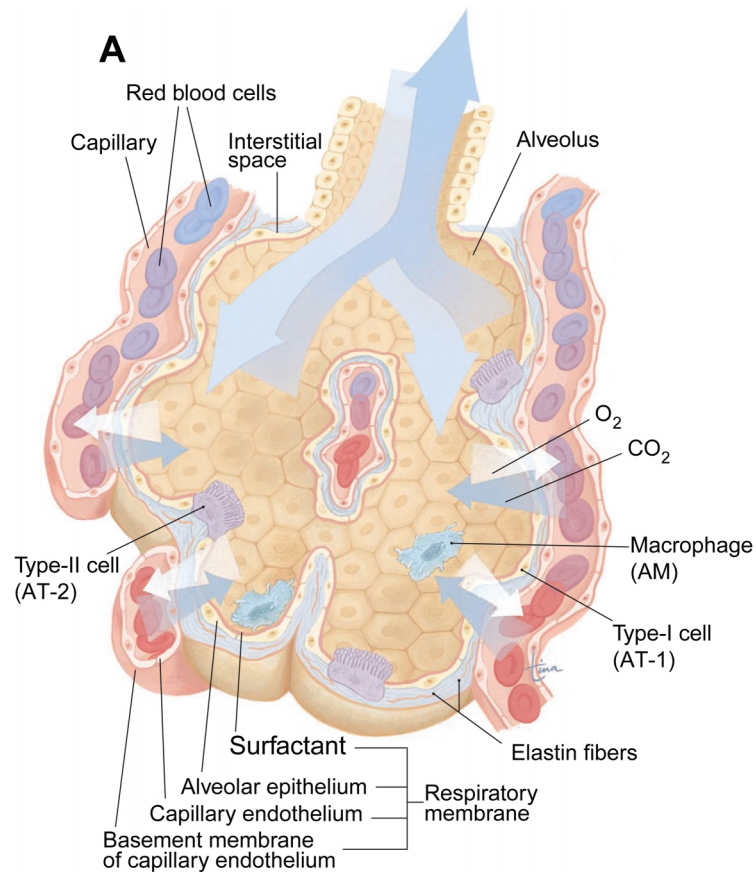


Figure 1-2: Structure of the alveolus (A) and transmission electron microscopy image of the alveolar space (B) with visible erythrocytes (ER). Reproduced from [12] and [13] with the permission of F.A. Davis and Elsevier respectively.

1.2 The Pulmonary Surfactant

The composition of PS is unique among the body fluids. It possesses a very high (mainly phospho-)lipid content that constitutes about 90% of its dry mass. The remaining 10% are proteins, some of which are uniquely expressed in the deep lung.

1.2.1 Lipids

An enormous range of lipids has been shown to be present in PS, most of which are phospholipids (PL) as mentioned above. As visible in Figure 1-3A, PL are amphiphilic, with a hydrophilic headgroup consisting of a phosphate group and a specific terminal moiety (*e.g.* choline), and a hydrophobic tail composed of two fatty acids which can vary in carbon chain length and degree of saturation. The specific headgroup determines the particular PL class and also strongly influences the PL properties; the headgroup can for instance hold a positive charge, resulting in no overall charge or in some cases a net negative charge of the molecule. Their amphipathic character allows PLs to organize themselves into different shapes and structures (examples are given in Figure 1-3B), the most prominent example being the plasma membrane of every mammalian cell (Figure 1-3B (ii)). In the case of PS, the most important aspect of structural organization is the ability of surfactant lipids to adsorb to the air-liquid interface and lower the surface tension (i), and to build reservoir-like micelles (iii) and (multi-)lamellar vesicles (iv).

All major PL classes have been detected in PS, *i.e.* phosphatidylcholine (GPChol), phosphatidylglycerol (GPGlyc), phosphatidylethanolamine (GPEth), phosphatidylserine (GPSer), and phosphatidylinositol (GPIno). The bulk of PLs are saturated and the composition is dominated by the presence of dipalmitoylphosphatidylcholine (DPPC) at up to 40 wt% [14].

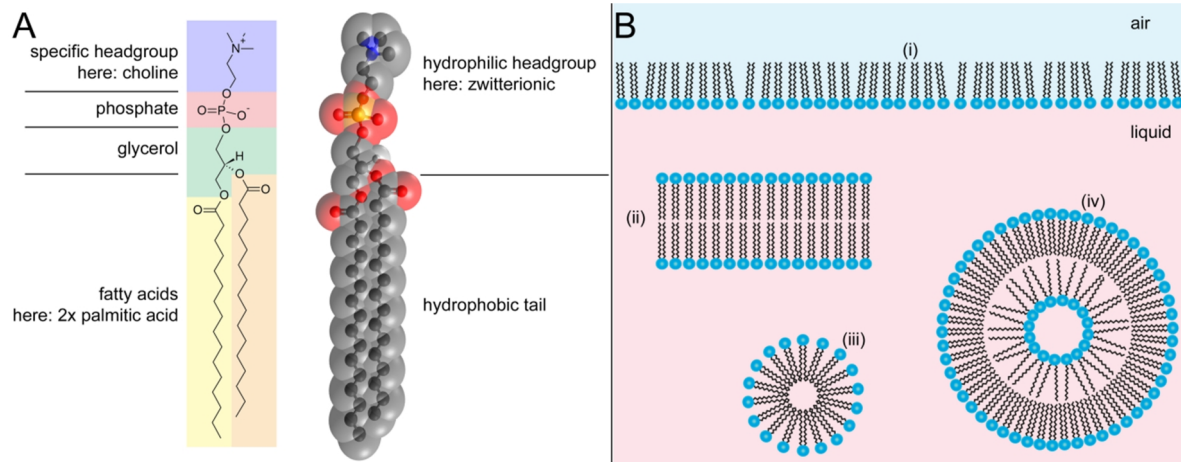


Figure 1-3: General structure of phospholipids using the example of dipalmitoylphosphatidylcholine, (DPPC) (A); possible structural organizations of phospholipids in aqueous medium (B).

The abundance of the lipid classes/species present in mammal PS differs among the reporting studies (an average distribution based on literature values is given in Table 1-1). PS lipids are however rather conserved among mammals [15, 16]. The variations in PS lipid composition that are found in non-mammal, air-breathing animals are likely due to their different body temperatures, meaning that surfactant lipids with different phase transition temperatures are required in order to function properly [17, 18].

Table 1-1: Lipid composition of pulmonary surfactant according to [14] and [19]

Lipids	DPPC	Other GPChol	GPGlyc + GPINo	Cholesterol	Other PLs	Other lipids
Abundance	~40%	~30%	10-15%	5-8%	<5%	<1%

The degree of saturation and PL class determines the packing density of the PL layers, and also the phase transition temperature at which the PLs change from a rigid ordered gel phase to the more flexible disordered liquid crystalline state.

1.2.2 Proteins

As stated above, only 10% of PS is constituted of proteins. Beside typical plasma proteins, such as albumin and hemoglobin, the largest fraction of proteins in PS consists of four different surfactant-associated proteins (SP-X) which are to a great extent uniquely expressed in the lungs. SP-X can be divided into two groups: SP-A and SP-D are large and hydrophilic, whereas SP-B and SP-C are small, highly hydrophobic proteins.

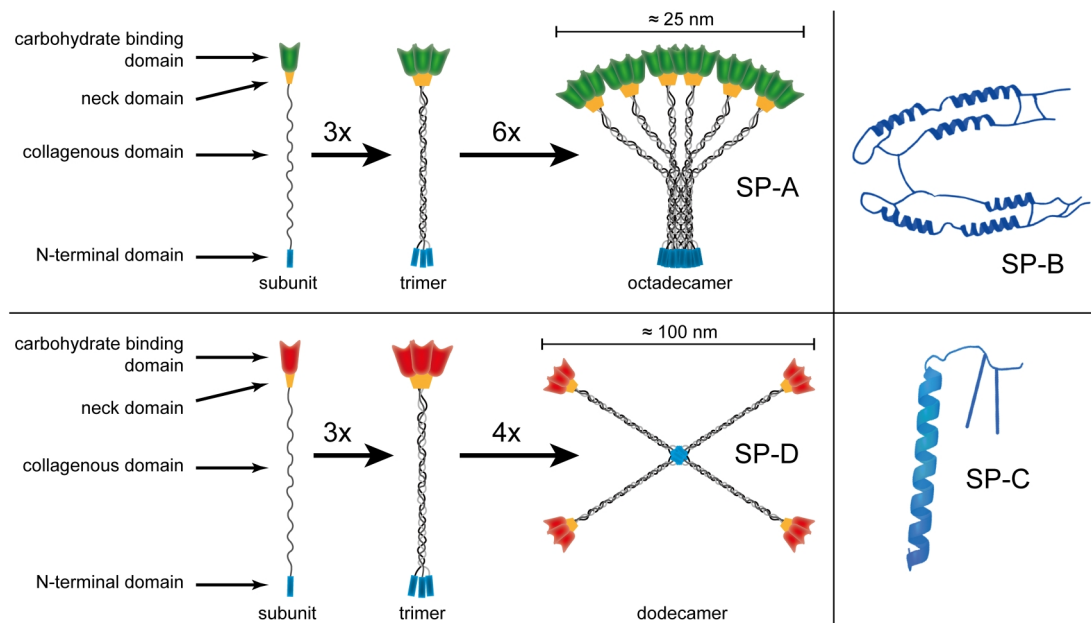


Figure 1-4: Structure of pulmonary surfactant-associated proteins A, B, C, and D.

SP-A and SP-D both belong to the collagen-containing C-type lectins, the collectins. This protein family currently has, 9 identified members, the most well-known being mannose binding lectin. Collectins in general are polymeric proteins whose monomers typically consist of four distinct regions: (1) a cysteine rich N-terminal tail region, (2) a collagen-like domain, (3) an α -helical coiled-coil region, the “neck”, and (4) a carbohydrate recognition domain (CRD). Three monomers form a trimeric subunit with a collagenous triple helix and closely attached neck regions, which then further form oligomers of several trimers (Figure 1-4). The monomer of SP-A is a 26-38 kDa protein, which assembles to a \sim 630 kDa octadecamer with a “flower bouquet” shape. SP-D monomers possess a longer collagenous domain and have a molecular weight of 43 kDa that forms an oligomeric “cruciform” structure of \sim 520 kDa by combination of 12 monomers. The final molecular weight varies as the proteins can potentially undergo partly underlie heavy glycosylation [20].

All collectins, as part of the host defense, possess several calcium dependent C-type CRDs, with affinity to a wide variety of mono- and polysaccharides. This allows them to recognize a broad spectrum of pathogens such as viruses [21, 22], bacteria [23], fungi [24] and other pollutants [25], as well as apoptotic and necrotic cells [26]. Collectins can then present such pathogens and damaged cells to leucocytes; as such, they constitute the first line defense in the lungs, and can be regarded as humoral receptors. SP-A/D are excreted into the alveolar space, where they not only interact with surfaces and molecules by receptor-ligand interactions, but also show affinity towards PLs. While for SP-D only a relatively selective binding to GPIIb/IIIa is observed.

has been observed [27], SP-A is closely associated with the PL membranes of the PS layer and as such has a major influence on the organization of the PL vesicles [28]. Furthermore, SP-A and SP-D have been found to exert, besides their antigen-presenting functionality, a direct antimicrobial effect, by disrupting the cell membranes of bacteria [29]; they are also involved in the regulation of PS homeostasis by a negative feedback mechanism [30]. SP-A is the most abundant protein in PS, constituting approximately 5-6% of the total dry weight, while SP-D is present in the lowest amounts, at about 0.5% of the dry weight of PS [31].

SP-B and SP-C each account for ~1% of PS dry weight. Their high degree of hydrophobicity makes them entirely insoluble in water in the absence of solubilizing PLs [32]. For this very reason, both proteins are expressed in AT-2 cells as soluble proproteins (proSP-B, proSP-C), carrying two hydrophilic flanking regions, and are post-translationally processed on their way to the air-liquid interface [33]. The quaternary structure of mature SP-B is a homodimer of 17.4 kDa, which consists to a large extent (~45%) of α -helices. SP-B belongs to the saposin-like proteins; a conceivable conformation of SP-B, based on other saposin-like structures [31] is shown in Figure 1-4. It is made up of 79 highly conserved amino acids of which 52% are hydrophobic, with one inter- and three intramolecular disulfide bonds, as well as one negatively charged and eight positively charged residues [34]. SP-B is essential for the organization of PS layers, their superstructure, and as a result, the surface tension lowering effect of PS. SP-B deficiency in neonates is associated with the usually fatal respiratory distress syndrome 1 [35]. How SP-B performs these functions is yet to be completely understood; it was found, however, that SP-B adsorbs very quickly to PL vesicles and leads to a fusion of preformed DPPC liposomes [36]. SP-B is very likely taking part in the organization of the PL vesicles of PS, by interfering with the multilamellar structures and by quick formation and stabilization of PL monolayers at the air-liquid interface [37, 38]. Furthermore, SP-B is involved in the processing of proSP-C - a deficiency of SP-B is therefore always accompanied by a lack of SP-C [39].

The role of SP-C is even more uncertain. It is a very small molecule (~4 kDa) that consists basically of just one α -helix with short sequences at each end, with the N-terminal region being typically palmitoylated twice [40]. SP-C is a transmembrane protein, intercalated within PL layers, and uniquely found in PS. Like SP-B, its overall net charge is positive and it therefore interacts mainly with anionic PLs. Unlike SP-B however, insufficient amounts of SP-C in neonates or in animal models do not lead necessarily to severe distress syndromes, although the manifestation of symptoms varies among patients [35]. Although this suggests that SP-C might not be absolutely necessary for the function of PS, it has been shown that the

presence of SP-C in artificial mixtures improves the surface tension lowering effect by means of enhancing respreading speed and compressibility [38]. A proper physical functioning of PS is also therefore only achieved in the presence of SP-A, -B, and -C and all lipids.

1.2.3 Secretion and Structural Organization

Having identified the main components of PS, one could easily conclude that PS consists of a simple PL monolayer containing additional proteins. In reality, its structure is more complex (see Figure 1-5): PS is already secreted in a highly organized manner by AT-2 cells, in the form of lamellar bodies (LBs). LBs can be stained within the cell and are a distinctive feature of AT-2 cells. Once outside the cell, LBs unravel to a mesh-like structure, the so-called tubular myelin (TM). TM serves as a reservoir for the membranous structure of PS, from which monolayers adsorb to the air-liquid interface. Besides the ability of PL monolayers to lower the surface tension at different surface pressures due to their compressibility, during exhalation (which means a reduction of surface area), the PLs return to the membranes in the sub-phase. This procedure is maintained by SP-A, -B, and -C - although a DPPC layer alone is stable at enormous surface pressure, the rapid re-adsorption and the structural organization can only be achieved in the presence of SP-X. Vesicles of PS can be recycled after reuptake by AT-2 cells or degraded by macrophages.

While DPPC alone exhibits a sharp phase transition at 41 °C, the complex lipid-protein mixture in PS allows a relatively broad phase transition range around the physiological temperature of 37 °C. For this reason, the PL layers of surfactant are in between the two PL membrane states, allowing for the coexistence of ordered and disordered phases which simultaneously exhibit high flexibility and high compressibility [28, 41, 42]. With this smart set-up and the interplay of the above mentioned factors, PS is capable of lowering the surface tension at the air-liquid interface to values close to 0 mN/m, and, more importantly, of maintaining these tensions during the relatively long periods of exhalation, preventing the collapse of alveoli at high surface pressures of up to 70 mN/m [43].

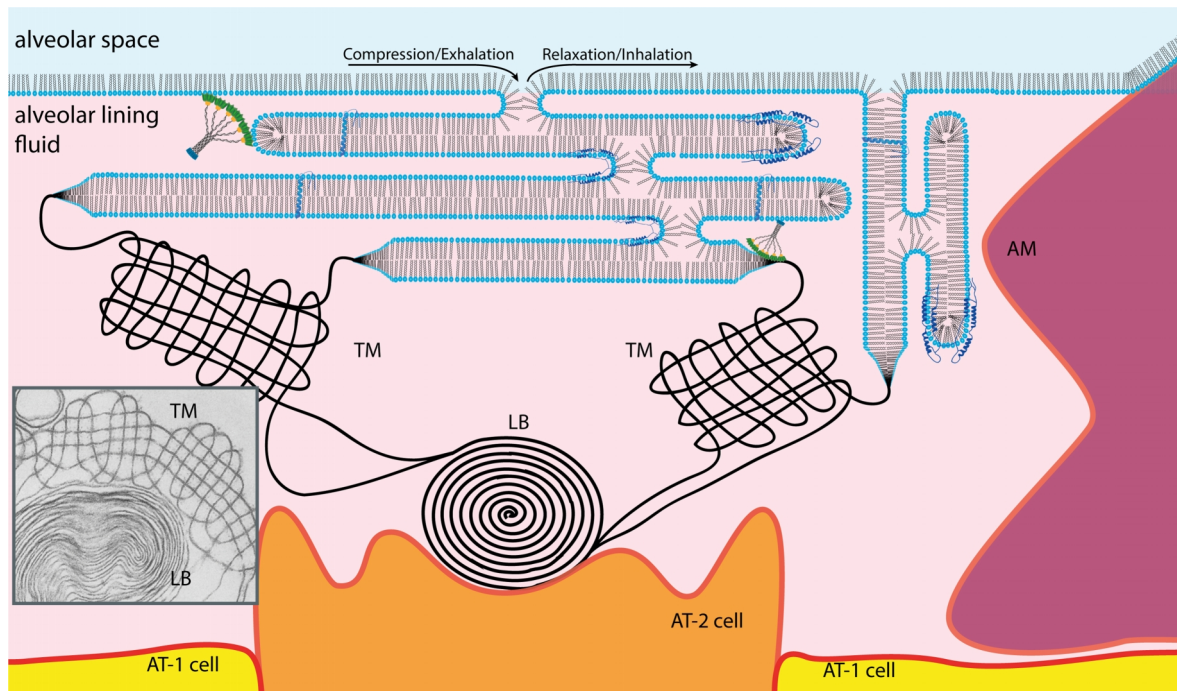


Figure 1-5: Structural organization of pulmonary surfactant at the air-liquid interface. PS is secreted by AT-2 cells as lamellar bodies (LBs) and is unraveled to tubular myelin (TM) which acts as a reservoir for the multi-lamellar structures at the air-liquid interface. For in- and exhalation, the monolayer can be expanded/diminished by this reservoir. The TEM image in the lower left corner is reproduced with permission from [44].

1.2.4 Pathophysiology of the Pulmonary Surfactant

As already mentioned, PS is essential for lung function and gas exchange. The lack of one or more PS components leads to either a physical inhibition or a deficiency of immune responses towards pathogens.

The most common clinical picture associated with abnormal PS is the infant respiratory distress syndrome (IRDS), which affects about 1% of neonates, with prematurely born infants most at risk of being affected. IRDS is caused by an insufficient surfactant production, leading to poor gas exchange in collapsed alveoli and manifesting in low blood oxygen levels. Beside the application of continuous positive airway pressure, clinical surfactant preparations are instilled as replacement therapies. There are several different preparations on the market for the treatment of IRDS, some of which are completely artificial and consist of a PL mixture with added recombinant hydrophobic proteins (i.e. Surfaxin®); most preparations, however, are obtained from animals. These animal derived surrogates are either gained by lavage of lungs (e.g. Alveofact®) or by extraction of minced lung tissue (e.g. Curosurf®). These

preparations differ in lipid concentration, but all have in common that they are protein depleted in order to reduce immunogenicity. Only the two hydrophobic surfactant proteins (SP-B and -C) remain in such preparations due to their importance for the physical functioning of PS [45].

An overproduction of PS, on the other hand, is also connected with decreased gas exchange, accompanied by dyspnea and cough. In lungs of patients affected by pulmonary alveolar proteinosis (PAP), PS accumulates in the alveoli and needs to be removed physically by lavage. Currently, the role of granulocyte-macrophage colony stimulating factor is being researched as a pharmacological target. Typically, in the lavage of PAP patients, an excess of SP-A can be found. SP-X levels in lavage fluid can be generally used as disease markers, not only for genetic disorders leading to a lack of a certain SP-X [35], but also for chronic disorders such as asthma, chronic obstructive pulmonary disorder, and cystic fibrosis [46-48], as well as infectious diseases [49], carcinomas [46], and acute lung injury (where SP-X is detectable in plasma) [50].

1.3 Inhalation of Particles

The inhalation of particles can be regarded from two different viewpoints. First of all, given the immense amounts of air which are inhaled every minute, and depending on the degree of pollution, scores of particles are inhaled every day; this could potentially prove harmful to the lungs by way of various mechanisms. The nanotoxicology of these particles is therefore an important factor to consider when it comes to assessment of the risks of airborne particles in working areas or polluted regions. On the other hand, for quite some time NPs have been in focus as drug delivery systems with the promise of sustained release, mucus- and cell layer penetrating features, and even the ability to facilitate targeted delivery [51]. With advancing techniques, the complexity of nanoparticulate formulations has increased from nanosized API (active pharmaceutical ingredients) crystals to liposomes and polymeric NPs, and further to core-shell structures and the employment of covalently bound ligands for active targeting (mainly for local/topical but also systemic delivery). The behavior of these particles, once they have reached their site of action, needs to be studied thoroughly, in order to predict the delivered dose, as well as the time-dependent release and/or dissolution of the drug. Especially the latter becomes important with respect to the low volume of liquid which is available in the lungs to dissolve drugs and excipients [7].

There are several definitions which have emerged for what NPs or nanomaterials actually are. The European Commission defined nanomaterials as “*A natural, incidental or manufactured material containing particles, in an unbound state or as an aggregate or as an agglomerate and where, for 50 % or more of the particles in the number size distribution, one or more external dimensions is in the size range 1 nm - 100 nm*” [52]. Most other standards also require at least one (SCCP) or two dimensions (ASTM, NIOSH), or the diameter (ISO) to be in the range between 1 and 100 nm, and thus all have in common that they define NPs in general. In terms of intended use, the definition of the European Science Foundation, which expands the classification of nanomedicine to particles of up to “*hundreds of nanometers*” [53], is more reasonable for the definition of NPs for the pharmaceutical delivery of drugs [54]. This is due to the fact that the delivery of APIs requires the application of a certain dose within a particle, and as a result a certain volume of the particle is required. Considering that decreasing the size of a NP decreases the volume to the third power, reasonable amounts of drug can only be delivered by nanoparticles of a certain minimum size. Therefore, in the scientific community for pharmaceutical technology, a diameter of 200-300 nm is regarded as a suitable and a common size for nanoparticulate delivery systems.

1.3.1 Size of Particles Intended for Pulmonary Drug Delivery

The deposition of particles in the lung is dependent on several characteristics of the single airborne particles, including size, density, shape, and charge. Whether or not a particle reaches the deep lung can be estimated by determining the mass median aerodynamic diameter (MMAD, denoting the flight characteristics of an equivalent sphere with the density of 1 g/cm^3), which can be measured by instruments simulating the lung architecture: so-called impactors. Interestingly, most pharmaceutical formulations for respiratory drug delivery have a comparatively large MMAD of around $1\text{-}5 \text{ }\mu\text{m}$ [51]. This particular MMAD range has been found to be optimal for targeting the respiratory region of the lungs (see Figure 1-6) by sedimentation. This is due to the deposition mechanisms that occur to airborne particles after inhalation [55] - particles with a large MMAD will impact very early in the airstream, *i.e.* the bronchi, pharynx, throat, mouth, or even the inhaler device itself. A small MMAD leads to less deposition in the tracheal region, as very small particles with an MMAD of less than $0.1 \text{ }\mu\text{m}$ mainly collide with the alveolar lining fluid as a result of Brownian motion (which is however no guarantee for efficient delivery as they are likely to be exhaled again). As already discussed in Chapter 1.3, NPs possess features which make them most interesting for pulmonary delivery, although effective drug delivery with complex delivery systems also demands a minimal particle size. The main problem with delivering such small particles in the nanometer range is their production as single airborne NPs, which is so far not feasible for administration via handheld inhalers. In the short- to mid-term, the delivery of NPs to lungs will be therefore within larger aggregates, droplets, or secondary particles with a deep lung-compatible MMAD of $1\text{-}5 \text{ }\mu\text{m}$, which then release the primary NPs after impaction.

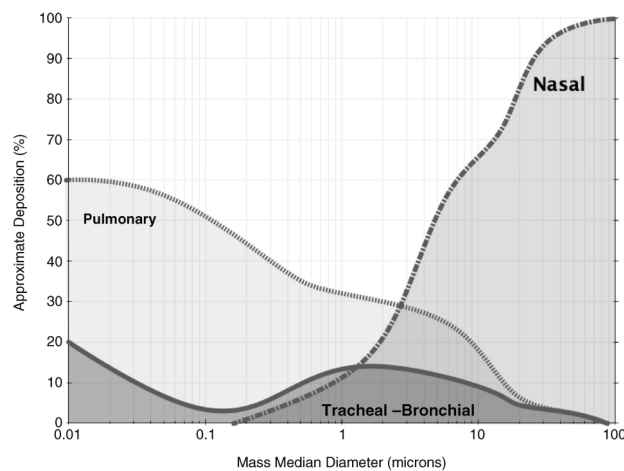


Figure 1-6: Deposition of inhaled particles in the lung as a function of their MMAD. Optimal deposition in the pulmonary region, *i.e.* the deep lung, can be achieved with particles in the range of $1\text{-}5 \text{ }\mu\text{m}$ or below 100 nm . Adopted from [56] with permission from John Wiley & Sons.

1.3.2 Particle Clearance and Cell Interactions

The immense surface area of the lung tissue and the constant inhalation of potentially polluted air make an efficient clearance mechanism essential. While the upper lung is able to mechanically remove inhaled particles by the cilia-mediated mucus transport along the bronchi and trachea towards the throat, the deep lung lacks such a mechanism. The respiratory region depends entirely on clearance by macrophages. AMs are professional phagocytes that are derived from monocytes after migration from the blood stream into the luminal alveolar space, where they are present in large numbers [57]. Approximately 12-14 AMs are to be found within one alveolus [58], where they engulf particles with high efficiency, not only due to their high mobility but also due to their ability to spread their pseudopodia (or “arms”) around large particles [59]. Unfortunately, the perfect particle size for pulmonary drug delivery of 1-5 μm MMAD is also a perfect size for engulfment by macrophages, while smaller NPs are taken up less efficiently [60].

Although it is more likely that particles are taken up by macrophages before they interact with epithelial cells, at least very small NPs might also be able to cross the epithelial barrier, allowing for systemic delivery [61, 62]. Nevertheless, regardless of whether intruding particles come in contact with AM or epithelial cells, or if they dissolve or persist in the alveolar fluid, they will encounter the outermost barrier structure of the deep lung: the thin layer of alveolar lining fluid and therewith the components of PS.

1.4 The Nanoparticle Corona

The most obvious aspect of the nano-bio interface is the interaction of NPs with cells; it also includes, nevertheless, the interaction of NPs with biological fluids. Since there are no “dry” cells in the human body, NPs will always encounter a fluid first before cell interactions can take place, regardless of the portal of entry and intended use [63, 64]. Depending on their nature, such extracellular fluids can be considered as non-cellular biological barriers (*e.g.* mucus and pulmonary surfactant).

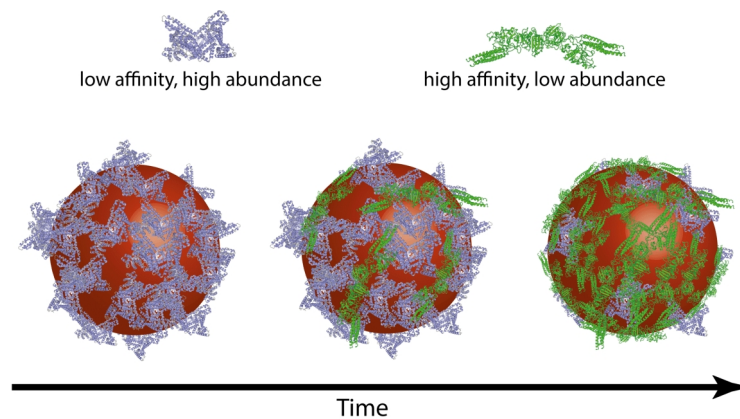


Figure 1-7: Corona evolution over time. According to the Vroman effect, the initially adsorbed highly abundant biomolecules on the surface of a solid are exchanged over time for less abundant molecules with higher affinity towards the surface.

Although protein adsorption onto NPs is a phenomenon that has been known for quite some time [65], the concept of the “nanoparticle corona” as it is understood today was established by Cedervall *et al.* in 2007 [66]. In principle, the term “corona” specifically describes the biomolecules (initially only proteins, therefore the term “protein corona” is still commonly used), that adsorb onto the surface of solid NPs, comparable to the process of opsonization of pathogens by antibodies. Opsonins, however, are considered as molecules which bind to the surface of pathogens, making them visible to phagocytic cells or promoting binding by receptor-ligand recognition [67]. Although this might be the eventual outcome in many cases, the NP corona encompasses the total adsorbed molecules without implying a certain effect, except for a masking of the actual NP surface. Vroman *et al.* elucidated in 1980 that the adsorption on solid surfaces, such as implants, is not static but a continuous process, where proteins with high abundance in the plasma adsorb first, but are exchanged over time by proteins that are less abundant, but possess a higher affinity towards the surface chemistry [68]. The very same, so-called Vroman effect can be observed on the surface of NPs (shown

in Figure 1-7). Each particle produces a specific adsorption pattern of biomolecules [69] which defines the new biological identity of the NP. A multitude of different molecules is present in biological fluids and as the number of produced NPs is immense, the NP corona has evolved to one of the most intensively investigated topics in nano-bio sciences following recognition of its importance [64, 70].

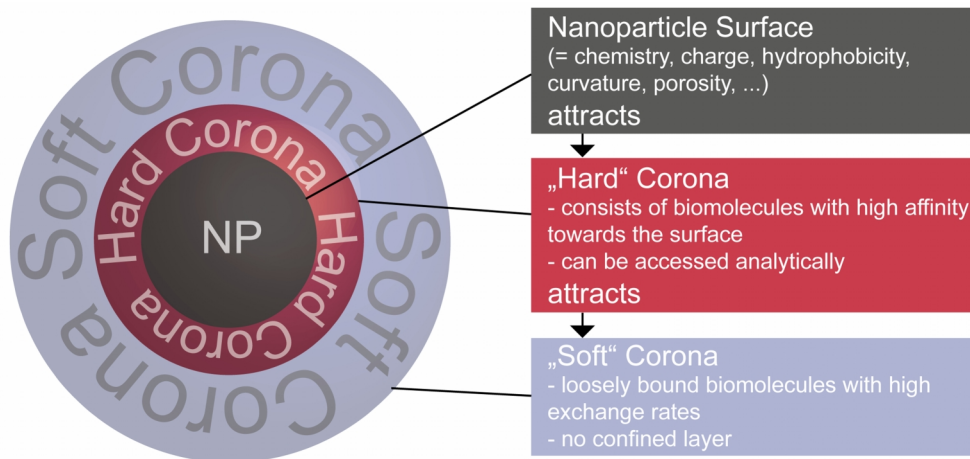


Figure 1-8: Schematic of the discrimination between "hard" and "soft" corona at equilibrium.

It has been extensively shown that the presence of the corona has a major impact on the further fate of NPs in terms of cell interactions, and furthermore on the stability of the NPs themselves [71-73]. In order to predict this fate, it is necessary to know the adsorbed biomolecules, and if one aims to quantify the biomolecules which selectively bind to a certain type of NP, the NP-corona complexes need to be separated from the non-binding supernatant. It has been widely accepted that the corona can be divided into a “hard” corona, the layer of proteins with high affinity towards the surface, and a “soft” corona, which is a layer of proteins loosely bound onto the hard corona, and which is characterized by low affinity and high exchange rates [66] (schematically shown in Figure 1-8). The high affinity corona is assumed to be the crucial layer for the biological identity [74] and is therefore commonly assessed by default for NPs produced for possible *in vivo* use.

1.4.1 The Nanoparticle Corona in Blood Plasma

A large number of studies have addressed the adsorption of plasma proteins on NPs. Starting with the kinetics of single proteins and the exchange against other proteins as well as the adsorption of the complex protein mixture in crude plasma, adsorption patterns of many technical and pharmaceutical NPs are known. The scientific community has begun to define what the consequences of protein adsorption are in terms of corona formation, stability *e.g.* agglomeration behavior, drug release, *etc.*, what the protein corona consists of and how the presence of proteins on the surface of NPs results in modified cell interactions. Commonly, the plasma protein corona is accessed by *in vitro* adsorption experiments, and Monopoli *et al.* were able to show that the separation technique does not actually influence the outcome of the detected corona [75]. The composition of this corona is unique for each type of NP, dictated by size/curvature [76], surface chemistry [77], charge [78], hydrophobicity [79], and morphology [80], as well as by the experimental conditions like exposure duration [81] and temperature [82], and protein concentration [83]. The corona itself in turn influences factors including NP clearance [84], cell uptake or association [72, 74], cytotoxicity [85], colloidal stability [73], and drug release [86]. Just recently, Ritz *et al.* were able to show on a rather small set of NPs, that just a few distinct proteins are responsible for an either enhanced (*e.g.* ApoH) or decreased (*e.g.* ApoA4, ApoC3) particle uptake [87], which again proves how thoroughly the corona formation of pharmaceutical NPs needs to be probed and characterized. As methods are advancing, the complex processes involved in corona formation become clearer but also reveal new challenges. Hadjidemetriou *et al.* for instance successfully showed that there are variations (and similarities) between the *in vivo* and *in vitro* corona in terms of composition and morphology [88]. Since new studies like the aforementioned are published on a daily basis, some more of the most recent findings regarding the plasma protein corona are summarized in Table 1-2 giving an example of the various topics.

Table 1-2: Summary of some of the most recent findings regarding the plasma protein corona.

Glycosylation of adsorbed proteins influences cell interaction	Wan <i>et al.</i> [89]
Pre-coating with immunoglobulins for targeting macrophages is inhibited by subsequent protein adsorption	Mirshafiee <i>et al.</i> [90]
Pre-formed epidermal growth factor corona stabilizes Au-NPs and enhances cellular deposition	Luby <i>et al.</i> [91]
Cloaking by platelet membranes shows reduced uptake of NPs by macrophages and plate-like effects such as selective adhesion	Hu <i>et al.</i> [92]
Protein corona around ZnO-NPs reduces cytotoxicity	Yin <i>et al.</i> [93]
BSA corona reduces drug release rate from NPs and enhances biostability	Peng <i>et al.</i> [94]
Antibody functionalized PMA-NPs retain their targeting ability in the presence of a corona	Dai <i>et al.</i> [95]
Protein corona provides a stealth effect for lipid and silica NPs by means of macrophage uptake	Caracciolo <i>et al.</i> [96]

Although this is still work in progress and comparatively little is known of how this plasma corona actually interacts with cells on a molecular level, another topic has been completely disregarded for quite some time – namely, the fact that direct contact with plasma is not a realistic means of exposure and corona formation for most NPs (except for those intended for *i.v.* application). NPs in consumer products such as Ag-NPs in antibacterial clothing or wound dressings, as part of air pollution, or as pharmaceutical delivery systems do not enter the blood stream directly, if at all, but will encounter the biological fluids at their portal of entry, *i.e.* sebum (in case of sebaceous glands of the skin) [97], gastrointestinal fluid and mucus (after ingestion), and in the case of the respiratory tract, mucus in the upper lung and PS in the deep lung. These local environments and their effects on NPs, however, have been addressed very little in the past [71].

1.4.2 The Nanoparticle Corona in the Lungs

In order to develop drug delivery systems for pulmonary administration, it is crucial to acquire information of the response mechanisms of the body involved in processing inhaled NPs [98, 99]. The conducting airways with their highly efficient clearance system are not addressed in this work, but have been found earlier to be a challenging environment for NP delivery [6]. As the deep lung offers also the possibility to make drugs systemically available by absorption across the thin air-blood barrier, alveolar delivery of APIs is in the spotlight. As clarified in Chapter 1.2, NPs will encounter a biological fluid which not only has a biochemical composition which is different to plasma, but which also possesses the physical properties of a membrane due to its structural organization. So far, it has always been assumed that the corona in a biological environment is simply formed based on kinetics and affinity of the individual protein to a particular NP. Whether this principle can be applied to PS is highly questionable. This peculiar environment will presumably lead to a NP corona which is not only biochemically different from the mere protein corona, but furthermore will have a major impact on the colloidal behavior of the NPs; and in reverse, NPs will have an impact on the functionality of PS [100].

It is somewhat surprising that so little is known about NPs impacting in the lung, considering that it is by far the largest portal to the body. The lack of an adequate model for PS presents a considerable, and perhaps even the biggest obstacle to accurate characterization of this behavior. Furthermore, there is a significant need to adapt commonly employed techniques in order to determine the NP corona in PS in its entirety, together with how it affects NPs in this local environment.

1.5 Aims of this Thesis

From the existing literature, it can be concluded that the corona of NPs has a major impact on the interaction of nanomaterials with cells. For the development of NPs as drug delivery systems, this corona has to be evaluated in detail in order to accurately gauge NP efficiency and safety *in vivo*. Exposure to inhaled NPs often occurs by accident and therefore corona evaluation applies not only to well-characterized and supposedly safe pharmaceuticals, but also to technical (nano-)materials. So far, research has only focused on the plasma corona, despite the fact that the inhalation of NPs is likely to result in a corona which is fundamentally different to the one in plasma. The existence of a unique corona formation in the presence of PS was the central working hypothesis behind this project. A principal issue is the difficulty in accessing this body liquid in order to study the interactions of NPs after deposition on the alveolar lining fluid and the formed PS corona. Although earlier studies have described interactions of NPs with single components or clinical surfactant preparations, and a few have addressed the interplay of NP with crude PS, there is no systematic approach which clarifies how one can access the formed PS corona, defines what it consists of and clarifies what the consequences of the formation are. The aims of this thesis were therefore:

1) To prepare and to characterize native porcine pulmonary surfactant suitable for studying the nano-bio interactions

By using an aforementioned PS preparation of lungs from slaughtered pigs (pPS), the surfactant can be extracted in moderate amounts without the need to euthanize the animals. A well characterized preparation of pPS, close to the described composition of human PS is essential in order to determine the lipid/protein adsorption onto cells, and to ensure a physiologically relevant behavior of the pPS preparation.

2) To study the colloidal behavior of nanoparticles in the presence of pulmonary surfactant and to evaluate various methods to access the corona

As it has been found that the size, and therewith agglomeration behavior of NPs can change in biological fluids, the particular colloidal properties of nanomaterials in the presence of PS are likely to modify the properties of the NPs as well. pPS however possesses vesicle-like properties that make size measurements difficult. Therefore a set of different tools for the measurement of NPs and the adsorbed PS layer were tested for their suitability.

- 3) To analyze and quantify the adsorption of surfactant components, *i.e.* proteins AND lipids, onto different nanoparticles, generating a “fingerprint” of their corona**

The composition of the NP corona determines the biological identity of the NP itself. From the viewpoint of pharmaceutical technology and the often proposed possibilities for NPs to be targeted to specific cells or tissues by surface-linked ligands, it is essential to know the very surface modifications that occur in the presence of PS in terms of lipid and protein adsorption, not only in a qualitative but also in a quantitative manner. Determination of the complete corona composition will allow for judging the interactions of NPs with cells, as well as the potential controllability of corona formation.

- 4) To study the influence of this corona on the nanoparticle-cell interaction with a lung relevant cell line**

Even though it seems obvious that the corona formation in PS modifies NP-cell interactions (e.g. uptake by cells, adhesion to the cell membrane), the influence of crude PS on NP adhesion in lung relevant cell lines is widely unknown. Studies have reported both increased and decreased cell association of particles in the presence of PS [101]. The factors influencing this phenomenon are far from being understood.

The gained information on the formation of the PS corona will help in relating *in vitro* experiments regarding the toxicity, dissolution, efficiency, and targeting of NPs to *in vivo* results. A more informed design of nanopharmaceutical drugs may be facilitated, allowing for specific interaction with the PS layer in a defined manner, in order to target cells or increase residence time by binding certain constituents of PS.

**2. PREPARATION AND
CHARACTERIZATION OF A PORCINE
NATIVE PULMONARY SURFACTANT**

2.1 Introduction

Blood is a readily accessible body fluid, and giving away a few deciliters causes only minor inconvenience to the donor. The interaction of nanomaterials with blood proteins is therefore one of the most extensively investigated fields in nano-bio-sciences [63]. When it comes to relevance, NPs entry *via* the respiratory tract is more likely to occur, either as a result of intended administration on purpose or accidentally in case of particulate matter, resulting in contact with the non-cellular barrier of the lungs. Obtaining sufficient amounts of PS to study its interaction with NPs is disproportionately more difficult than obtaining blood, as PS is typically gathered by bronchoalveolar lavage (BAL) - a rather invasive procedure resulting in only small quantities of BAL fluid (BALF), insufficient for studying nano-bio interactions. Patients who suffer from respiratory diseases such as pulmonary alveolar proteinosis require lavages as part of their medical treatment, presenting an option for both BALF and PS collection; however, the composition of both BALF and PS is typically altered in these patients [102, 103], making it unusable for such experiments. *In vivo* or *ex vivo* experiments in small animals may be utilized to evaluate NP toxicity [104, 105], especially since inhalation, the actual mode of exposure, can only be mimicked *in vivo*. However, for sake of animal welfare following the “three Rs” principle (reduce – replace – refine), experiments in small animals such as mice are not adequate as a future model to screen NP–PS interaction.

An alternative option, which has already been used several times to study the effects of NPs on PS and vice versa, is that of commercially available surrogates. There are a number of different, typically animal derived, preparations for use in clinics to treat neonatal respiratory distress syndrome in infants which do not produce sufficient amounts of PS. Most of these are organic extractions from minced or lavaged lungs, *e.g.* Alveofact® (Lyomark, bovine lavaged lung), Curosurf® (Chiesi, porcine minced lung) and Survanta® (AbbVie, bovine minced lung). All these preparations have in common that they are depleted of proteins in order to prevent immunogenic reactions against the contained foreign matter. To maintain the required function of lowering the surface tension and because their immunogenicity is low, the hydrophobic surfactant associated proteins SP-B and SP-C remain in the extracts or are eventually added [106]. Recently, efforts have been made to replace the animal derived preparations with artificial formulations of lipids and recombinant SP-B and SP-C; such similarly functioning synthetic substitutes including “Super mini-B peptide”, “KL₄ peptide”, and “SP-Css ion-lock 1” and first, highly standardized, products bearing no risks of immunogenicity have hit the market (*e.g.* Surfaxin®/Aerosurf®, DPPC, POPG + KL₄

peptide, Discovery Laboratories, Warrington, PA.). These products have been found to be equivalent to animal derived preparations [107-109].

The above mentioned clinical surfactants are produced with the aim to mimic the physical PS function using the smallest set of compounds possible. Using such formulations to study the interactions of inhaled NPs with the PS barrier therefore compares to confining plasma-NP interactions to solely the contribution of albumin. Beck-Broichsitter *et al.* could furthermore show that PS preparations with different complexity also react in a diverse manner to polymeric NPs in terms of surface activity inhibition. While an artificial plain PL mixture was heavily affected, the effects were reduced with increasing complexity of the preparation, with a native PS being almost unaffected [110].

To compare the properties of artificial PS and to elucidate the fascinating mechanisms of PS organization, biophysicists often use a native PS preparation which is obtained from pig lungs. It has been demonstrated to possess the physical properties of human PS and features in its native state all essential components, *i.e.* lipids and proteins [43, 111-113]. Although the isolation of pPS is still labor intensive, the process ensures the most realistic composition of the final product, by applying lavage (not mincing) and a density gradient centrifugation to remove non lipid-associated proteins. The resulting pPS is highly concentrated, allowing a realistic interaction scenario, and since the isolation starts with lungs from slaughtered pigs, it can be gained without being affected by ethical issues. In order to adequately address the *in vivo* situation of NP-PS interactions, this chapter describes the preparation of porcine pulmonary surfactant as a surrogate. pPS is characterized in terms of lipid/protein composition and its colloidal behavior.

2.2 Reagents and Methods

2.2.1 Reagents

All standards for thin layer chromatography (TLC) and liquid chromatography mass spectrometry (LC-MS) analysis were purchased from Avanti Polar Lipids (Alabaster, AL, USA). All other reagents and solvents were purchased from Sigma-Aldrich (Munich, Germany) and were at least of analytical grade, while mobile phase solvents were of LC-MS grade. The water used in all experiments was purified to a resistivity of 18.2 M Ω *cm (Milli-Q®, Merck Millipore, Germany).

2.2.2 Broncho Alveolar Lavage of Porcine Lungs

Lungs were selected in the slaughterhouse (Faerber, Zweibruecken, Germany) immediately after evisceration of the animals on the basis of their apparent non-damaged and uninfected appearance. Any blood which could be present in the trachea was removed by adding a small amount of cold 0.9% sodium chloride solution. The lungs were then lavaged under application of gentle massage with ~2-4 L of 0.9% NaCl. The lavage fluid (= pBALF) was filtered and, providing its appearance was colorless (indicating no large scale contamination), stored on ice. After centrifugation (Hettich Rotina 420R + rotor 4794, Tuttlingen, Germany) for 5 min at 2000 rpm and 4 °C for removal of cell debris, the pBALF was frozen until further purification. In the event of blood stain occurrence in the cell pellets, the pBALF was discarded.

2.2.3 Preparation of Concentrated Native Pulmonary Surfactant

pBALF was purified using a modified method of Shelley *et al.* [112] as described by Taeusch *et al.* [114], *videlicet* a density gradient centrifugation. The thawed pBALF was initially centrifuged for 1 h at 31000 rpm and 4 °C in an Optima L 90 K ultracentrifuge, (Beckman Coulter, Krefeld, Germany) equipped with type 70 Ti rotor. While the supernatant was discarded, the accumulated pellets were dispersed in a 16 ml of 16% (w/v) NaBr + 0.9% (w/v) NaCl and 4 ml each transferred to centrifugation vials. This layer was covered first with a 6 ml layer of 13% (w/v) NaBr + 0.9% (w/v) NaCl, and subsequently with a layer of 0.9% NaCl solution. The pPS vesicles, which typically have a density lower than 1.10 g/cm³, were isolated by centrifugation in a swinging bucket rotor (SW 40 Ti, Beckman Coulter) for 3 h at 28000 rpm and 4 °C without braking. To remove excess NaBr, the resulting pPS was again dispersed in

0.9% (w/v) NaCl and centrifuged (1 h at 31000 rpm, 4 °C). The white pellets were stored at -80 °C until use. An overview of the complete process is given in Figure 2-1.

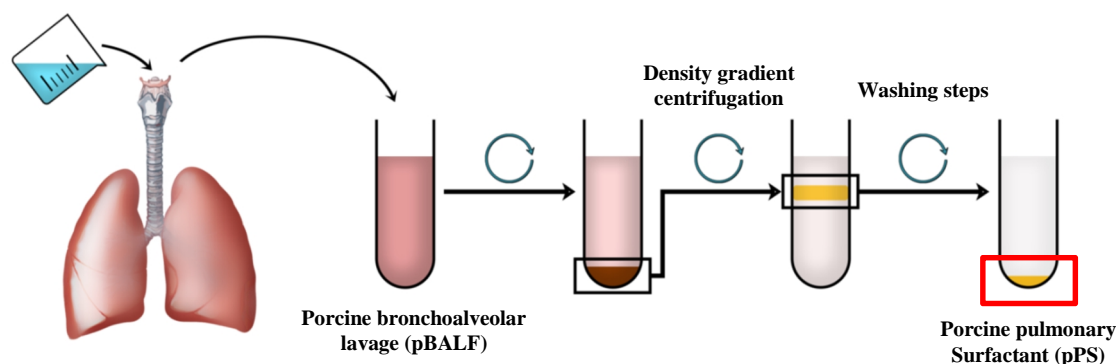


Figure 2-1: Schematic representation of the pPS isolation process. Reproduced from [115].

2.2.4 Total Protein Quantification

Total protein content of the pooled pPS was quantified using a bicinchoninic acid assay (BCA Kit or QuantiPro™ Kit, Sigma Aldrich) as recommended by the manufacturer. In brief, 200 μl of BCA solution, consisting of bicinchoninic acid, sodium carbonate, sodium tartrate, and sodium bicarbonate in 0.1 N NaOH and a 4% (w/v) copper(II) sulfate pentahydrate solution, was added to 25 μl sample in a 96-well plate (Greiner Bio-One, Austria). Blank and standard samples, prepared from bovine serum albumin for the purposes of preparing a standard curve, were treated equally. The plates were sealed and incubated at 37 °C for 30 min. The absorbance of each well at 520 nm was measured in a microplate reader (Infinite 200M, Tecan GmbH, Crailsheim, Germany) and the total protein concentration was calculated by comparison to the standard curve.

2.2.5 Total Phospholipid Quantification (Phosphorous Assay)

Total PL content was estimated by determining the phosphorus content, based on a protocol of Barenholz and Amselem [116]. In short, samples and standards (KH_2PO_4) were dried in borosilicate glass vials using a laboratory sand bath. After addition of 450 μl of 70% perchloric acid, the vials were loosely closed using glass marbles and the organic contents were incinerated at 250-260 °C for 30 min. The vials were allowed to cool to room temperature and incubated together with 3.5 ml water, 500 μl ammonium molybdate tetrahydrate solution 2.5% (w/v), and 500 μl freshly prepared ascorbic acid solution 10% (w/v) for 7 min in a boiling

water bath. The colorimetric reaction, which produces a blue phosphomolybdate, was stopped by placing the tubes in ice water. The absorbance was read in a microplate reader (Infinite 200M, Tecan) after a transfer of 200 μ l sample to a 96-well plate. The PL concentration was calculated assuming an average molecular weight of the measured PLs of 734 g/mol, the molar mass of DPPC.

2.2.6 Dynamic Light Scattering

The average vesicle size of pPS and their temperature dependency was determined by dynamic light scattering (DLS) using a ZetaSizer Nano ZS (Malvern Instruments Ltd., Worcestershire, UK). pPS was diluted to a protein concentration of 40 μ g/ml in tris-buffered saline (=TBS, consisting of 10 mM Tris, and 150 mM NaCl in water, pH adjusted to 7.4 with concentrated HCl) and measured in disposable polystyrene cuvettes. In temperature ramp experiments, average size and scattering intensity was determined in 1 $^{\circ}$ C steps after 2 min equilibration time from 5 to 65 $^{\circ}$ C.

2.2.7 LC-MS Analysis of Phospholipids

PLs were determined by liquid chromatography mass spectrometry as extensively described in Chapter 2.3.

2.2.8 Cholesterol Quantification

Cholesterol and cholesteryl ester content was determined using a fluorometric assay kit (Amplex[®] Red Cholesterol Assay Kit, Thermo Fisher Scientific) according to the manufacturer's manual. Briefly, 50 μ l of samples and cholesterol standards were pipetted into wells of a 96-well plate (Greiner Bio-One) and incubated with 50 μ l of a freshly prepared mixture of 300 μ M Amplex[®] Red, 2 U/ml horseradish peroxidase, 2 U/ml cholesterol oxidase, and 0.2 U/mL cholesterol esterase. After 30-60 min incubation at 37 $^{\circ}$ C protected from light, the fluorescence emission was detected at 550 nm with an excitation wavelength of 550 nm in a microplate reader (Infinite 200M, Tecan). Due to the presence of cholesterol esterase, all cholesteryl esters are hydrolyzed and subsequently detected as free cholesterol. Cholesterol oxidase produces H₂O₂ from free cholesterol which is afterwards probed by 10-acetyl-3,7-dihydroxyphenoxazine (Amplex[®] Red reagent) in the presence of horseradish peroxidase, resulting in the highly fluorescent resorufin.

2.2.9 Thin Layer Chromatography

In general, 10 μ l of samples and 5 μ l of qualitative lipid standards (10 mg/ml dissolved in TBS) were applied on a HPTLC silica gel 60 plate (Merck, Germany) and eluted in a saturated chamber with a mixture of chloroform:methanol:water 65:25:4 by volume. Elution was stopped shortly before the solvent running front reached the end of the HPTLC plate. Lipids were stained with iodine vapor in a glass chamber until sufficiently visible.

2.2.10 SDS-PAGE and Western Blotting

If not stated otherwise, for sodium dodecyl sulfate polyacrylamide gel electrophoresis (SDS-PAGE) equal volumes of samples and 2x SDS-PAGE Laemmli loading buffer (Bio-Rad, Munich, Germany) were mixed and proteins were denatured under reducing conditions at 99 °C for 10 min. The samples were applied to a 12% polyacrylamide gel and electrophoresis performed at 120 V in a Mini-Protean TetraCell (Bio-Rad, Munich, Germany). Spectra Multicolor Broad range protein ladder (Fermentas, St.Leon-Rot, Germany) was used as a molecular weight marker. Gels were either stained with coomassie (PageBlue™ Protein Staining Solution, Thermo Fisher Scientific, Schwerte Germany) or silver (Pierce™ Silver Stain for Mass Spec, Thermo Fisher Scientific, Schwerte Germany) according to the manufacturer's protocol.

In the case of TLC separation prior to SDS-PAGE, the iodine stain was evaporated under the fume hood overnight. The predefined spots were wetted with 10 μ l water and the silica carefully scratched from the underlying glass plate. After addition of 60 μ l SDS-PAGE loading buffer, gel electrophoresis was performed as described above.

For subsequent western blotting, proteins were transferred onto a PVDF membrane (Immun-Blot®, Bio-Rad, Munich, Germany) in a Trans-Blot® SD Semi-Dry Transfer Cell (Bio-Rad, Munich, Germany) for 90 min at 80 mA per gel. Membranes were blocked for 90 min in blocking buffer (consisting of 5% non-fat milk, 0.1% Tween 80, 150 mM NaCl, 10 mM Tris, pH 7) and incubated overnight at 4 °C with either SP-B or SP-C antibodies (both rabbit anti-human, SevenHills Bioreagents, Cincinnati, OH, USA) diluted 1:1000 in blocking buffer. After washing, secondary antibodies (1:2000, anti-rabbit immunoglobulin HRP, Dako, Hamburg Germany) were applied to the blots for 2 h at room temperature (RT) and subsequently incubated in HRP substrate (Immobilon™ Western Chemiluminescent HRP Substrate, Merck Millipore, Germany). Chemiluminescence was detected on X-ray film.

2.2.11 Label-free Shotgun Proteomics

Protein quantification was performed at the Institute for Immunology, Johannes Gutenberg University of Mainz by Dr. Stefan Tenzer. Before measurements, a buffer consisting of 7 M urea, 2 M thiourea and 2% of 3-[(3-Cholamidopropyl)dimethylammonio]-1-propanesulfonate (CHAPS) was used to elute the proteins from phospholipids *etc.* in a filter aided sample preparation (FASP) after trypsinization. Subsequently, samples were analyzed by mass spectrometry with ion-mobility enhanced data-independent acquisition [81, 117]. Relative amounts (in ppm) of total protein were calculated within each sample automatically in the ISOQuant software featuring the TOP3 quantification approach, as described elsewhere [76]. Due to poor annotations of porcine proteins in the common databases, all pig identifiers of the proteins were blasted against the human Swiss-Prot database. The homologue human protein was chosen by E-value and Blast Score. Proteins were annotated with STRAP 1.5 [118]. Gravy Score was calculated according to the method of Kyte and Doolittle [119].

2.3 Excursus: Establishment of an HPLC-MS Method for Phospholipid Quantification

The complex mixture of lipids which are to be found in PS requires sophisticated methods for its analysis. Basic information about the lipid classes making up the PS can be gained by simple methods such as TLC, but due to the amount of different lipid species which have been detected in the PS, a precise quantification can only be achieved by LC-MS. Although the major constituents of PS are phosphatidylcholines, with DPPC being the single most prominent lipid, other groups were able to determine nearly all PL classes in PS: phosphatidylglycerol (GPGlyc), phosphatidylethanolamine (GPEth), phosphatidylserine (GPSer), phosphatidylinositol (GPIIno), sphingomyelins (SM), and lyso-PLs of all classes. Furthermore, cholesterol is present in PS in amounts of up to 10 wt%; this can be easily quantified with an enzymatic assay however, and was therefore not included in the current method development. The requirements for the LC-MS to be established were as follows:

- Sample preparation workflow which allows for analysis of crude pPS samples and pPS adsorbed to NPs
- Detection and quantification of all PL classes: GPChol, GPGlyc, GPEth, GPSer, GPIIno, SM
- Quantification of each species against an external standard of its class
- Detection and quantification of all lyso-forms of the aforementioned classes
- The ability to distinguish between overall chain length of the PLs

To achieve this goal, ultra-high performance liquid chromatography (U-HPLC) and triple quadrupole MS after heated electrospray ionization were deployed. The separation and detection methods are based on recommendations of the LIPID MAPS® consortium [120].

2.3.1 Sample Preparation

In the case of crude pPS, no further processing of the samples would be needed for LC-MS analysis besides dissolution in an LC-MS compatible solvent, since the proteins would hardly produce overlapping ions in the range of PLs. Samples, however, that contain metal ions in higher concentrations, such as the magnetite primary NPs to be used for the corona experiments, do not interfere with the measurements by building adducts with the monitored ions, but their deposition also results in a diminished life time of the quadrupole (QP).

Therefore, all samples were treated in order to remove all nanoparticulate metal oxides, as schematically shown in Figure 2-2A. To avoid the involved process of the standard lipid extraction method developed by Bligh and Dyer [121], which aims to remove cellular components, all samples were lyophilized overnight (Christ Alpha 2-4 LSC, Martin Christ GmbH, Germany) and the lipids dissolved. Unfortunately, the standard (phospho-)lipid solvent, chloroform:methanol 2:1, was not applicable from the beginning of the procedure due to poor NP stability under such conditions. Therefore, an intensive dissolution procedure in a mixture to be utilized as the LC solvent B (isopropanol:hexane:ammonium formate 1% 50:40:10 v/v +0.1% formic acid, 5 repetitions), followed by a last dissolution step in chloroform:methanol was employed. By TLC (Figure 2-2B) of the freeze dried pellets and the supernatant after each dissolution step, exhaustive extraction was ensured with this protocol. The pooled extractions were evaporated (Concentrator Plus, Eppendorf) and the samples dissolved in LC solvent B.

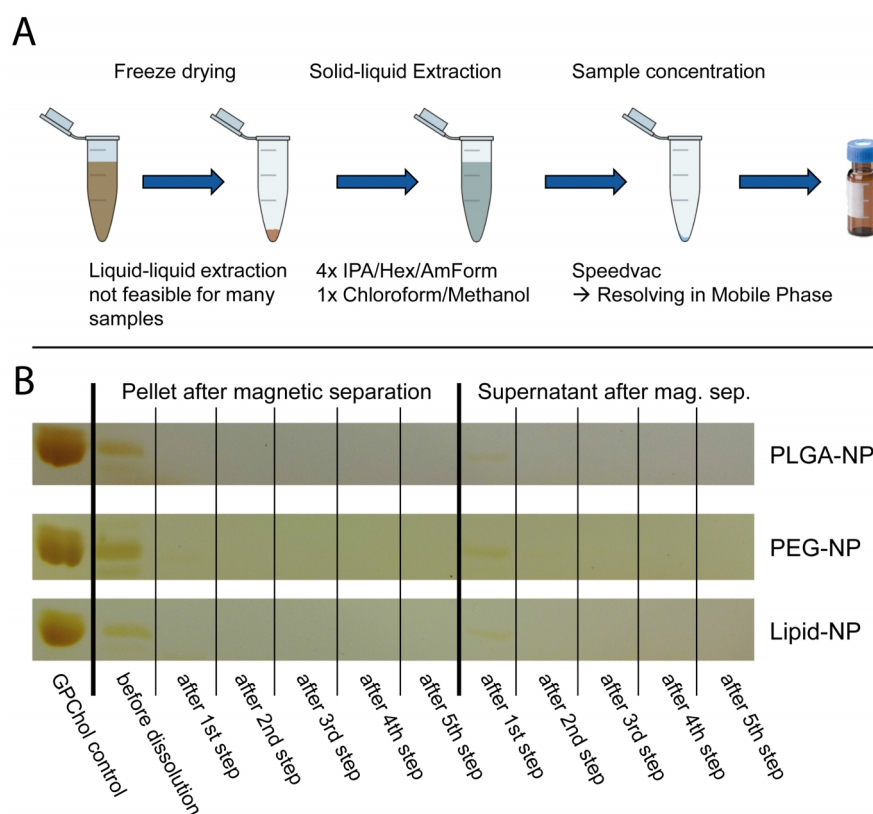


Figure 2-2: Scheme of sample preparation procedure (A), and TLC as control of exhaustive extraction (B), shown exemplarily for three different NPs (see Chapter 3 for further information on the used NPs, IPA/Hex/AmForm = isopropanol/hexane/ammonium formate).

2.3.2 Identification of Distinct Headgroup Fragments

The general structure of PL, with their ionic headgroup as described in Chapter 1.2.1, allows for a relatively easy ionization of the molecule, making the PL precursor ions an optimal candidate for MS analysis. The triple quadrupole set-up allows for fragmentation of the PLs in the second QP and selection again of product ions in the third QP (= MS², Figure 2-3A). Because the molecule charge differs between the PL classes and some (i.e. GPChol, SM, GPEth, and GPSer) are zwitterions, all classes were screened in negative and positive ionization mode to find the most intense break down signal of an class-specific fragment allowing the lowest detection limit. A TSQ Quantum™ Access MAX Triple Quadrupole Mass Spectrometer (Thermo Scientific) equipped with an heated electrospray ionization source (HESI-II, Thermo Scientific) was used in all experiments.

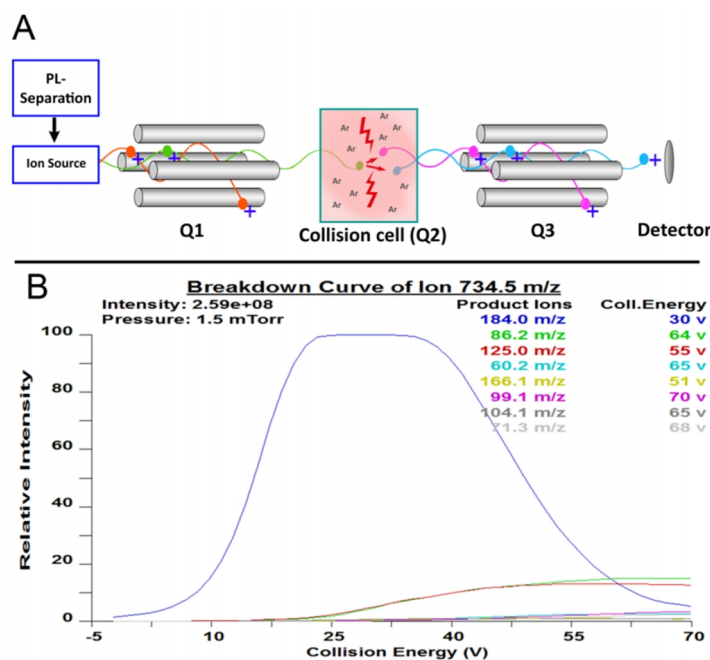


Figure 2-3: Principle of PL detection in an LC- triple quadrupole set-up (A). Example breakdown curve of a DPPC standard during direct injection (B).

By direct injection of single PL species of different classes, the most prominent headgroup fragment was determined together with the optimal collision energy (CE) and skimmer offset (SO). A breakdown curve of DPPC is shown representatively in Figure 2-3B. Since the headgroup fragments of some PL classes cannot be ionized, they are not detected by the product ion scan mode. Instead the precursor ions were scanned for a neutral loss of a certain m/z value. The applied scan parameters and the chemical structures of the PL classes together with the separated fragment are presented in Table 2-1.

Table 2-1: Structures of the measured phospholipid classes shown together with the monitored fragment (in brackets).

Phospholipid class and External Standard	Structure	Monitored fragment m/z
Phosphatidylcholines (GPChol) 16:0 GPChol 14:0 GPChol 18:1 lyso-GPChol		+184
Phosphatidylglycerol (GPGlyc) 16:0-18:1 GPGlyc		NL +172
Phosphatidylethanolamine (GPEth) 16:0-18:1 GPEth		NL +141
Phosphatidylserine (GPSer) 16:0-18:1 GPSer		NL -87
Phosphatidylinositol (GPIIno) 16:0-18:1 GPIIno		-241
Sphingomyelin (SM) 16:0 GPChol		+184

2.3.3 Normal Phase vs. Reversed Phase

In most HPLC application there is only one reasonable option when selecting either reversed (RP) or normal phase separation. Due to the properties of PLs however, both methods can be applied. While RP columns separate the PLs species by chain length, disregarding the charge of the headgroup, normal phase columns distinguish by headgroup charge and protonation state with only minimal impact of chain length on retention time. Both principles have their rationale for use; RP however results in elution of PL species with different headgroups but the same chain length at the same time, which requires parallel scanning for different fragments, reducing the sensitivity for all classes. Additionally, the concurrent elution of the PL classes can also cause an overlap of m/z values, which can only be resolved in MS^X instruments. Normal phase (Triart Diol-HILIC, 150 x 2.0 mm, 3 μm particle size, YMC, Japan) separation was therefore chosen as most suitable. The LC set-up consisted of an Accela Autosampler, Accela PDA and Accela 1250 pump (Thermo Fisher Scientific).

2.3.4 Separation of Phospholipid Classes

The mobile phases were adopted from those recommended by the LIPID MAPS[®] consortium and consisted of isopropanol:hexane 60:40 +0.1% formic acid (= solvent A) and isopropanol:hexane:ammonium formate 1% 50:40:10 +0.1% formic acid (= solvent B). The addition of formic acid improved the shape of most peaks. GPI_{no} with its pK_a of 2.5 however, is only partially charged in acidic pH and therefore elutes in twin peaks.

Time [min]	A%	B%	Flow [$\mu l/min$]
0	85	15	250
3	85	15	250
8	25	75	250
9	10	90	250
11	0	100	250
15	10	90	250
16	85	15	250
21	85	15	250

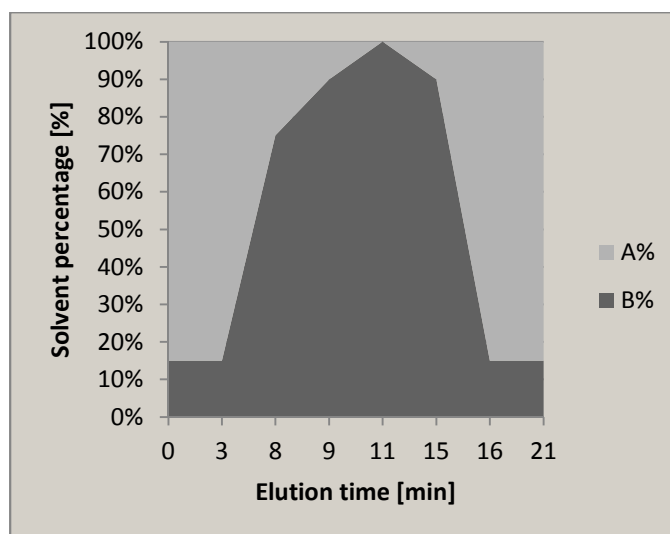


Figure 2-4: Final gradient, allowing separation of all PL classes (with A = isopropanol:hexane 60:40 and B = isopropanol:hexane:ammonium formate 1% 50:40:10, both +0.1% formic acid).

With the final solvent gradient as shown in Figure 2-4, the PLs eluted in the order GPGlyc, GPEth, GPIIno, GPSer, GPChol, as seen in Figure 2-5. Understandably, the PLs with longer fatty acid chains eluted earlier than shorter fatty acid chains within each class, with lyso-PLs appearing as the last species of the class. The complete separation of the PL classes allowed for deploying a scan segment for each class, analyzing only the headgroup fragment of the respective class. Without the need to switch between positive and negative scan mode, the scan time for each m/z and correspondingly the sensitivity could be enhanced.

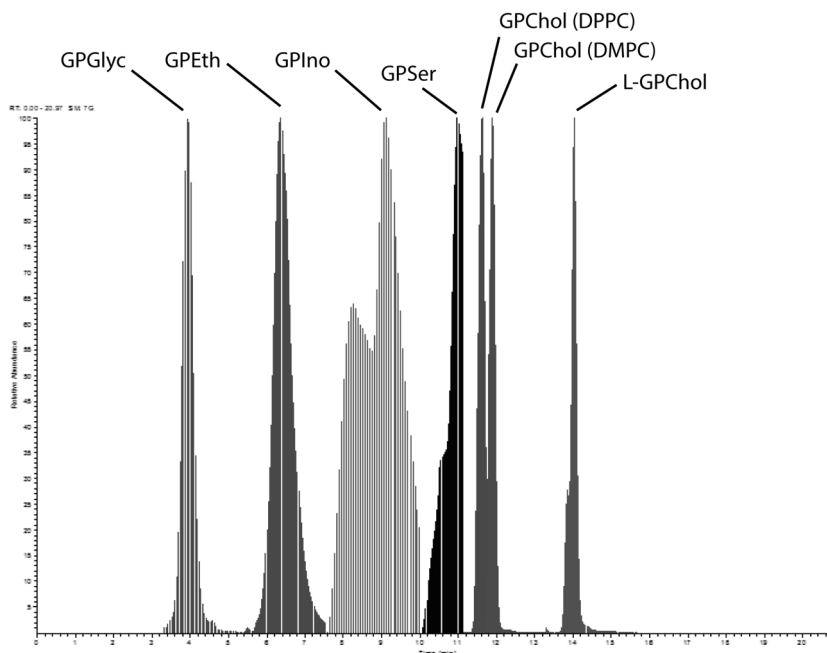


Figure 2-5: Typical separation of all standards injected. Due to the separation of all classes, it was possible to deploy scan segments for each class, increasing sensibility for the respective headgroup fragments.

2.3.5 Data Acquisition and Processing

The vast amounts of data in an analysis that covers 276 m/z values of 6 different PL classes which have to be compared to the external standards of each class, requires careful data handling with a high degree of automation. Only the initial data acquisition was performed in the instrument-specific software Thermo Xcalibur™, which is not suitable for large data sets or several analytes. The foundation of the data processing workflow (Figure 2-6) was the peak detection in MZmine [122], resulting in chromatograms for every single species monitored. The area under the curve (AUC) of the deconvoluted chromatograms were deisotoped by applying an algorithm with the help of an R script to the whole data set, to eliminate the

effect of overlapping m/z value isotopes. The comparison of the AUC of each PL species to an external standard and all further processing took place in Microsoft Excel 2010. To enhance the signal to noise ratio of the peaks, pPS was scanned for all occurring PL species, the m/z value was assigned to the related PL by a tool which is part of the LIPID MAPS® project [123], and further measurements were performed in SRM-mode (single reaction monitoring). Since the range of the PL classes as well as their concentration in the samples differed, each sample was injected twice at different concentrations to ensure a response for each species in a linear range.

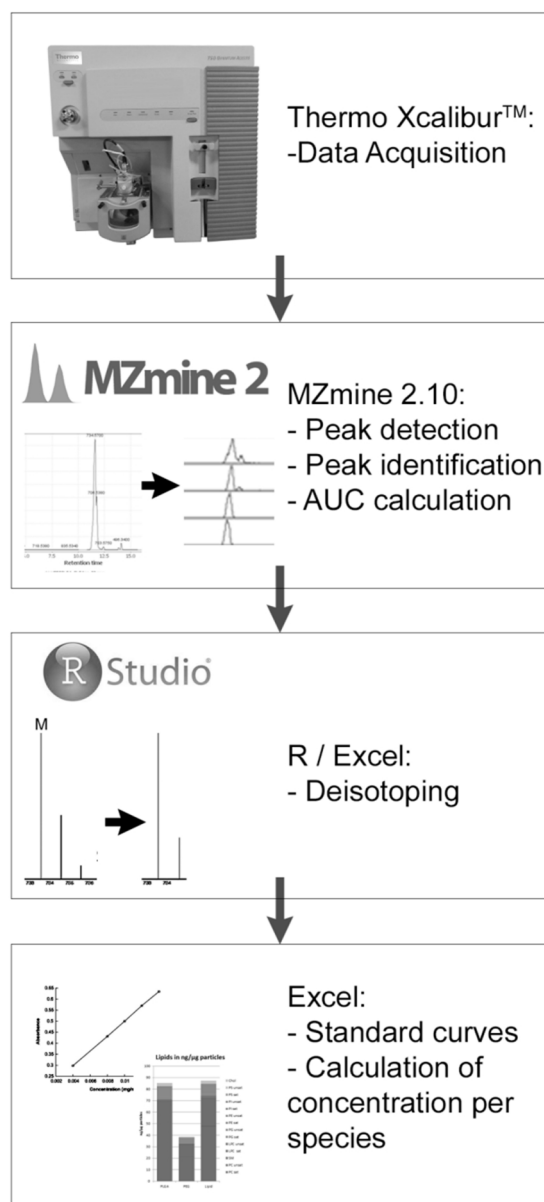


Figure 2-6: Data processing workflow of the established phospholipid analysis.

2.3.6 Validation

Due to the tremendous number of analytes, validation was only employed for the standard substances, assuming an equal behavior for all PL species of a class. Validation was carried out according to the ICH guideline for the validation of analytical procedures [124].

The specificity of the method is already given by the exact mass determination and the headgroup of the PL, and did not need any further evaluation.

The linearity of the measured concentration range was determined after each data set acquisition from the correlation coefficient R^2 , which was based on the regression line of the standard curve and was always better than 0.99. The range was derived from the linearity (=upper limit) and the quantification limit (=lower limit, see Equation 2.2).

The detection (L_D) and quantification limit (L_Q) were calculated based on the standard deviation (SD) of multiple blanks (σ_B) and the slope of the calibration curve (m) according to Equation 2.1 and 2.2 respectively. Values are presented in Table 2-2.

$$L_D = \frac{3.3 \sigma_B}{m} \quad (2.1)$$

$$L_Q = \frac{10 \sigma_B}{m} \quad (2.2)$$

Table 2-2: Limit of Detection (L_D), limit of quantification (L_Q) and total number of species measured

PL class	L_D [ng/ml]	L_Q [ng/ml]	Used measuring range [ng/ml]	Number of scanned masses
GPChol/SM	0.09	0.26	5-500	72/6
GP Glyc	0.66	2.01	5-500	42
GP Eth	0.14	0.42	5-2500	37
GP Ino	0.04	0.12	5-2500	58
GP Ser	0.14	0.42	5-2500	27
L-GPChol	0.18	0.56	5-2500	35

The repeatability of the method as an assessment of precision was measured in terms of an intraday and interday comparison, and judged based on the coefficient of variation (C_V , Equation 2.3, with σ_μ = standard deviation of mean value; μ = mean value). These values were also used to determine the accuracy in terms of the relative error (E_R , Equation 2.4, with C_{exp} = experimentally determined concentration; C_t = theoretical concentration). Intraday and interday C_V values were always lower than 20% and 25% respectively in the used measuring range, which is acceptable for such analysis. E_R was for more than 75% of values lower than 20% and therefore met the requirements.

$$C_V = \frac{\sigma_\mu}{\mu} * 100 \quad (2.3)$$

$$E_R = \frac{(C_{exp} - C_t)}{C_t} * 100 \quad (2.4)$$

The developed LC-MS method met all demands that were defined to determine the PL content of pPS samples with sufficient correctness. The method is tailored to the typical PL mixture, and the sample preparation allows not only the analysis of crude samples, but also the quantification of PLs on the surface of NPs.

2.4 Results and Characterization of pPS

In order to lavage the non-collapsed lungs immediately after the slaughtering process, lavage was performed at the slaughtering line. Only macroscopically healthy, undamaged lungs were used (Figure 2-7A) and in the case of blood contamination of the lavage, pBALF was discarded to maximize pPS purity. Additionally, all pBALF that showed larger red blood cell stains in the first centrifugation step was not further processed. By applying these high standards, a pPS preparation was gained which ultimately showed no sign of contamination in the density centrifugation (Figure 2-7B).

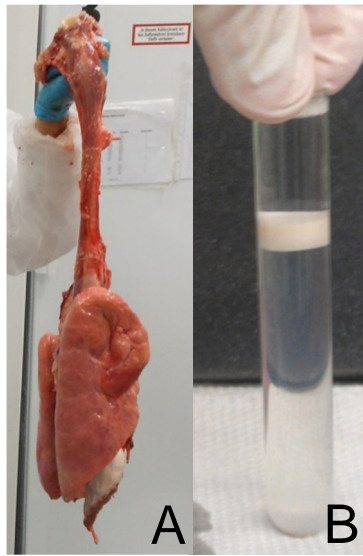


Figure 2-7: Example images of the pPS preparation steps. Healthy, non-damaged lungs (A) were lavaged immediately after slaughtering. The native pPS preparation was successfully purified after density gradient centrifugation (B).

More than 25 lungs were lavaged with only 8 lungs complying with the aforementioned requirements. All pellets were pooled and diluted in TBS (~21 ml) to improve handling; the total protein content and PL content was found to be 3 mg/ml and 34 mg/ml respectively.

2.4.1 Phase Transition Temperature

As already described in Chapter 1, every PL mixture has a specific phase transition temperature, at which the PLs change from the ordered gel phase to the liquid crystalline phase. Above this temperature, the lipids are highly versatile, while below this temperature the PL layer is densely packed. In the case of PS the phase transition temperature is lower and broader in comparison to the transition temperatures of the component PLs alone, due to the effects of SP-B and SP-C. In the range of the phase transition temperature (about 25-41 °C) both ordered gel and liquid crystalline phases exist in PS [41]. By looking at the polydispersity index (PDI) and the average size of vesicles within pPS in buffer ramped from 5 to 65 °C (Figure 2-8) it becomes obvious that some major restructuration is taking place at phase transition. By comparing single consecutive measurements at a temperature below (Figure 2-9A) and within (Figure 2-9B) the phase transition temperature range, this effect is even more clearly visible: The lipid layers behave like relatively monodisperse liposomes below the phase transition temperature, but are changing in size and as a result, structure, within seconds (roughly 20 seconds per measurement). It was therefore concluded that all experiments which aim to elucidate the interaction of NPs with PS must be performed at physiological temperature in order to expose the NPs to the highly variable PS structures that would be expected to occur *in vivo*.

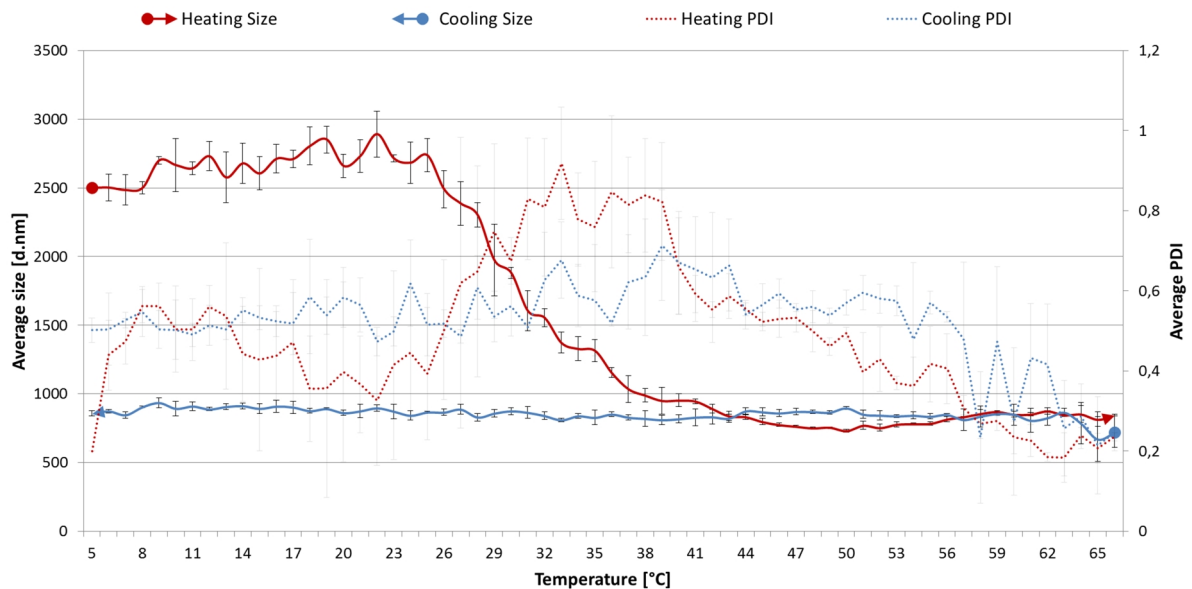


Figure 2-8: Temperature ramp of pPS showing increased activity (as inferred from the PDI) and average size decrease of vesicular structures between 25 and 41 °C, the phase transition temperature of PS [41]. After heating to 65 °C, pPS does not return to its initial state in the cooling phase - the physical properties of pPS are inhibited by degeneration of proteins.

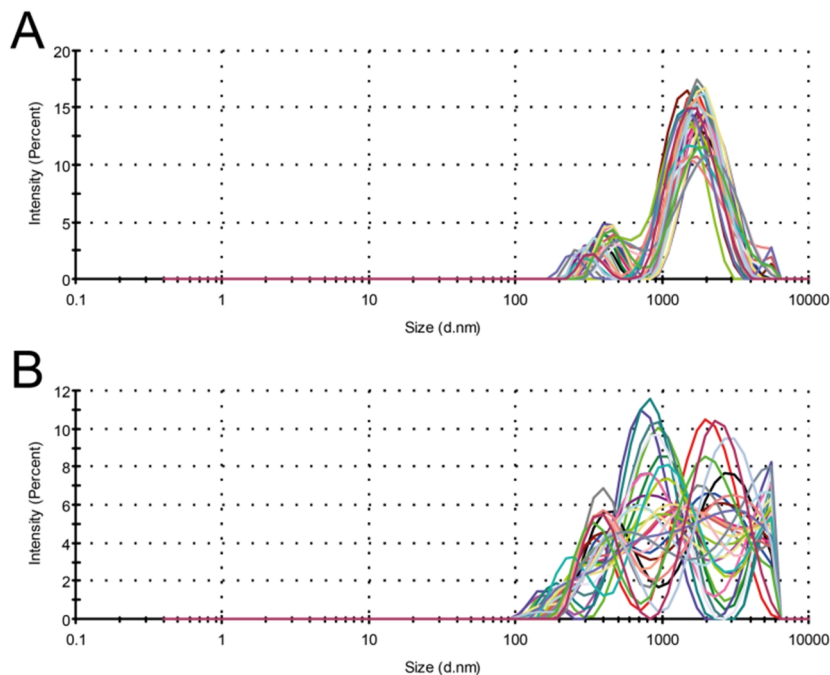


Figure 2-9: Influence of temperature on pPS vesicle size. DLS analysis of pPS (40 $\mu\text{g}/\text{ml}$ protein in TBS) at 4 °C (A) and 37 °C (B) reveals a liposome-like monodisperse behavior of the vesicles below the phase transition temperature. Reproduced from [115].

2.4.2 Lipid Composition

The analysis of pPS by TLC (Figure 2-10) revealed that pPS consists of several lipid classes, dominated as expected by GPChol. The limitations of this method, however, became obvious: With only one elution condition a complete separation of all classes cannot be achieved. Furthermore, the disproportionality of the lipid classes present within PS leads to either a concealing of the closely running classes by GPChol or concentrations below the detection limit for the less abundant species. Since for the further work regarding NP-corona analysis no tremendous changes within lipid concentration were expected, a more sophisticated method for lipid analysis was established as described in Chapter 2.3, allowing an in-depth analysis of all present species.

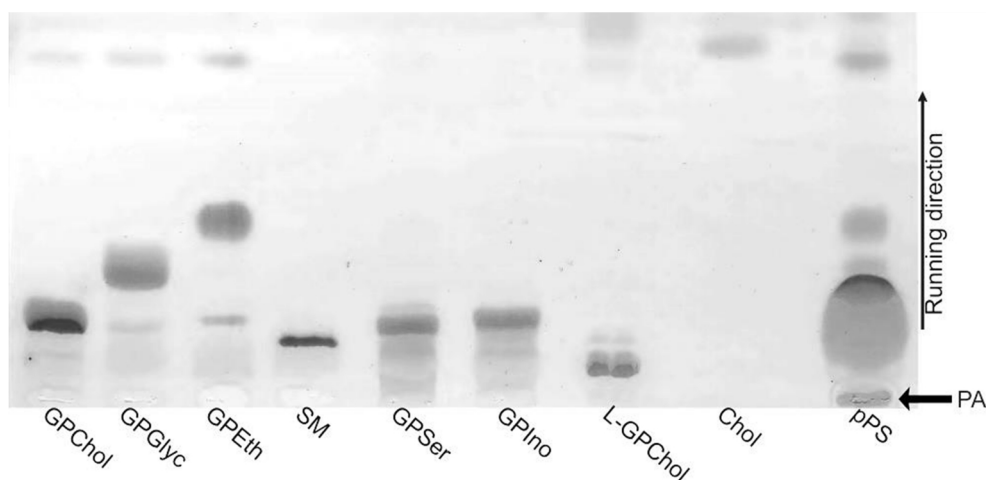


Figure 2-10: Separation of pPS lipids by normal phase TLC. (PA= point of application)

With the application of this method, it was possible to produce the most complete lipid profile of pPS performed to date. The results are summarized in Table 2-3 and Figure 2-11. A total of 249 different lipid species were detected, with the ten most abundant species accounting for 78% of the total weight of lipid present. The relative concentration of DPPC (37%) was found to be lower than stated in the literature, which could be a result of the sum of classes detected. Surprisingly, GPIIno (16.8%) was the second most abundant class after GPChol (67.1%), followed by cholesterol and its esters (7.9%).

The absolute concentration of lipids in pPS is difficult to determine and is still debated. Regardless of the isolation methods used (with the exception of invasive procedures), the PS layer is diluted, and depending on the recovery rate [125], results scatter along with the estimation of surface area.

Table 2-3: Detailed lipid composition of pPS as determined by normal phase HPLC-MS, and enzymatic assay (Chol).

Lipid	GPChol	SM	GPGlyc	GPEth	GPIIno	GPSer	Chol	Total
Total number of lipids quantified	94	3	41	35	58	17	1	249
wt% of total Lipids	67.1±3.8	0.2±0.1	5.9±1.2	2.0±0.3	16.8±1.9	0.1±0.0	7.9±1.0	100
% thereof Lyso-PL	3.5±0.4	0	4.8±0.6	0.5±0.0	0	0	-	2.6
% thereof saturated	71.3±4.2	72.0±1.8	27.2±2.1	0.4±0.0	7.4±0.6	0.0	-	48.0
most abundant species	32:0 (DPPC) 54.7±5.0	34:1 63.2±2.3	34:1 36.4±1.1	36:2 17.5±0.2	34:1 14.1±0.6	36:1 71.0±7.8		
	30:0 13.3±2.4	32:2 28.0±1.8	32:0 18.2±2.2	34:1 15.3±0.2	36:2 5.8±0.2	36:2 7.2±4.3		
	34:1 13.3±2.3	32:1 8.8±0.9	34:2 8.7±0.4	34:2 13.7±0.2	36:1 5.2±0.4	38:4 7.0±5.1		
	32:1 10.5±1.5		32:1 8.6±0.3	36:3 13.6±0.3	others 74.9	others 14.8		
	others 8.2		others 28.0	others 39.8				

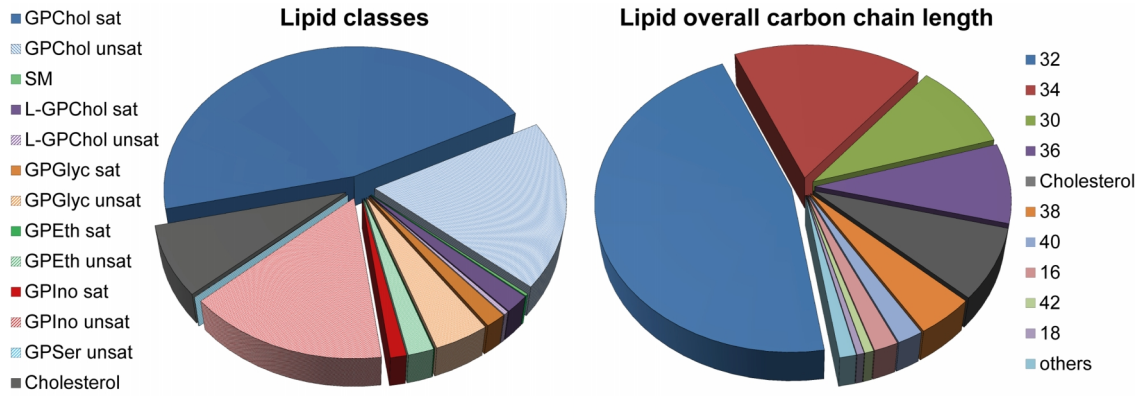


Figure 2-11: Relative distribution of lipids found in pulmonary surfactant by means of lipid classes and overall chain length of phospholipids by wt%.

2.4.3 Protein-Lipid Interactions

Similar to lipid analysis, basic methods, *i.e.* SDS-PAGE, were primarily deployed to analyze the protein composition of pPS. It became obvious that the high amounts of lipids in pPS do not allow for the application of gel electrophoresis without prior sample preparation. Precipitation of proteins by ice-cold acetone did not improve the running behavior of pPS; purification by chloroform/methanol precipitation led to better results (Figure 2-12).

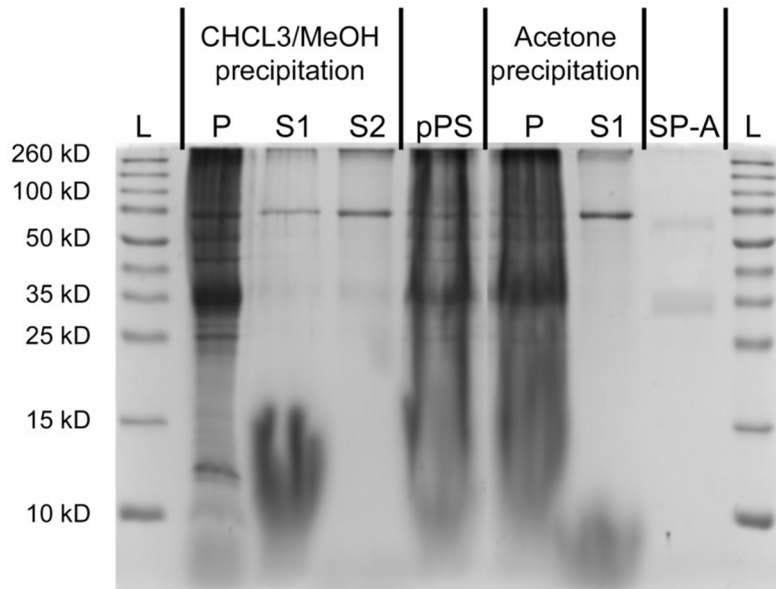


Figure 2-12: Comparison of chloroform/methanol and acetone protein precipitation by SDS-PAGE. Although precipitation by CHCl₃/MeOH showed improvement in lipid depletion, specific proteins are lost in the process (see S1). L = ladder, P = protein pellet after precipitation, S1/S2 = 1st and 2nd supernatant of precipitation, pPS pulmonary Surfactant, SP-A = Surfactant Protein A.

Both protocols, however, depleted not only the lipids, but also extracted proteins from pPS. The most prominent band appearing in the supernatant of precipitation had a size of ~ 70 kDa, with a second faint band of 35 kDa being present. SP-A, which is typically seen in SDS-PAGE gels as monomer and dimer, shows the same bands. Considering the fact that SP-A takes part in lipid organization these result are not surprising. SP-B and SP-C are very likely to be lost during the purification as well, since the two proteins are only sparingly soluble in aqueous solvents and will eventually remain within the organic solvents and the PLs.

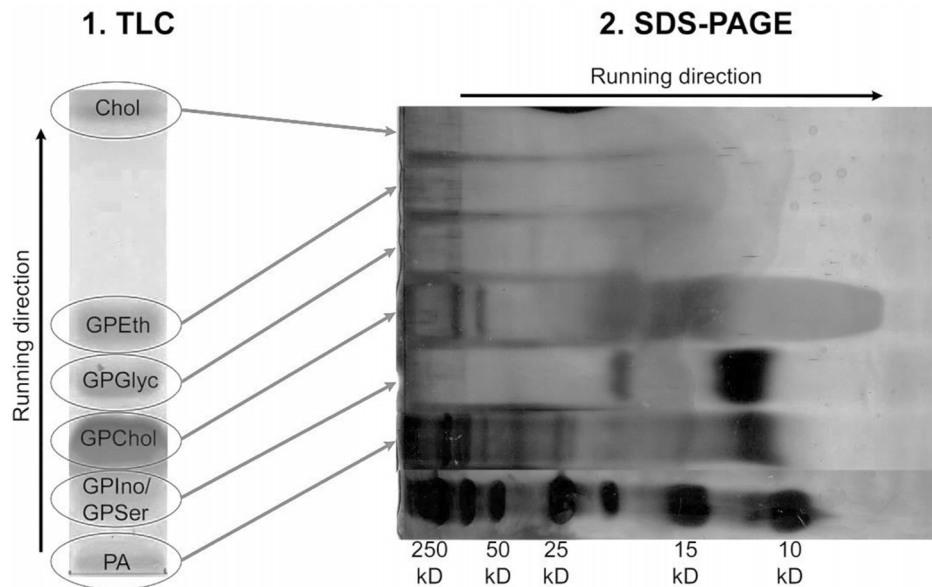


Figure 2-13: "2-Dimensional"-separation of pPS proteins. TLC was deployed for the first separation, single lipid spots were extracted and subsequently resolved by SDS-PAGE (PA = point of application).

To further investigate the connection between lipids and proteins, pPS was first separated into lipid classes by TLC as described in the previous chapter. In a second step, the spots of the lipid classes were scratched from the TLC plates and resolved by SDS-PAGE (Figure 2-13). The point of application showed, as expected, most protein bands; interestingly, the following lipid spots did not show the same, but fainter, bands on the gel. Apparently, only specific proteins elute together with the classes: The scratched spot of the first eluting GPIIno/GPSer (could not be resolved) showed two very distinct bands (~ 18 kDa and ~ 12 kDa), which are not visible in the next spot of GPChol. Together with the GPChol spot, however, two more proteins larger than 50 kDa are eluted. Due to the high concentration of lipids in this band no further bands can be recognized in the lower size range. While in GPGlyc a faint band is still visible, no proteins elute together with GPEth and cholesterol. The identity of these proteins was not further elucidated, but it became clear that a different method is required to get sufficiently accurate results.

2.4.4 Protein Composition

With respect to the study aim, to study the complete PS corona of NPs rather than just single proteins, more sophisticated methods were employed to analyze the proteins occurring in pPS. By label-free shotgun proteomics (performed by Dr. Stefan Tenzer, Institute for Immunology, Mainz), a total of 386 different proteins/peptides were determined to be present in crude pPS. The 30 most abundant proteins that were found in pPS in comparison to the most prevalent proteins in plasma (as determined by Tenzer *et al.* in [76]) are shown in Table 2-4. While plasma proteins are dominated by albumins and globulins, the pPS proteins are considerably more diverse. SP-A has the highest concentration in pPS (10.2%), yet does not occur in plasma at all. It can certainly be expected that there are plasma proteins present in pPS; given the close connection of blood vessels with the alveolar lining fluid at the air-blood barrier, this seems rather likely. The occurrence of hemoglobin in pPS has indeed been linked to the fact that alveolar cells express this themselves, and as such it has been found to associate with the PS vesicle membranes without disturbing the physiological function of PS [126, 127]. Beside SP-A, the second collectin SP-D was also detected in pPS, although in low amounts (0.5%); it was thought to be lost during the purification steps since it is the most hydrophilic SP-X, and is therefore not as closely connected to the lipid vesicles. The concentration of SP-B (1.4%) is in agreement with values published earlier [41]. The sample preparation as described in 0, together with the need for cleavage sites in the protein, allowed only peptides which have a minimal molecular weight of 10 kDa to be analyzed. Therefore, the very small SP-C could not be detected with this method. Its presence was proven however by western blotting with specific antibodies (see Figure 2-14). In total, it was found that the pPS proteome includes much less immunoglobulin (Ig) than plasma, although the surfactant interacts on a daily basis with intruding pathogens and particulate matter.

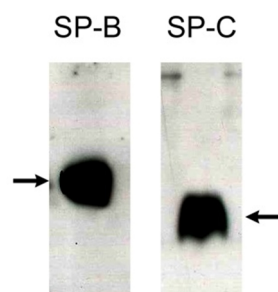


Figure 2-14: Western blotting of pPS after SDS-PAGE proved the presence of SP-B and SP-C in the preparation.

Table 2-4: Top 30 most abundant proteins in pulmonary Surfactant and plasma (data taken from Tenzer *et al.*, proteins occurring in both lists in bold)

Pulmonary Surfactant			Plasma				
No.	Protein name	%	STD	No.	Protein name	%	STD
1	Pulmonary surfactant-associated protein A1	10,19	0,39	1	Serum albumin	23,15	4,80
2	Serum albumin	5,77	0,18	2	Alpha-2-macroglobulin	11,04	0,98
3	Sodium-dependent phosphate transport protein 2B	2,31	0,11	3	Complement C3	8,80	0,39
4	Tubulin alpha-4A chain	2,27	0,04	4	Ig gamma-1 chain C region	7,70	0,77
5	Fibronectin	2,23	0,07	5	Serotransferrin	5,01	0,24
6	Myosin-9	2,09	0,11	6	Alpha-1-antitrypsin	4,60	0,86
7	Deleted in malignant brain tumors 1 protein	1,99	0,11	7	Haptoglobin	3,51	0,36
8	Complement C5	1,85	0,09	8	Apolipoprotein A-I	3,26	0,60
9	Actin, cytoplasmic 1	1,80	0,10	9	Ig kappa chain C region	2,42	0,16
10	Complement C3	1,68	0,19	10	Ig gamma-2 chain C region	2,20	0,25
11	Pulmonary surfactant-associated protein B	1,39	0,11	11	Complement C4-A	2,09	0,14
12	Ig alpha-1 chain C region	1,28	0,08	12	Ig alpha-1 chain C region	2,07	0,31
13	Hemoglobin subunit beta	1,23	0,01	13	Ig gamma-4 chain C region	2,05	0,06
14	L-xylulose reductase	1,14	0,06	14	Hemopexin	1,79	0,13
15	Tubulin beta-4B chain	1,02	0,07	15	Ceruloplasmin	1,35	0,12
16	Tubulin alpha-1A chain	1,02	0,07	16	Ig lambda chain C regions	0,91	0,04
17	Calcium-activated chloride channel regulator 1	0,96	0,04	17	Alpha-1-antichymotrypsin	0,89	0,05
18	Polymetric immunoglobulin receptor	0,94	0,03	18	Inter-alpha-trypsin inhibitor heavy chain H2	0,88	0,07
19	AP-2 complex subunit beta	0,94	0,08	19	Complement factor H	0,81	0,07
20	Serotransferrin	0,92	0,03	20	Ig mu chain C region	0,80	0,08
21	Tubulin beta 5 chain	0,88	0,06	21	Vitamin D-binding protein	0,77	0,19
22	BPI fold-containing family B member 1	0,88	0,07	22	Inter-alpha-trypsin inhibitor heavy chain H1	0,74	0,05
23	Alpha-2-macroglobulin	0,84	0,05	23	Kininogen-1	0,64	0,08
24	Myosin-14	0,82	0,01	24	Clusterin	0,58	0,11
25	Myosin-7B	0,82	0,37	25	Inter-alpha-trypsin inhibitor heavy chain H4	0,57	0,05
26	C4b-binding protein alpha chain	0,75	0,02	26	Complement factor B	0,56	0,03
27	Ig lambda-1 chain C regions	0,74	0,04	27	Plasminogen	0,54	0,03
28	Coatmer subunit alpha	0,73	0,04	28	Vitronectin	0,48	0,05
29	EH domain-containing protein 2	0,69	0,06	29	Plasma protease C1 inhibitor	0,47	0,01
30	Fatty acid synthase	0,69	0,04	30	Alpha-1B-glycoprotein	0,47	0,05

2.5 Summary and Conclusion

The isolation of pPS by the method of Shelley *et al.* [112], is an established model in biophysics, which has helped in understanding the astonishing properties of the air-blood barrier [128, 129]. Most studies so far have however only employed artificial, lipid-based clinical PS preparations (e.g. Alveofact®, Surfacten®, Curosurf®, *etc.*), making the assumption that only lipids from PS will interact with NP. Such preparations are commercially available and standardized; nevertheless, the use of these preparations for elucidating the NP corona and even the impact of NPs on the surfactant layer is not appropriate. By indirect measurements of phase transition temperature, it could be shown, that pPS undergoes massive structural reorganization in the physiological temperature range.

Table 2-5: Comparison of the determined concentrations of lipids in the used surfactant preparation to values found in the literature. The in-house analysis included for the first time an advanced quantification method for all lipid classes that were previously detected. Mol% and wt% are fairly comparable due to the narrow mass range of most occurring lipids.

PL class	[111] by TLC [mol%]	[128] by HPLC-UV [mol%]	pPS [wt%]
GPChol	79.5 ± 1	85.6 ± 1.8	67.1 ± 3.8
GPIIno	10-15	2.0 ± 0.2	16.8 ± 1.9
GPGLyc	4-8	8.6 ± 0.7	5.9 ± 1.2
GPEth		2.9 ± 0.8	2.0 ± 0.3
GPSer	n.a.	Traces	0.1 ± 0.0
Cholesterol	3.2 ± 0.2	n.a.	7.9 ± 1.0
SM	n.a.	1.0 ± 0.5	0.2 ± 0.1

The composition of both lipids and proteins was determined to a very high level. Lipid composition was dominated, as expected, by DPPC, with GPIIno as the second most abundant class. The determined concentrations were in agreement with values from the literature (Table 2-5) and furthermore, all PL classes were determined in pPS simultaneously for the first time. pPS contains all naturally occurring lipids including cholesterol, which is depleted in commercial surfactants [111].

By deploying sophisticated lipidomics, an immense diversity of proteins was detected, and the occurrence of all SP-X was proven. Due to the nature of biophysical experiments performed with PS, minor plasma protein concentrations are negligible. Comparison of the generalized gene ontology terms of pPS and plasma (Figure 2-15) shows that protein properties of these biological fluids differ, further confirming that the plasma corona cannot be regarded as relevant for airborne NPs in the deep lung. Therefore, it can be concluded that the isolated

porcine native pulmonary surfactant is a most realistic model to study the interplay of NPs with the non-cellular barrier of the deep lung, which will not only interact with the NPs in a physically correct manner, but, as it contains all relevant lipids and proteins, also constitutes the perfect preparation to elucidate the NP corona *in vitro*.

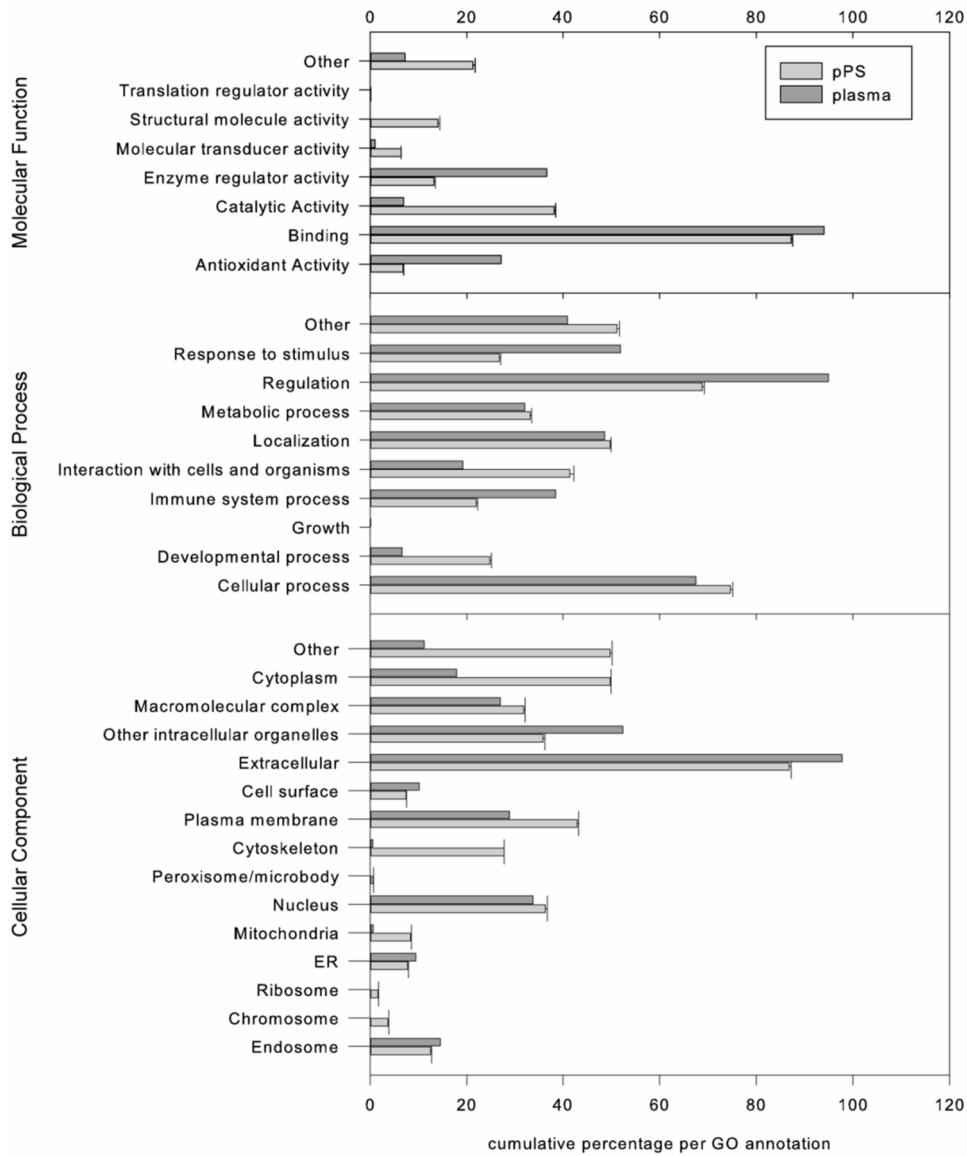


Figure 2-15: Comparison of the relative cumulated gene ontology terms of the entity of proteins found in crude plasma (data taken from [76]) and pPS.

3. THE NANOPARTICLE CORONA IN PULMONARY SURFACTANT

3.1 Introduction

NPs that are intended to be used in patients have to be tested for toxicity, drug release, colloidal stability, cell uptake, *etc.*, and the route of application and site of action have to be taken into account for these tests. In the case of inhalable NPs for pulmonary delivery, the site of action is the alveoli; NP properties and behavior needs therefore to be studied in this environment. Most *in vitro* experiments on the efficiency and safety of NPs are still performed under questionable conditions, *e.g.* using unrelated cell lines, measuring NP stability in water or cell medium with and without fetal calf serum (FCS), and performing cytotoxicity and uptake experiments ignoring the fact that in the human body NPs will be covered, or opsonized, by biomolecules prior to cell contact [71]. Whenever the term ‘nanoparticle’ is used, it usually refers to a particle which possesses characteristics that a macroscopic solid does not. An NP however which is actually nano-sized after production may not necessarily be within the nano-range after its administration into the body. Several factors can lead to agglomeration, to a degree at which the NP loses its specific abilities and characteristics [130]. The tendency of macrophages to engulf single NPs is quite low; larger agglomerates however are taken up easily by either phagocytosis or pinocytosis [131].

NPs that enter the deep lung may be inhaled by accident, *i.e.* “technical particles” such as contained within exhaust fumes, meaning they are deposited as single particles. Alternatively, NPs may be inhaled on purpose, as drug delivery vehicles. The aerosol generation of single NPs is not yet feasible in the latter case; the NPs are therefore incorporated into microparticles or aerosolized within liquid droplets. Regardless of the intention, solid NPs that enter the alveolar region will come in contact with the very first barrier of the lungs: the PS. The proteins and lipids of the PS will adsorb to the surface of the NPs, altering surface properties such as hydrophobicity, surface charge and surface chemistry, and in doing so affecting NP stability, drug release, agglomeration tendency [132], and most importantly, cellular recognition of and interaction with NPs [87]. How the layer around NPs is formed and what it does to the NP itself when it comes into contact with a biological fluid has been extensively researched in the last years [69]. Plasma proteins have been largely accepted in this respect as a general model for the non-cellular nano-bio-interactions that occur in the body. A number of factors such as how single proteins adsorb to the NP surface [133], how fast the corona is formed [81] and how thick this layer is [79], how many proteins adsorb per surface area [133], what orientation these proteins have [134], whether the binding can be modified by size/curvature [135], and the surface chemistry [136] and charge [135] of the corona have

been studied. However, the dissimilar environment in the deep lung in comparison to plasma is quite obvious, and the manner in which this affects the outcome of the latter mentioned effects on NPs is almost completely unknown.

Although researchers who are looking into nano-bio interactions have accepted the fact that they need to include the adsorption of biomolecules into the testing of their newly formulated particles, various methods rather than standardized procedures are commonly used to probe the corona formation. Most groups keep it as simple as possible and gain suitable results by incubating NPs in plasma and separating the NPs with their adherent corona by centrifugation [137], or visualize the corona *in situ* by measuring the size change in protein-containing solutions [138]. Just recently Hadjideometriou *et al.* were able to observe the corona formation *in vivo* [88]. All of these techniques, however, presume that there is a hard corona, as already introduced in Chapter 1, which needs to be divided from the soft corona.

When looking at this very peculiar body fluid, one must realize, that PS is neither a colloidal system nor a solution, but a membranous and vesicular system, which organizes itself not only at the air-liquid interface but also in the submerged phase [41]. Once an NP interacts with any component of PS, it can be expected to become a part of the whole system rather than continuing to be seen as a single NP. Not only adsorption but also lipid bilayer dynamics have to be considered for the interactions of NPs with PS. Nevertheless, if this leads to an agglomeration of the particles or to an excessive adsorption of lipids/proteins has never been documented. Other researchers have been looking into the effects of single components of PS [101] or artificial models [132]; this chapter will focus on the interaction of NPs with crude pPS, as it was described in Chapter 2. It is most likely that all lipids and proteins present within PS interact with the NP surface, and therefore only the entire system will reflect the actual *in vivo* situation. It is expected, that PS requires completely different approaches to visualize the NP corona, as it is not simply a protein solution and therefore does not act like one. In this chapter, it was attempted to observe and access the corona on NPs by different options that are commonly used for the plasma corona, by means of size measurement methods. Besides the typical techniques such as DLS and nanoparticle tracking analysis (NTA), the approach of differential centrifugal sedimentation (DCS), as recently established by Monopoli *et al.*, was investigated [79]; separation by asymmetric flow field flow fractionation (AF4) was also employed. These methods partly depend on special characteristics of the nanomaterial; therefore, NPs compliant to these requirements had to be used according to the respective method, giving valuable insights into the largely ignored factor of the ‘nanoparticle corona in pulmonary surfactant’.

3.2 Reagents and Methods

3.2.1 Reagents

Poly(D,L-lactide-co-glycolide) (PLGA) with a lactide:glycolide ratio of 50:50 (Resomer RG 503 H) and Eudragit® RS 100 were purchased from Evonik (Essen, Germany). Polyvinyl alcohol was obtained from Carl Roth (Karlsruhe, Germany; Mowiol® 4-88). The non-synthesized magnetite-containing NPs were bought from the following suppliers: PEG-NPs (nanomag®-D PEG 5000 250 nm) and ProtA-NPs (nanomag®-D Protein-A 250 nm) were ordered from Micromod (Rostock, Germany), Lipid-NPs (fluidMAG-Lipid 200 nm) and Starch-NPs (fluidMAG-D 200 nm) from Chemicell GmbH (Berlin, Germany), and PS-NPs (PS-MAG-COOH 350 nm) from Microparticles GmbH (Berlin, Germany). All NP were used as received. Fluorescent carboxylated polystyrene NPs (Fluoresbrite® COOH YG 0.05/0.2 µm and Fluoresbrite® Multifluorescent 0.2 µm, further referred to as PS-COOH NPs) were obtained from Polysciences Europe GmbH (Eppelheim, Germany); all other reagents and solvents were purchased from Sigma Aldrich (Munich, Germany).

3.2.2 Preparation of magPLGA and magEu Nanoparticles

Magnetite-loaded PLGA NPs (magPLGA-NPs) and magnetite-loaded Eudragit® RS 100 NPs (magEu-NPs) were synthesized as described in detail in Chapter 0.

3.2.3 Electron Microscopy

For scanning electron microscopy (SEM), NPs were diluted appropriately (1:100 – 1:1000) and applied on a carbon disc. The suspensions were dried overnight, sputtered with gold (Q150R, Quorum Technologies, Laughton, UK) and imaged with an EVO HD 15 microscope (Zeiss, Germany). Transmission electron microscopy (TEM) was performed on a JEM 2011 (Jeol, Japan) after drying NP dispersions on a copper grid.

3.2.4 Dynamic Light Scattering

DLS was performed as described in Chapter 2.2.6. The zeta potential of the NPs was also measured with the Zetasizer ZSP based on the electrophoretic mobility using a disposable folded capillary cell in automatic mode. For titration experiments, an automatic titration system (MPT-2, Malvern) was additionally connected to the instrument. Where possible, the titrant was kept under permanent stirring and the mixing chamber at 37 °C.

3.2.5 Nanoparticle Tracking Analysis

NP number count was measured using a NanoSight LM10 (Malvern). The NP suspensions were diluted appropriately and injected into the measuring chamber with a syringe. Measurements were performed with a green laser (532 nm) in triplicate. If not stated otherwise, NPs were analyzed three times for 60 seconds with sample agitation between the measurements. Agglomeration behavior of fluorescent NPs was measured with an applied green filter using the live view mode (Software: NanoSight NTA 2.3).

3.2.6 Adsorption Experiments

pPS was diluted to meet an NP to protein ratio in μg of 1:2 in TBS buffer. NP stock solutions were dispersed thoroughly by vortexing and brief sonication in an ultrasonic bath before the appropriate amount was added to the pPS. The mixture was incubated at 37 °C under agitation (400 rpm) in a thermal shaker (Thermomixer comfort, Eppendorf, Hamburg Germany) to prevent pelleting of the pPS vesicles. As this work represents the first study looking into the adsorption of PS onto NPs in such a level of detail, a set incubation time of 1 h was chosen based on several considerations:

- Previous work which has been performed in-house and by other groups regarding single lipids or proteins showed fast corona evolution within minutes [81]. To ensure that the protein and lipid adsorption has reached equilibrium, a significantly longer incubation time was chosen.
- The lower limit of incubation time has also to be regarded. The magnetic separation of NPs is not as fast as the separation by centrifugation. Therefore, no shorter incubation times were evaluated, considering the introduced error in comparison to the subsequent separation time.
- Using the kinetic parameters for estimating the equilibration time is difficult. There are no kinetic parameters available which describe the behavior of the PS towards a solid. There are descriptive parameters regarding lipids and single proteins alone; a reliable prediction of the affinity of a protein-lipid mixture, however, is impossible at the moment, since the PS behaves neither as liposomes, nor as protein solution. To gain such data, a time-dependent resolution of the evolution of such PS corona around NPs must be first performed.

3.2.7 Asymmetric Flow Field Flow Fractionation

The used AF4 set-up consisted of a common HPLC configuration (Pump, Autosampler, RS Variable Wavelength Detector, Fraction collector, all Ultimate 3000, Dionex™, Sunnyvale, USA), a flow controller (Eclipse DualTec), a refractometer (Optilab T-rEX) and a multi angle (or static) light scattering (MALS) device (DAWN HELEOS II, all by Wyatt Technology, Dernbach, Germany). The medium sized separation chamber was used, equipped with a regenerated cellulose membrane (cutoff 10 kDa) and a mobile phase consisting of freshly prepared phosphate buffered saline (PBS). A volume of 15 μ l per sample was focused and subsequently eluted with a constant detector flow of 1 ml/min and the following settings:

Mode	Step Duration	Crossflow
Elution	2	3
Focus	1	
Focus + Injection	2	
Focus	7	
Elution	5	1 \rightarrow 0.1
Elution	25	0.1 \rightarrow 0
Elution	25	0
Elution + Injection	5	0
Elution	4	0 \rightarrow 1

3.2.8 Differential Centrifugal Sedimentation

DCS was performed on a DC24000 (CPS Instruments, Inc. Prairieville, LA, USA). If not stated otherwise, the experimental set-up was as follows: A gradient of sucrose in PBS was prepared by injecting consecutively nine solutions of decreasing sucrose concentration (each 1.6 ml). As stated for the individual experiments, three different gradients and speeds were used (2-8% Sucrose at 14000 rpm; 8-24% at 18000 rpm; 12-48% at 18000 rpm). After the last injection of sucrose solution, the gradient was overlaid with 1 ml of dodecane to prevent evaporation and therewith changes in gradient composition. The gradient was allowed to stabilize for 20 minutes before measurement. Standard polyvinyl chloride NPs (CPS Instruments, Inc.) with a size of 239 nm were injected prior to each sample injection and the sample size was calculated in relation to the run time of the standard. The sample volume was always 100 μ l with an NP concentration of 0.1 mg/ml. Data was acquired using CPSV95C software, supplied by the instrument manufacturer.

3.3 Excursus: Preparation of Magnetite-Loaded Nanoparticles

Early experiments with PS already revealed the complicated nature of polymeric NPs and pPS separation following their incubation in PS from the latter. In order to facilitate the use of magnetic separation and to exploit the additional advantages to be gained by using high density NPs, different NPs with incorporated magnetite primary nanoparticles were prepared.

Extremely small magnetite NPs (depending on the material) possess the advantage of being superparamagnetic, which means that each NP acts as a single magnetic domain. When an external magnetic field is applied, for instance as produced by a neodymium magnet, superparamagnetic NPs align themselves in the same direction as this field. As soon as the magnetic field is removed, the NPs lose their magnetic moment and show no susceptibility to self-agglomeration by remaining magnetism. The most commonly used material for such NPs is iron oxide, in particular the ferrimagnetic magnetite (Fe_3O_4) and maghemite ($\gamma\text{-Fe}_2\text{O}_3$). Iron oxide NPs of sizes smaller than 20 nm show superparamagnetism [139], and have - in comparison to most polymers - a high density. As an interesting polymer for potential drug delivery to the lungs, PLGA was chosen. As an additional polymer which exhibits positive charge, Eudragit RS 100 was used to synthesize NPs with a positive zeta potential.

3.3.1 Preparation Method

Primary magnetite NPs were prepared by Dr. Christian Cavelius (INM, Saarbruecken) by a co-precipitation method [140]. In short, ferrous and ferric salts were mixed under alkaline, non-oxidizing conditions, forming magnetite (Equation 3-1). The precipitated magnetite was coated with oleic acid, and the now highly hydrophobic NPs were collected in an organic phase such as hexane or chloroform. Since magnetite is sensitive to oxidation, it is likely to be partly transformed into the likewise superparamagnetic maghemite (Equation 3-2).



NPs were prepared using an emulsification-evaporation method as schematically shown in Figure 3-1. Briefly, primary magnetite NPs were dispersed under vortexing and sonication in chloroform together with either PLGA or Eudragit® RS 100, and added to an aqueous solution of polyvinyl alcohol. After brief mixing, the two-phase system was sonicated on ice

for 70 s at 30% intensity with a tip-sonicator (250 Digital Sonifier, Branson, Danbury, USA) equipped with a 1/8" tapered microtip. The dispersion was quickly transferred into a beaker and under mechanical stirring (Eurostar digital, IKA-Werke, Staufen, Germany), water was added to 40 ml. The chloroform was then allowed to evaporate overnight. After filtration through a 0.45 μm membrane in the case of magPLGA-NPs, magnetite-loaded NPs were separated from insufficiently loaded NPs by separation in a magnetic rack (PureProteome™ Magnetic Stand, Merck Millipore, Germany) for 5 min. Magnetic NP pellets were dispersed in water and stored until use at 4 °C. The mass concentration was determined gravimetrically after lyophilization (Christ Alpha 2-4 LSC, Martin Christ GmbH, Osterode am Harz, Germany). Additionally, it was possible to coat magPLGA-NPs with the positively charged polymer chitosan to produce positively charged core-shell NPs as described by Kumar *et al.* [141].

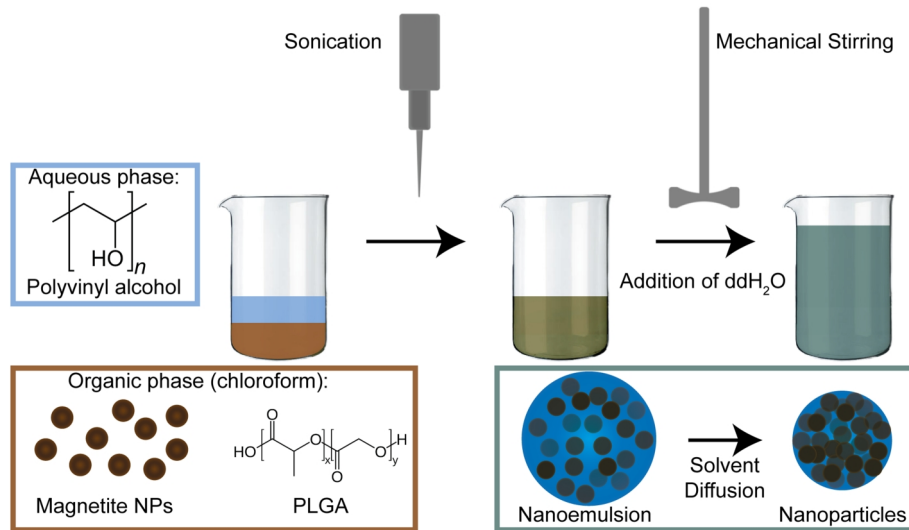


Figure 3-1: Schematic of the nanoparticle preparation process, here magPLGA-NPs. ddH₂O = double distilled water.

3.3.2 Characterization

The magPLGA- and magEu-NPs that were produced by the above described method were monodisperse, spherical, and highly magnetic (as described in Table 3-1). In small volumes (Eppendorf tubes) of pure water, it was possible to attract all particles of the dispersion by an externally applied permanent magnet (Figure 3-2); particles were still dispersible by vortexing however, a necessary condition for the planned adsorption experiments which would require multiple cycles of redispersion following washing steps.

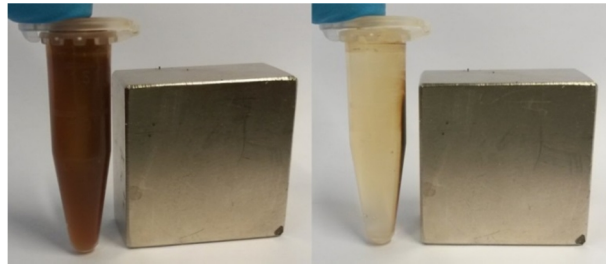
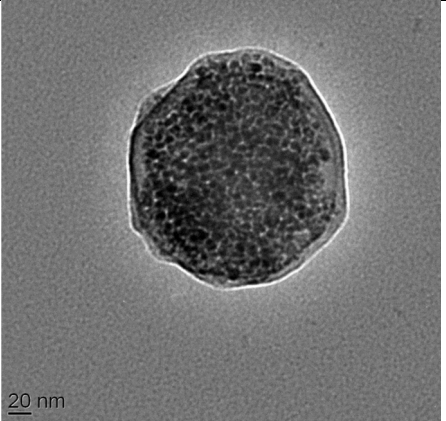
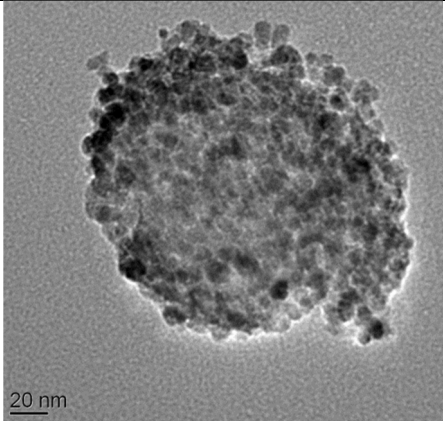
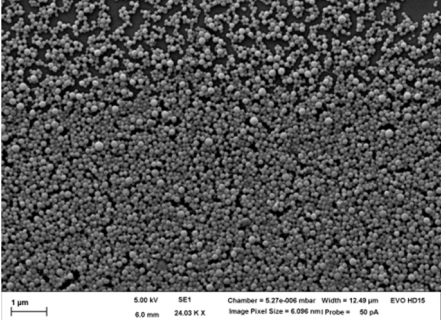
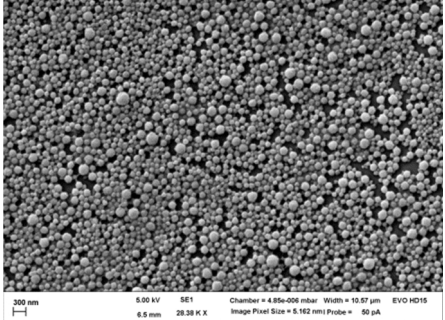


Figure 3-2: magPLGA-NPs are attracted by a permanent neodymium magnet within minutes.

Table 3-1: Average properties of the produced magPLGA- and magEu-NPs

NPs	magPLGA	magEu
Size (DLS) [d.nm]	180–210	200–220
PDI	<0.1	<0.1
Zeta potential [mV]	-25 ±0.2	+34 ±0.5
TEM		
SEM		

3.4 Results and Discussion

3.4.1 Dynamic Light Scattering of Nanoparticles in the Presence of Porcine Pulmonary Surfactant

DLS offers the possibility for size analysis of submicron particles, down to the scale of single proteins. There is, however, a major drawback: polydisperse samples or samples with several size fractions are not resolved well. In the presence of larger structures, DLS is limited by the high amount of light scattered by the large particles, which masks the signal of smaller particles. As shown already in Chapter 2 (Figure 2-9), the membranes of PS scatter light like coalescenting liposomes which, therefore, results in a signal over a large size range. This makes it impossible to accurately determine the size of concurrently present NPs. This effect on the results of NP size measurements is exemplified by polystyrene NPs in presence of different amounts of pPS, shown in Figure 3-3A. The amount of scattered light by either particles or pPS is however dependent on their concentration. By slow titration of NPs with increasing amounts of pPS it was attempted to measure the size increase and therewith the corona layer formation at least at the early stage, given that the added pPS immediately adsorbs to the particles and does not remain in solution. For all used NPs the titration diagram was very similar (PS-COOH shown in Figure 3-3C as a representative example). Starting from the very first addition of pPS, the average size slowly increased. PS-COOH NPs that are exposed to plasma proteins, even at high concentrations of 10% FCS, only show a certain size increase when the whole NP surface is covered with hard- and soft-corona (Figure 3-3B). The additional free proteins are not visible in DLS, as single proteins scatter very little in comparison to the large NPs. In case of pPS however, the size continues to increase until it resembles the polydisperse graphs of solely pPS in solution. Furthermore, the overall intensity of the sample is decreasing during addition of pPS. It could therefore be inferred, that the increasing size of the sample is not due to the corona formation but is more likely a function of the increasing strength of the signal coming from the membranous structures of pPS. Although the application of this method was evaluated for the whole set of NPs with different surface properties and particles sizes, the thickness of the corona could not be judged by DLS.

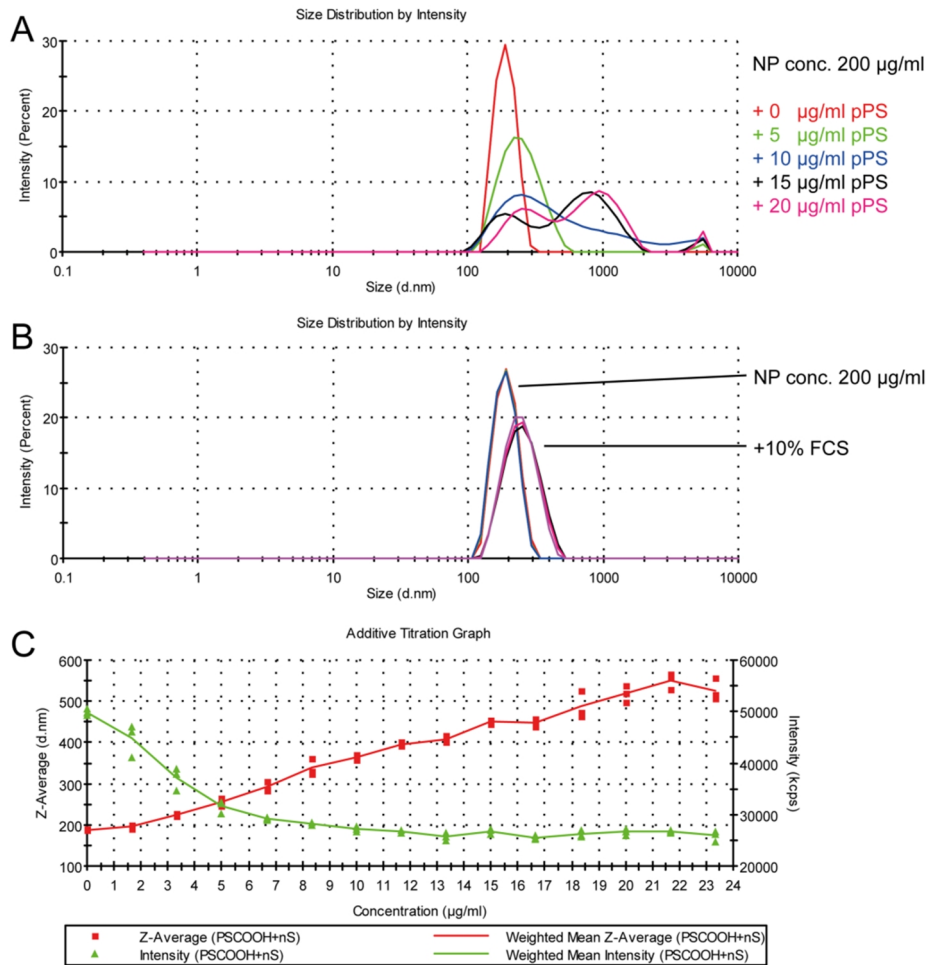


Figure 3-3: DLS measurements of 200 nm PS-COOH NPs during titration with pPS. Single measurements (A) show that already small amounts of pPS cause the monodisperse NP peak to vanish. In comparison, NPs in a solution of plasma proteins (B),, even at high concentrations, does not show such behavior. During the titration with pPS (C), the z-average of all peaks is increasing to values to more than double the initial size, while the intensity of the sample decreases.

3.4.2 Nanoparticle Tracking Analysis

Although the size determination of NPs by NTA is, like DLS, based on Brownian motion, the two methods show many points of difference. Both use a laser to produce a scattering signal, however the method used to calculate particle size from this scattered light signal is markedly different: DLS detects the change in the scattered light signal, while NTA tracks the scattered light of single particles which are illuminated by a laser beam through a microscope set-up. This gives the advantage of being able to manually select which signals should be counted as particles. On the other hand, NTA detects far fewer particles at one time in comparison to DLS, making longer measurements necessary in order to get reliable results. By simple

tracking analysis, pPS produced such a high background scattering signal that the software was hardly able to extract real NP trajectories from the obtained videos. NTA possesses another option to refine the values of samples with high background noise: The use of fluorescent signals. By filtering the directly scattered light with a green filter, only red light signals are permitted to reach the camera. By using such a discriminatory filter, only NPs with certain excitation/emission spectra can be measured and the signal intensity is much lower, although the obtained trajectories are highly distinctive for the NPs. As it can be seen in Figure 3-4 (dotted line), the results of NPs after incubation with pPS are similar to the ones from DLS measurements, although NTA interprets the fast changes in the scattering as large amounts of smaller particles. By applying a fluorescence filter to the measurements, the signal pPS-only vesicles are entirely disregarded (solid line). A drawback of this method is, however, the need for fluorescent NPs.

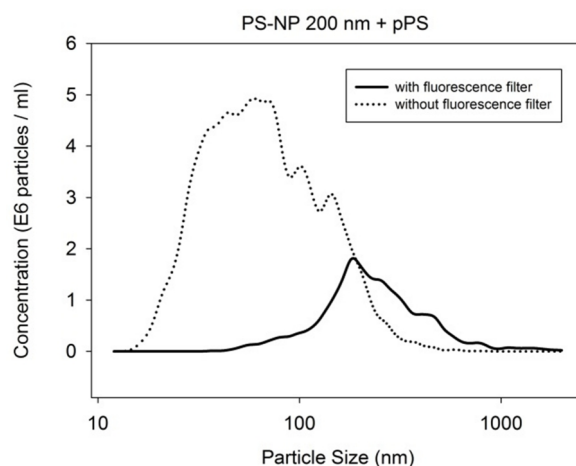


Figure 3-4: Influence of fluorescence filter on nanoparticle tracking analysis in presence of pPS. Without filter the structures of pPS result in a scattering signal that the software assumes to be small particles in high concentrations. By filtering the non-fluorescent signal out, a signal in the particle range becomes visible (20 μg PS-COOH 200 nm + 40 μg pPS incubated for 1 h at 37 $^{\circ}\text{C}$).

By incubating multi-fluorescent PS-COOH NPs in medium supplemented with different additives for 1 h at 37 $^{\circ}\text{C}$, it was possible to observe the particle movement *in situ* without being misled by the additional signals of the excess additives. The NP distributions are shown in Figure 3-5 (summary of the measured d_{max} values in Table 3-2). Several effects can be observed. As reported before by Monopoli *et al.* [79], FCS leads to a homogenous corona formation, with a slight increase in thickness with increasing FCS concentration. NPs after incubation with pPS show a main peak, slightly larger than the control and similar to the plasma corona formation; however, the distribution is broadened towards larger particles/agglomerates. Alveofact[®] in the same concentration as pPS leads to an apparent

agglomeration of the NPs, which is most surprisingly entirely indiscernible if FCS is simultaneously present in low concentrations.

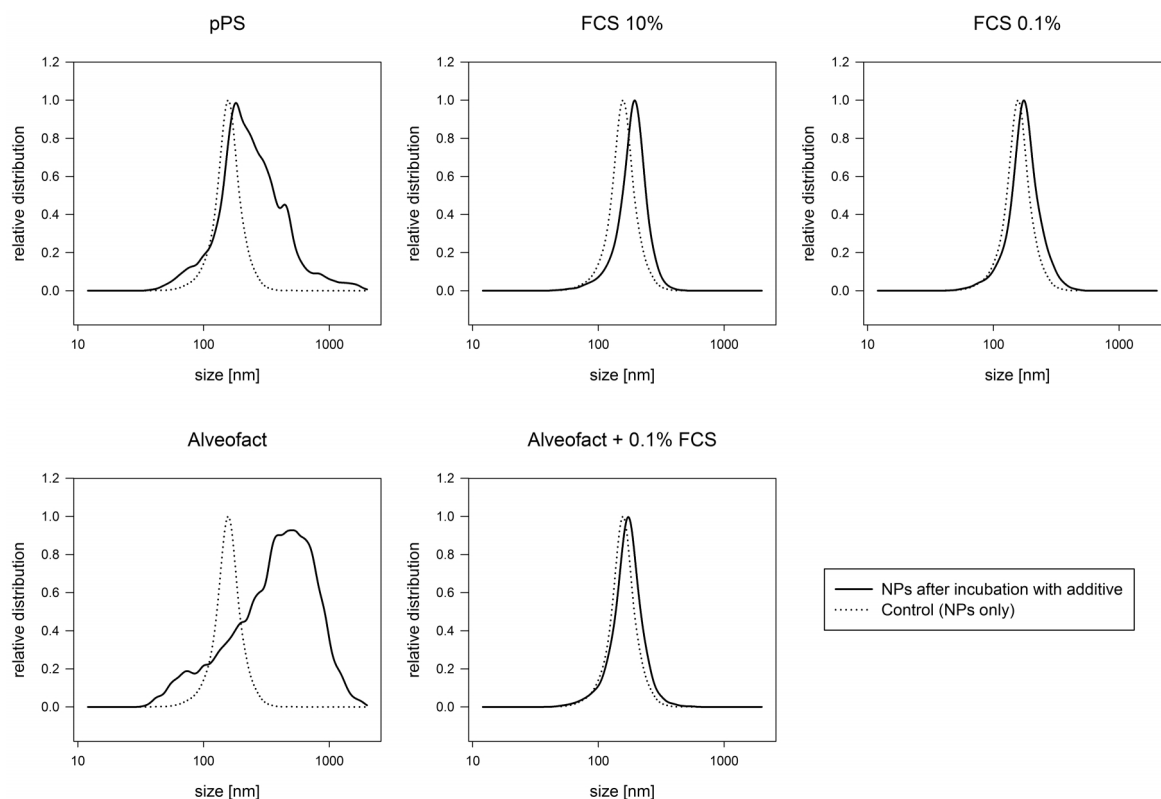


Figure 3-5: NTA measurements of 200 nm multifluorescent PS-COOH NPs with different incubation additives. In the presence of FCS at two different concentrations (10 and 0.1%) a homogenous corona forms, while pPS leads to a broadening towards larger particle sizes and Alveofact® to an apparent agglomeration of the NPs. In the presence of 0.1% FCS, NPs do not interact with Alveofact®.

From these observations it can be concluded that PS-COOH NPs definitely interact with the pPS, leading to corona formation. Apparently, the vesicles of the protein-depleted Alveofact® are either more rigid and impede the movement of the particles more, or they lead to a higher agglomeration of NPs than pPS. The main peak d_{\max} of NPs after incubation with pPS shows a shift of 22 nm in comparison to the control, resulting in an apparent thickness of the corona of 11 nm. Assuming a thickness of roughly 5 nm for a DPPC bilayer [142], it appears that the minimal corona around the NPs consists of more than one bilayer. For the fraction of particles appearing larger in the measurement however, it remains unclear from the measured trajectories if the NPs move more slowly due to agglomeration mediated by the pPS adsorption, or if they are entrapped within the membranous structure of pPS, slowing down their Brownian motion. For the same reasons, it cannot be judged if the addition of FCS to Alveofact® inhibits the membranous system or if the corona formation is disturbed and no agglomeration takes place. Several groups found an inhibition of PS functionality in terms of

surface activity [114], although this effect is dependent on the complexity of the preparation [143] and might be limited to the adsorption at the air-liquid interface [144].

Table 3-2: Average peak maxima of the measured PS-COOH NPs after incubation with different additives.

	mean d_{\max} [nm \pm SD]	apparent corona thickness [[d_{\max} - d_{\max} Control]/2]
Control	157 \pm 2	-
pPS	179 \pm 7	11
FCS 10%	194 \pm 2	19
Alveofact[®]	515 \pm 161	179
FCS 0.1%	175 \pm 2	9
Alveofact[®] + FCS 0.1%	173 \pm 3	8

3.4.3 Asymmetrical Flow Field Flow Fractionation

AF4 is a powerful tool to separate objects over a large size range of \sim 1 nm to 100 μ m, allowing separation of single proteins from large particle agglomerates. The separation principle is based on the fact that Brownian motion is more likely to move smaller particles into the faster zone of the laminar flow. This principle allows a separation and subsequent detection by particle size only. After testing different elution settings, buffers, and membranes it became clear that pPS, either due to the size of its vesicles/membranes or due to interactions with the semipermeable membrane, requires very long elution times and can only be washed completely out of the chamber with an aqueous ethanol solution. The crossflow needed to be minimal, as the surfactant produced otherwise a strong signal over the entire elution period as shown by Hupfeld *et al.* [145]. However, it was not possible to completely separate pPS from NPs, even though the main pPS peak appeared notably later; the tested NPs always eluted concurrently with pPS. As a representative example, a chromatogram displaying the elution of magPLGA-NPs, pPS, and magPLGA-NPs incubated in pPS is shown in Figure 3-6A. Although the NP peak was shifted to a longer elution time after incubation with pPS and the particles could be identified within the collected fraction (Figure 3-6B; inset shows identification of iron by energy-dispersive X-ray spectroscopy (EDX), it was not possible to obtain meaningful values for the size and mass of the detected peaks either by MALS or by DLS, presumably due to the high variability in online measurements of pPS size as observed before.

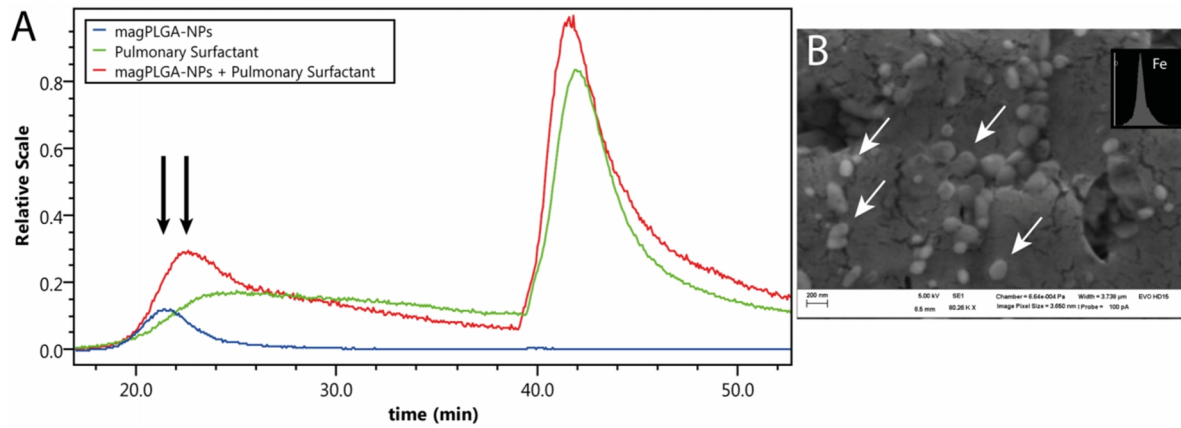


Figure 3-6: Surfactant-NPs interactions as observed by AF4. Chromatogram of magPLGA-NPs after incubation with PS shows peak shift to larger particles (A). NPs were found within the peak by SEM (B) and their presence proven by EDX (inset).

A4F is very well suited to separate different fractions of distinctive sizes; it is however limited to the separation by different particle sizes. The separation of NPs from proteins or other complex media such as soil or cell lysate has already been shown to be feasible by others [146, 147]. Lipid-rich samples, however, interact strongly with the AF4 membrane and, therefore, no conditions could be found at which pPS was separated from NPs. In the future, the technique might be used for this very application, provided that the online scattering detectors become more powerful and inert or modifiable membranes become available.

3.4.4 Differential Centrifugal Sedimentation

DCS is a type of analytical ultracentrifugation in the form of a spinning disk, in which particles are detected after a separation based on centrifugal velocity which, in turn, is based on a modified Stokes law (Equation 3-3):

$$\frac{D}{\eta} = \frac{R_f^2 - R_0^2}{\omega^2 t} \left(\frac{\rho_p - \rho_f}{\rho_p} \right) \quad (3-3)$$

Where D is the particle diameter, η is the viscosity of the fluid, R_f is the outer radius of the spinning disk, R_0 is the inner radius of the disk, ρ_p is the density of the particle, ρ_f is the density of the fluid, ω is the rotational velocity and t is the time the particles need to move from R_0 to R_f .

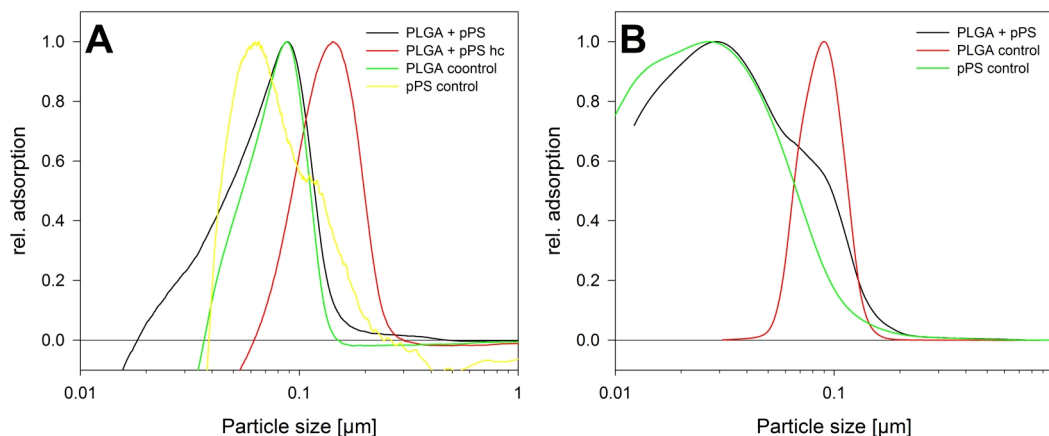


Figure 3-7: Analysis of magPLGA-NPs in the presence of pPS, by DCS. **A:** In a gradient of 12-24% sucrose the pPS peak overlaps with the magPLGA peak. No difference can be seen after incubation of both (PLGA + pPS). After magnetic separation and washing, the “hard corona” was analysed, but the washing procedure lead to agglomeration (PLGA + pPS hc). **B:** In a less dense gradient (2-8% sucrose) pPS elutes first; the detector signal increases however, making an analysis impossible.

The time needed to reach the detector at the outer part of the disk for a sample is therefore dependent on particle diameter and particle density, as distinguished from AF4, which discriminates only by size. By choosing different gradient densities, this method can be adopted for a variety of particles sizes and densities. pPS however not only forms vesicles over an wide size range, resulting in overlapping particle peaks, but also has a density equal to the density of polymers ($\sim 1.3\text{g}/\text{cm}^3$). Therefore, in order to achieve separation of NPs from surfactant, only magnetite-loaded NPs with a higher density were used in these experiments.

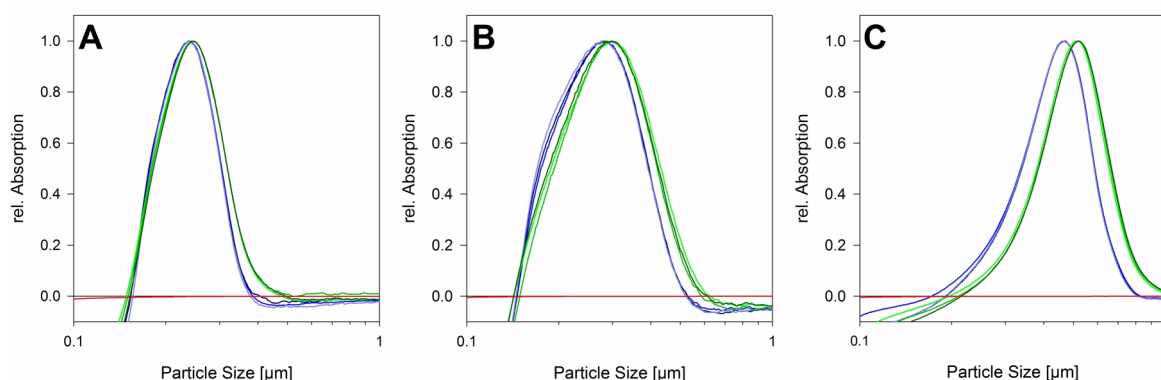


Figure 3-8: DCS measurements of different NPs in a 24-48% sucrose gradient. magPLGA- (A), Lipid- (B), and PEG-NPs (C) were either incubated in buffer (blue lines) or in buffer supplemented with pPS (green lines). Under these conditions no signal for pPS was detected (red line), only a size increase of NPs.

Using DCS for such purposes was initially described by the group of Dawson [79]. Their protocol with a gradient ranging from 12 to 24% sucrose, however, was optimized for measuring particles with an adherent protein corona after incubation in blood plasma, with and without removing the loosely bound soft corona. Reproducing this set-up for measuring the surfactant corona did not result in any meaningful outcome, as under these conditions peaks of NPs and pPS overlapped (see Figure 3-7A). Furthermore, the magnetic separation of NPs after incubation with pPS and repeated washing, which is supposed to result in removing the soft corona, has shown to cause an irreversible agglomeration of the particles, presumably due to the strong interaction forces of the hydrophobic PS coronas (compare plots *PLGA + pPS* and *PLGA + pPS bc* in Figure 3-7A). Decreasing the gradient density aiming at a fast sedimentation of the surfactant vesicles was also not successful (Figure 3-7B). Although density, size, and weight of PS vesicles change constantly, the vesicles eluted first but still overlapped with the particles peak and caused an intensified detector signal.

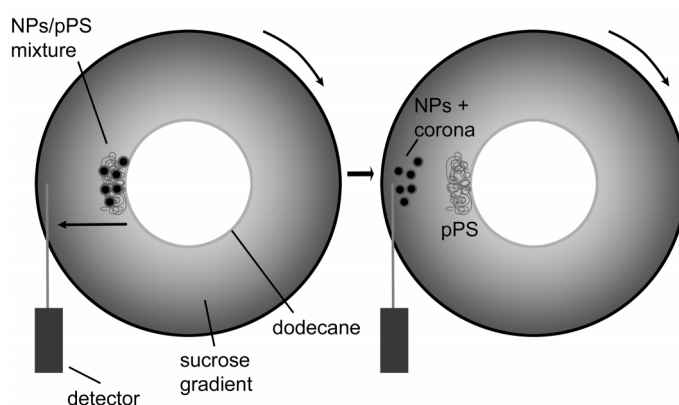


Figure 3-9: Mode of detection in differential centrifugal sedimentation. By using a sufficiently dense gradient material, only the relatively heavy magnetite-loaded NPs sediment, while the lighter pPS vesicles do not despite their size.

By increasing the concentration and therewith the density of the gradient to 24-48% sucrose, it was possible to entrap the pPS vesicles within the gradient (schematically shown in Figure 3-9). Subsequently, the background of pPS was practically non-existent and all peaks after injection of incubated samples are accounted for by NPs and the attached corona. Figure 3-8 shows DCS results of magPLGA- (A), Lipid- (B), and PEG-NPs (C) with and without corona. By comparing the peak shape and the overall shift of the NPs with corona, it is fair to say, that the NPs do not agglomerate in presence of pPS, but form a corona. Although interactions of magPLGA- and Lipid-NPs with pPS were expected, it is rather surprising, that hydrophilic PEG-NPs interact equally with surfactant, also resulting in a corona formation. More particles (Starch, Eudragit, Protein A-coated) were also tested with very similar results.

The apparent size increase of all tested NPs is shown in Figure 3-10. Interestingly, Starch-NPs showed agglomeration at room temperature, but not at 37 °C, resulting in a continual increase in size together with a large standard deviation. In contrast, the positively charged magEU-NPs agglomerated only if incubated at 37 °C in absence of pPS. Incubated at RT, their size did not increase, and in presence of surfactant they were also stable at 37 °C, showing minimal corona formation. So far no explanation could be found for this behavior, although positively charged NPs are known to readily agglomerate and interact with surfaces such as the used Eppendorf tubes.

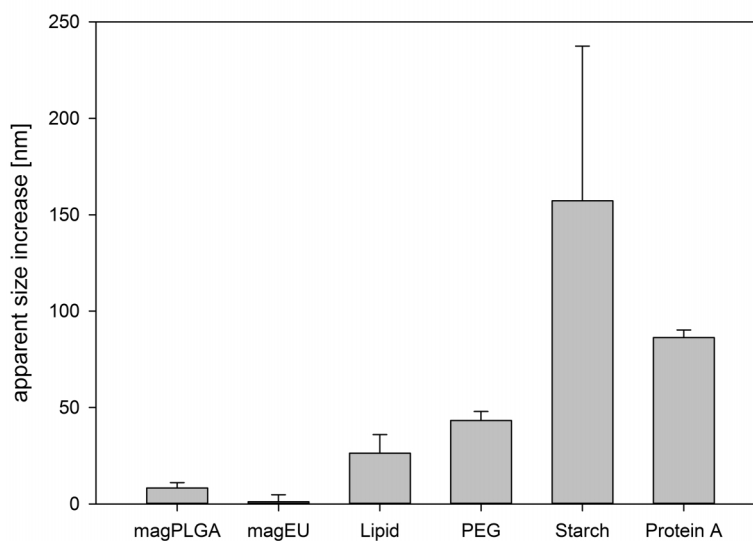


Figure 3-10: Apparent size increase in nm of different NPs after incubation with pPS.

The measured particle size increase is not the real thickness of the corona, as the software calculates the size based on a given density for the whole measured object, although the density of the particles differs from the corona. In order to apply the so-called core-shell model as proposed by Monopoli *et al.* [79], which approximates the real thickness of the additional layer on the surface of NPs by taking account of the different densities of core and shell, the density of the NPs needs to be precisely known. The densities of the used nanomaterials were calculated in accordance with Equation 3-3, assuming a monodisperse size. Unfortunately, the magnetite-loading of NPs is never homogenous; therefore, the particle density varies among the particles, making it impossible so far to calculate a real coating thickness based on the core-shell model. The shown measurements can therefore only be regarded as qualitative results. They certainly prove the presence of a pPS corona on all tested NPs, however to be able to make a statement about the real thickness of the corona, the procedure still needs to be adjusted.

3.5 Summary and Conclusion

Overall it can undoubtedly be said that accessing the NP corona in PS is more challenging than probing the plasma corona. Comparable to looking at an integral membrane protein, which can hardly be isolated in its natural form without the lipids of the membrane surrounding it, NPs with an adherent PS coating are as hard to separate from their surroundings without disturbing the actual direct interaction with the membranes of pPS. Although this *in vitro* approach is always artificial, the more one tries to separate the particles, the more artificial the results become. Nevertheless, as the above described experiments have shown, NPs need to be separated from the surfactant vesicles before measurement, either by optical methods such as filtering for only fluorescent NPs, as is feasible with NTA, or by physical separation before detection as in the AF4. Most of these methods require special particle characteristics, such fluorescence or high density and are therefore not applicable to pharmaceutical preparations or fine dust. No matter what method is applied, however, all effects of the pPS and the forming corona on the colloidal behavior of NPs cannot be visualized with a single method. DLS for instance did not allow for drawing any conclusions about the colloidal state of NPs, since it is too easily disturbed by the pPS vesicles. AF4 could be a useful tool in the future, although the current state of the art with respect to the set-up and membrane properties cannot separate NPS from pPS. A shift in NPs size and therewith a proof of corona formation was nevertheless observed. AF4 has a great potential as a standard analytical tool for measuring the colloidal state of nanomaterials in biological fluids, and after complete separation the sample collection would allow for further analysis of the attached biomolecules. NTA proved to be able to track NP trajectories while ignoring the background of PS. The obtained results need to be carefully interpreted however: Brownian motion of NPs is, of course, dependent on the size of the particles and will therefore decrease with an adherent PS corona. PS, however, is a self-organizing interconnected membranous system. NPs that are once coated by the hydrophobic PS, will strongly interact with the membranes and cannot move freely anymore, making them appear large in experiments which measure size by particle motion.

Hence a next question evolves that is rather difficult to answer: Can the PS corona be divided into a hard and soft corona? If ones aims to separate hard-corona complexes from supernatants by centrifugation in presence of pPS, the NPs cannot be fully resuspended and show much larger particle sizes in DLS, NTA, and DCS. Thus, the corona can only be measured “*in situ*”, without prior separation from non-binding PS. Although the NTA

measurements showed no monodisperse corona formation, as it was observed for the plasma protein corona, even at high concentrations of plasma proteins, they did not agglomerate entirely in the presence of pPS, but remained rather stable in size. One could interpret that this apparent size of the NPs is rather the size of the pPS vesicles they are connected to. Once an NP has adsorbed lipids onto its surface, it becomes part of the vesicular structure of pPS and its movement. Therefore its measured size *in situ* appears to be as large as the vesicle itself. Transferring the soft/hard corona approach to the deep lung, it would be rational to say that regardless of what is considered as hard corona, due to the interconnection, the soft corona consists basically of all the other membranes of the PS. By using DCS, it was possible to show that NPs can be separated and detected with adherent pPS. It remains to be clarified, however, if the detected size increase is the hard corona, or if the degree of separation is strictly depending on centrifugal forces or shear forces. Although the extent varied, DCS data proved an interaction of all NPs with pPS, regardless of their surface properties. Especially the highly hydrophilic PEG-NPs were expected to behave more reluctantly. The biochemical composition of the bound molecules will be addressed in the following chapter.

4. THE MOLECULAR COMPOSITION OF THE PULMONARY SURFACTANT CORONA

4.1 Introduction

The biomolecule corona of NPs in plasma is one of the most intensively studied areas in bio-nano sciences. It has been extensively shown that the adherent proteins on the surface of NPs influence their fate within the body in terms of clearance [84], cell uptake or association [72, 74], cytotoxicity [85], colloidal stability [73], and drug release [86]. With advancing analytical methods, the protein corona in plasma has been researched in detail and a standard corona screening for fabricated NPs is starting to emerge [148]. Accessing the NP corona in PS is however more challenging, and has been disregarded for quite some time. PS possesses unique physical properties, as already discussed in Chapter 1.2, and these make the analysis of the corona challenging. Not only must one look into the adsorbed proteins on the surface of the NPs (as in the case of the plasma corona), but the lipids must also be regarded as interacting molecules which alter the surface appearance of the NPs and need therefore to be analyzed. The temperature influence on the structural behavior of PS illustrates that the incubation of NPs with PS for analytical purposes must take place at physiological temperature, at which dynamic and inhomogeneous liposome-like PS vesicles are present. By providing for formation of these structures, utilization of such a temperature would most accurately mimic the *in vivo* interaction of PS with NPs. At lower temperatures – at which plasma protein adsorption experiments are commonly performed – the NPs will only interact with the accessible biomolecules in the comparably more fluid PS regions, while not coming in contact with molecules entrapped in the rigid PL membranes that are present below the phase transition temperature. Additionally and most importantly the PS with its membranous structure acts unlike a solution of proteins. The lipid layers present within PS connect the NPs, or in other words, the NPs are trapped inside the PS membranes. Therefore, one of the major challenges is to separate the NPs, following their contact with a full PS model and the formation of a bound corona, from non-binding supernatant, to allow for the detection of the actually bound “hard corona”-biomolecules. But, as already discussed in Chapter 3, a differentiation into a hard and a soft corona might not be feasible due to this very reason, which may even be a deliberate defense mechanism of the respiratory tract: the assimilation of NP properties by the adsorption of proteins and lipids.

Only little effort has been invested in the examination of this particular nano-bio interface. The difficulty in gaining access to PS has brought most researchers interested in this topic to use artificial PS preparations which are intended for clinical use and are therefore protein-depleted. These fluids, which include preparations such as Curosurf®, are not capable of

accurately forming an NP corona. Studies focusing on the physical interactions of a clinical surfactant with NPs are also questionable, given the high evidence for the existence of strong lipid-protein interactions [27, 41, 149, 150], as well as the fact, shown by Beck-Broichsitter *et al.*, that the PS response to NPs varies with PS preparation complexity [110]. Our group was able to show that the surfactant proteins SP-A and SP-D show varying affinity to different NPs, and that the effect of this binding on cell uptake *in vitro* was further modified in the presence of lipids [101], proving that only a crude PS preparation will interact in a physiologically relevant manner. Kapralov *et al.* [151] took a first step towards determining the complete PS corona after *in vivo* administration of single walled carbon nanotubes (SWCNT) to mice, showing that lipids and proteins are found on the nanomaterials after lavage; from the opposite perspective, the lipidomic profile of the lung was altered by SWCNT [152].

Having selected an adequate whole PS preparation, we decided to evaluate the different methods to access the NP corona in PS, using pPS as a model, and to deploy a complete analysis thereof, *i.e.* the component lipids and proteins. These results are urgently needed to understand how NPs interact with the PS membranes in the deep lung, and whether it will be possible to modify NPs for targeted delivery. By applying label-free shotgun proteomics, which has been successfully used to analyze the NP protein corona [76, 81] and is also employable in the presence of high amounts of lipids [153], and a lipidomic approach by HPLC-MS, the corona was determined by state-of-the-art techniques. In order to be able to use different separation methods and to see maximal variation in NP-PS interactions, we chose a set of magnetite-loaded NPs with varying surface chemistry: hydrophobic phosphatidylcholine-coated Lipid-NPs, and hydrophilic NPs coated with PEG 5000. Hu *et al.* [154] predicted by *ab initio* calculations *in silico* that particle hydrophobicity will dictate the interaction with a DPPC/POPG/SP-C/SP-B layer, resulting in a more superficial localization in the lipid layer for a hydrophilic NP in comparison to a lipophilic one which was incorporated into the lipid layer. Furthermore, we investigated magnetite-loaded NPs synthesized from PLGA, as a pharmaceutical excipient that was approved by the FDA for human use and therefore could be used as vesicle for future nanopharmaceuticals intended for respiratory application.

4.2 Reagents and Methods

4.2.1 Reagents

Buffer reagents and solvents were purchased from Sigma Aldrich (Munich, Germany), while FCS was purchased from Lonza (Basel, Switzerland). PS was isolated as described in Chapter 2, and Alveofact® was kindly provided by Lyomark Pharma GmbH. All samples were always diluted in TBS.

4.2.2 Nanoparticles

The magnetic PEG-NPs (nanomag®-D PEG 5000) were manufactured to specification by Micromod (Rostock, Germany), the magnetic Lipid-NPs (fluidMAG-Lipid) used in this study were purchased from Chemicell GmbH (Berlin, Germany); both were used as received. Magnetic PLGA-NPs were prepared as described in section 3.3. The characterization of the used NPs, performed by the same methods as described in Chapter 3, is shown in Table 4-1 and Figure 4-1.

Table 4-1: Characterization of the used NPs.

	PLGA-NPs	PEG-NPs	Lipid-NPs
Surface properties	Carboxylic acid	PEG5000	Phosphatidylcholine
Core	Magnetite/PLGA 50:50	Magnetite/Dextran	Magnetite/GPChol
Source	Emulsification-evaporation	Micromod nanomag®-D PEG5000	Chemicell fluidMAG®-Lipid
Size nominal [d.nm]	n.a.	250	200
Z-average (DLS) [d.nm]	217.3 ±3.4	380.0 ±2.1	245.2 ±2.3
PDI (DLS)	<0.1	<0.15	<0.3
Size (NTA) [d.nm]	177 (±47)	160 (±54)	169 (±64)
Zeta potential (DLS) [mV]	-25.1 ±0.3	-13.8 ±0.9	-32.4 ±1.1
Number conc. (NTA) [# /mg]	8.54*10 ¹¹ (±1.77*10 ¹¹)	7.49*10 ¹¹ (±1.97*10 ¹¹)	4.34*10 ¹¹ (±1.38*10 ¹¹)
Calc. surface area [m²/g]	127	184	82

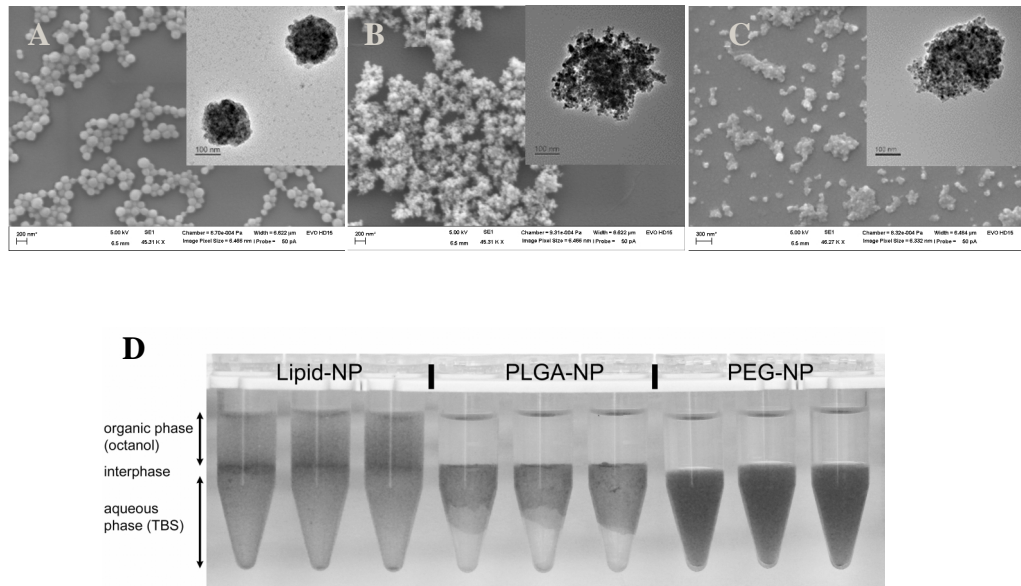


Figure 4-1: Characterization of NPs used in Chapter 4 by means of electron microscopy (A-C) and octanol-water distribution (D). Reproduced from [115].

4.2.3 Adsorption Experiments

The incubation of NPs with pPS was performed as described in Chapter 3.2.6.

4.2.4 Separation of NPs from Pulmonary Surfactant

For the proteomic and lipidomic analysis, NPs with the adherent corona were separated as follows: Immediately after incubation, the samples in 1.5 ml Eppendorf tubes were inserted in a magnetic Separator with a sideward magnet (PureProteome™ Magnetic Stand, Merck Millipore, Germany) which was kept at 37 °C in an incubator. After 15 min, the supernatant was carefully removed - without disturbing the pellet – and discarded. Fresh buffer warmed to 37 °C was added to a volume of 1.4 ml and the samples were subsequently vortexed briefly. This procedure was repeated three times, with the last step being performed without addition of buffer. The remaining pellet was spun down at 10000 rpm in a tabletop centrifuge for 5 min and the remaining supernatant was again discarded. The pellets were frozen at -80 °C until further processing. All experiments were performed in triplicates.

Additional methods, used to access the plasma protein corona, were adapted from methods described in the literature. Simple centrifugation was carried out according to a protocol of Monopoli *et al* [137]. This method was equivalent to the magnetic separation described above,

however in this case the process of magnetic separation was substituted with a centrifugation step for 10000 rpm at 37 °C for 10 min. Gradient centrifugation was performed equally for all three buffers (see below) similar to the method established by Docter *et al.* [117]. Briefly, the incubated samples were pipetted carefully onto a 0.5 ml cushion of the respective buffer. Density gradient centrifugation was performed at 20000 rpm for 30 min at 4 °C and the supernatant discarded. Samples were washed with TBS without disturbing the pellets and frozen until use. Three different buffers based on TBS were used, all of them at a concentration that resulted in a density of 1.1 g/cm³ to prevent a pelleting of the pPS: 26% sucrose (adopted from Docter *et al.*), 13% sodium bromide (adopted from the initial pPS preparation procedure), and TBS in which water was replaced by deuterium oxide (adopted from [155]).

4.2.5 SDS-PAGE

Gel electrophoresis of the proteins adsorbed to the NPs was performed as described in Chapter 2.2.10.

4.2.6 Thin Layer Chromatography

TLC was performed as described previously in Chapter 2.2.9. If not stated otherwise, 10 µl of the NPs-PS complexes were applied as received after adsorption experiments.

4.2.7 Label-free Shotgun Proteomics

Corona proteins were determined as described in Chapter 2.2.11. The filter aided sample preparation allowed a direct trypsinization of the proteins without desorption from the NPs.

4.2.8 Lipid Determination

PLs and cholesterol were quantified as described in Chapter 2.3 and 2.2.8 respectively.

4.2.9 Statistical Analysis

Statistical tests were performed with the help of Alexander Rurainski and Dominik Selzer (Scientific Consilience GmbH, Saarbruecken). Significantly different data was detected by applying a moderated *t*-test known as limma [156], which was initially developed to find significant differences among microarrays (“linear models for microarray and RNA-seq data”) but has been shown to be valid for protein data as well [157]. As an implementation for the R computing environment [158] a limma package [159] from the Bioconductor software project

[160] was used. While the standard Student's *t*-test calculates the variance of a protein in a data set only based on the protein's data, the moderated *t*-test fits a linear model to a complete data set and employs the empirical Bayes approach. As a result, a modified *p*-value for each comparison was obtained according to the Benjamini-Hochberg procedure [161], which was regarded as significant if $p < 0.05$. Statistical difference between the absolute amounts of adsorbed lipids was tested by one-way ANOVA (SigmaPlot Version 12.5).

4.3 Results and Discussion

4.3.1 Analyzing the Surfactant Corona

In order to access the effectively bound corona, we compared different separation techniques. Since a concentrated pPS preparation already shows sedimentation without centrifugal forces due to the size of the membranous vesicles, a separation by centrifugation as was proposed by Monopoli *et al.* [137] for the analysis of the plasma protein corona led to a complete sedimentation of NPs and pPS, in accordance with expectations (Figure 4-2B). To circumvent the sedimentation of pPS we deployed density centrifugation to spin down only the NPs. To achieve rapid partitioning, Tenzer *et al.* [117] developed a simple method to separate NPs from plasma proteins by centrifuging samples through a cushion of 22% sucrose solution. This method was adopted to meet a density (26% sucrose = 1.1 g/cm³) which is used in pPS purification and was only applicable in this study due to the high density of magnetite-loaded NPs. Unfortunately, the density of pPS vesicles is in the same range as most polymeric NPs, making basically all separation techniques using centrifugation impractical. Although it was expected that a clear segregation of pPS and NPs was possible under these circumstances, density centrifugation still however produced a pellet in the blank control without the NPs (Figure 4-2D). Furthermore, adsorption to all three NPs appeared very similar. We assumed an influence of the high sucrose concentration on the structural dynamics of the pPS, and exchanged sucrose against a sodium bromide buffer (which is used in PS purification), as well as a deuterium oxide buffer. Nevertheless, both attempts resulted in a visible pellet in the blank, possibly a result of the permanent structural change of the pPS and therewith the density of the vesicles. The comparison of PEG- and Lipid-NPs showed differences in the total adsorbed protein, which were albeit minimal and not as distinct as expected. Magnetic separation, which allows a lateral attraction of the particles even in the presence of sedimenting pPS, was the only employed method which showed a negligible pellet in the blank control (Figure 4-2C). Moreover, only this procedure resulted in a clear distinction of the total adsorbed proteins in the order PEG-<PLGA-<Lipid-NPs as assumed from NP hydrophobicity. These results are in contrast to the study performed for the plasma corona by Monopoli *et al.*, in which different separation methods resulted in equal adsorption profiles [75]. SDS-PAGE and densitometric evaluation was sufficient to compare the overall adsorption, though as visible in the representative gel shown in Figure 4-2A, due to the high amounts of lipids which were depletable, further information cannot be gained from this basic analysis.

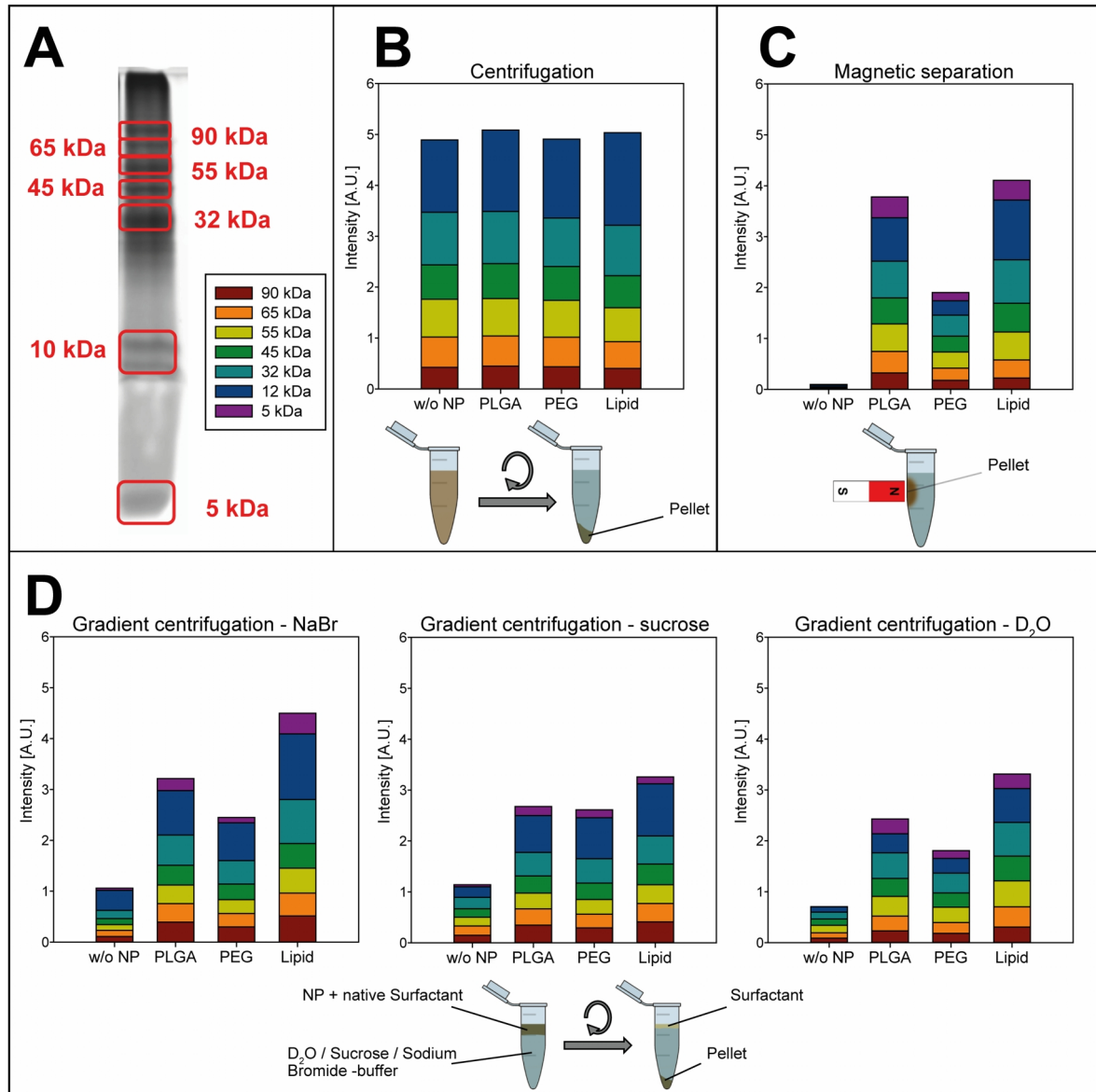


Figure 4-2: Comparison of separation methods to access the PS corona. Adsorption was determined after SDS-PAGE and subsequent coomassie staining by densitometric analysis of the spots as shown in A. While common centrifugation spins down pPS in all samples (B), gradient centrifugation (D) with different buffer compositions shows a separation but fails to produce blank values. Magnetic separation achieves a successful cleaning of the NP-pPS complexes (C). NaBr = sodium bromide, D₂O = deuterium oxide. Reproduced from [115].

4.3.2 Lipid Corona

The overall amount of lipids that adsorbed to NPs under the chosen conditions was determined by HPLC-MS/enzymatic assay. Surprisingly, no significantly different amounts of lipids on the Lipid- (87.1 ng lipids/ μg NPs) and PLGA-NPs (86.4 ng lipids/ μg NPs) were shown when related to the particle concentration (Figure 4-3A), although such NPs possess diverging surface hydrophobicity. Even more strangely, the PEG-NPs showed about half as much lipid adsorption (37.1 ng lipids/ μg NPs). As the particle corona is surface related, it is rather meaningful to compare the absolute values to the particle surface. The actual surface of the NPs was unfortunately not accessible for the chosen particles, because the typically used BET (Brunauer–Emmett–Teller) analysis by gas adsorption requires NPs which are at least somehow dispersible in gases, which the three used NP types are not. With their most extreme surface hydrophobicity/hydrophilicity they will unavoidably agglomerate if dried, and as such BET analysis will not produce realistic values. Therefore, the NP surface area was estimated based on the absolute number concentration (as determined by NTA) and the measured diameter of the particle (measured by DLS), assuming a spherical shape. These derived data can be found in Table 4-1 (section 4.2.2). Based on this surface area corrected data, the adsorbed amounts of lipids per m^2 surface area of all three particles are significantly different (Figure 4-3B), in the increasing order of PEG- (0.12 mg/m^2), PLGA- (0.38 mg/m^2), and Lipid-NPs (0.61 mg/m^2). These results for the binding affinity mirror the hydrophobicity of the particles, and confirm the expected lack of attraction of lipids by the hydrophilic NPs (as predicted by molecular dynamics simulations from Hu *et al.* [154]).

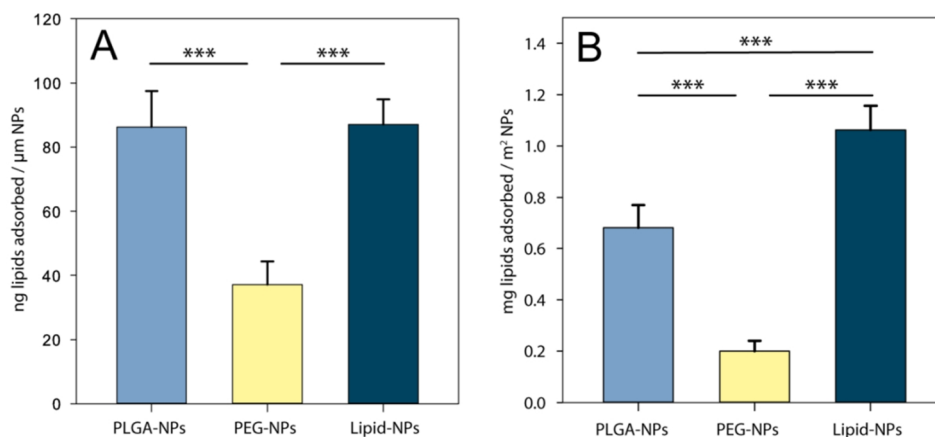


Figure 4-3: Absolute amounts of lipids determined in the corona of PLGA-, PEG-, and Lipid-NPs as determined by HPLC-MS related to particle mass concentration (A) and to particle surface area (B). Reproduced with permission from [115].

The relative lipid composition in the corona of all particles was divergent from the one in crude pPS (see Figure 4-4). Disregarding lipid classes, there were significant differences in the concentration of GPChol, which on average increased in the corona by 11.2% for saturated and 9.6% for unsaturated lipids (Figure 4-4A). The relative concentrations of the other classes were decreased. As described in Chapter 1, the carbon chain length of the lipids is a measure of lipid flexibility and affects (together with the number of double bonds) the phase transition temperature. By comparing the overall chain length of the lipids in the corona with the employed pPS (Figure 4-4B), it is obvious that PL with a total chain length (= number of carbons in both acyl chains) of 32 and 30 carbons, less than the average chain length, preferably adsorb to the NPs. Since these binding effects occurred on all NPs regardless of their surface properties, one could speculate that NPs mostly interact with the most dynamic regions within the PS structure where short-chained PLs with higher fluidity predominate.

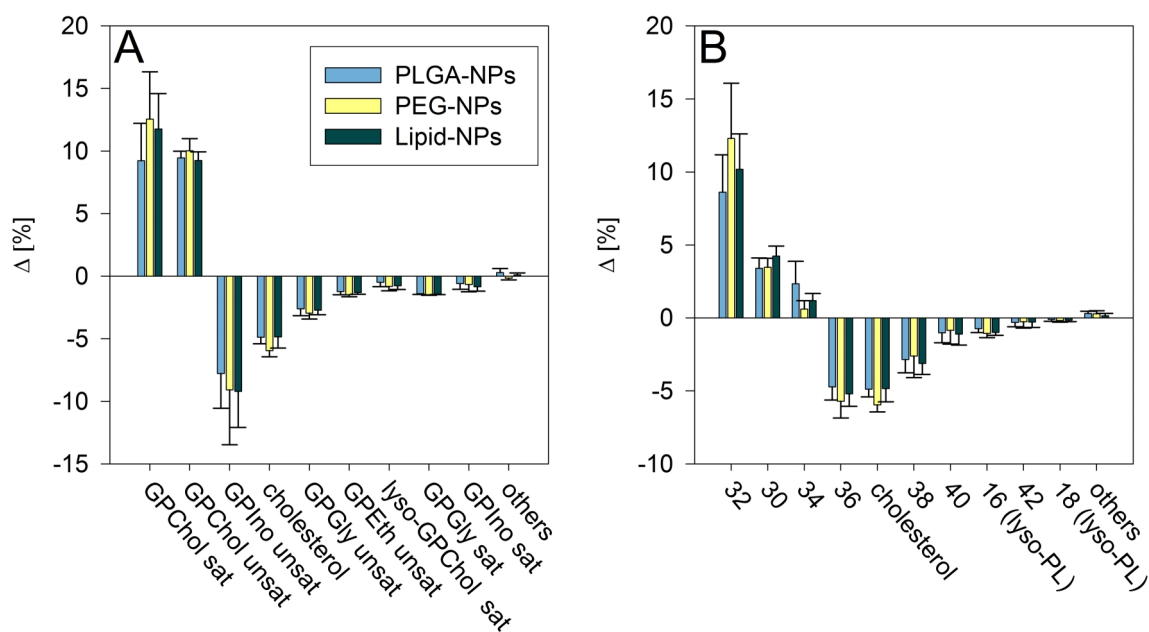


Figure 4-4: Relative comparison of the lipids found in the corona of PLGA-, PEG-, and Lipid-NPs in comparison to crude pPS, by lipid class (A) and overall chain length (B). Reproduced with permission from [115].

Among the NPs, almost no variation was observed, as there were no significant changes either within classes or chain lengths between PLGA- and Lipid-NPs, meaning that their lipid corona has to be regarded as equal. With respect to the comparison of the relative composition of the PEG-NPs corona with that of PLGA- and Lipid-NPs, the amount of cholesterol present was slightly lower on PEG-NPs by 1.1% (see Table 4-2), while

GPIno(34:1) was reduced in comparison to PLGA-NPs (1.3%). All other differences were only minor (< 0.1%) and were therefore not regarded as relevant.

From this data it was concluded that the hydrophobicity of NPs does not relate to an adsorption of different lipid species, but only to different amounts of corona lipids. As it can be assumed that the same forces were applied to all NPs during the separation and washing of the complexes, and therefore a once lipid-covered NP could arbitrarily attract additional lipid layers, it is hardly conceivable that the different lipid amounts on NPs, and the binding to PEG-NPs in particular, can be explained without a mediating effect of PS proteins.

Table 4-2: Top 10 most abundant lipid species found in crude pPS and in the corona of PLGA-, PEG-, and Lipid-NPs.

pPS		PLGA-NPs		PEG-NPs		Lipid-NPs	
Lipid species	Abundance [%]						
GPChol(32:0)	36.8 ±4.9	GPChol(32:0)	42.5 ±2.4	GPChol(32:0)	45.8 ±3.1	GPChol(32:0)	44.2 ±2.2
GPChol(30:0)	9.0 ±2.1	GPChol(30:0)	12.4 ±0.8	GPChol(30:0)	12.6 ±0.8	GPChol(30:0)	13.3 ±0.8
GPChol(34:1)	8.9 ±1.2	GPChol(32:1)	11.3 ±0.5	GPChol(32:1)	12.0 ±1.0	GPChol(34:1)	11.6 ±0.6
Cholesterol	7.9 ±1.1	GPChol(34:1)	11.1 ±0.7	GPChol(34:1)	11.2 ±1.0	GPChol(32:1)	11.5 ±0.6
GPChol(32:1)	7.0 ±0.8	Cholesterol	3.0 ±0.5	Cholesterol	1.9 ±0.5	Cholesterol	3.1 ±0.9
GPIno(34:1)	2.4 ±0.3	GPIno(34:1)	2.8 ±0.9	GPChol(34:2)	1.6 ±0.4	GPIno(34:1)	2.1 ±0.5
GPGLyc(34:1)	2.1 ±0.4	GPChol(34:2)	1.4 ±0.3	GPIno(34:1)	1.5 ±0.4	GPChol(34:2)	1.2 ±0.2
LGPCHol(16:0)	1.6 ±0.1	GPChol(34:9)	1.2 ±0.3	GPChol(34:9)	1.3 ±0.3	GPChol(34:9)	1.0 ±0.1
GPGLyc(32:0)	1.1 ±0.3	LGPCHol(16:0)	1.0 ±0.3	GPGLyc(34:1)	0.8 ±0.3	GPGLyc(34:1)	0.9 ±0.2
GPIno(36:2)	1.0 ±0.1	GPGLyc(34:1)	1.0 ±0.3	LGPCHol(16:0)	0.7 ±0.3	LGPCHol(16:0)	0.8 ±0.2
Top10 Total	77.7	Top10 Total	87.8	Top10 Total	89.4	Top10 Total	89.6

4.3.3 Lipid Corona Formation of an Artificial Surfactant Preparation and the Influence of Plasma Proteins

In order to test this hypothesis, adsorption experiments were performed with an organic PS extract, the clinical surfactant Alveofact®, which contains only the lipid fraction and additionally SP-B and SP-C. The same concentration of PLs relative to NPs (~20 µg PLs/µg NPs) was used and incubation took place under the same conditions as the preceding experiments with pPS. TLC analysis revealed that the organic extract only interacted with Lipid-NPs; there was no adsorption to either PEG- or to PLGA-NPs (Figure 4-5A, only GPChol as most prominent band shown). Indeed, the addition of serum proteins in a similar amount as present in complete pPS, in the form of FCS, did not change the outcome (Figure 4-5B), while pPS showed again adsorption to all NPs. Assuming that the protein-depleted

organic extract possesses an identical phase behavior, the binding to both PEG- and PLGA-NPs requires the presence of surfactant-specific proteins, capable of binding surfaces on the one hand and lipids on the other.

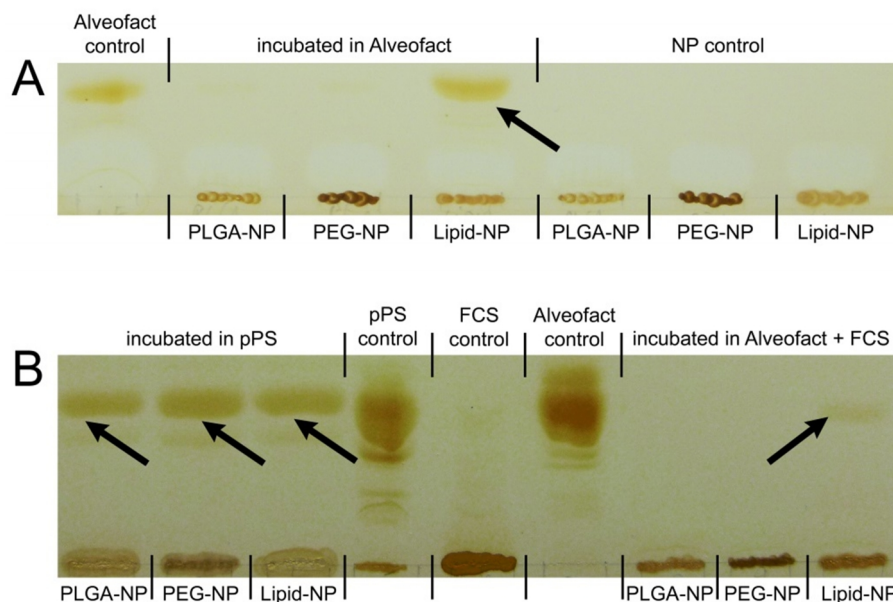


Figure 4-5: Incubation of PLGA-, PEG-, and Lipid-NPs with Alveofact® (A) shows no adsorption of lipids on PEG-, and PLGA-NPs. The addition of FCS to Alveofact® does not improve lipid binding (B). Adsorption of native pulmonary surfactant shown in comparison. Reproduced from [115].

4.3.4 The Protein Corona

The extremely high lipid content in PS interferes with most techniques aiming at the determination of proteins, and allows for only an approximation of protein amounts. By using the BCA assay and a calculation based on the proteomic approach, it was estimated that the ratio of lipid to protein was 10:1 in the corona of all particles and was therefore similar to the ratio in crude pPS. These results are in agreement with the ratio reported by Kapralov *et al.* [151]. Label-free shotgun analysis, however, provides relative data of protein abundance which allows for comparison of the protein coronas, and is highly sensitive: 414 proteins were detected in the corona of PLGA-NPs, 376 in the corona of PEG-NPs and 417 proteins on Lipid-NPs (the complete list of determined proteins was published in [115]).

The protein corona composition in relation to the makeup of crude pPS shows a similar behavior as the lipid corona: Proteins which are most abundant in native pPS (Table 2-4) are not necessarily the major proteins found in NP coronas (Table 4-3). While SP-A is dominant

in crude pPS, the proteins with the highest concentration on NPs are tubulin alpha-4A chain, actin cytoplasmic 1, hemoglobin subunit beta, and L-xylulose reductase, all of which do not appear to be closely connected with PS. Nevertheless, it was recently found, that hemoglobin is synthesized and secreted by AT-2 cells, jointly with the lamellar bodies of PS [126, 162], and altered variants of the hemoglobin beta chain are strongly associated with the PS membranes [127]. Actin, myosin, and tubulin, which are ubiquitous in microtubules, take part in the secretion of PS [30], and tubulin especially was found to be closely associated with GPChol vesicles [163]. Furthermore, it is presumed that L-xylulose reductase is a membranous protein which might interact with GPI_{no}.

The analysis of molecular weight, isoelectric point and overall hydrophobicity (depicted as GRAVY Score) distribution on all particles show no significant correlations of these attributes to certain NP surfaces (Figure 4-6). It appears that physico-chemical properties are not the driving force for protein adsorption, although it is unclear how much of the determined proteins actually bind to the NP surface itself, and how much is actually incorporated in additional lipid layers.

Table 4-3: Top 30 most abundant proteins in the corona of PLGA-, PEG-, and Lipid-NPs.

PLGA-NPs		PEG-NPs		Lipid-NPs	
No.	Protein name	No.	Protein name	No.	Protein name
1	Tubulin alpha-4A chain	1	Tubulin alpha-4A chain	1	Tubulin alpha-4A chain
2	Actin, cytoplasmic 1	2	Actin, cytoplasmic 1	2	Actin, cytoplasmic 1
3	Hemoglobin subunit beta	3	Hemoglobin subunit beta	3	Hemoglobin subunit beta
4	L-xylulose reductase	4	L-xylulose reductase	4	L-xylulose reductase
5	Tubulin beta-4B chain	5	Tubulin beta-4B chain	5	Myosin-9
6	Tubulin alpha-1A chain	6	Tubulin alpha-1A chain	6	Tubulin beta-4B chain
7	Deleted in malignant brain tumors 1 protein	7	Tubulin beta chain	7	Pulmonary surfactant-associated protein A1
8	Tubulin beta 5 chain	8	Myosin-9	8	Deleted in malignant brain tumors 1 protein
9	Pulmonary surfactant-associated protein A1	9	Fibronectin	9	Tubulin alpha-1A chain
10	Myosin-9	10	Glyceraldehyde-3-phosphate dehydrogenase	10	Tubulin beta chain
11	BPI fold-containing family B member 1	11	Deleted in malignant brain tumors 1 protein	11	Fibronectin
12	Fibronectin	12	Elongation factor 1-alpha 1	12	BPI fold-containing family B member 1
13	Serum albumin	13	BPI fold-containing family B member 1	13	Serum albumin
14	Glyceraldehyde-3-phosphate dehydrogenase	14	Serum albumin	14	Glyceraldehyde-3-phosphate dehydrogenase
15	Elongation factor 1-alpha 1	15	Pulmonary surfactant-associated protein D	15	Elongation factor 1-alpha 1
16	ADP-ribosylation factor 1	16	Pulmonary surfactant-associated protein A1	16	Calcium-activated chloride channel regulator 1
17	Tubulin beta-2B chain	17	ADP-ribosylation factor 1	17	ADP-ribosylation factor 1
18	Retinal dehydrogenase 1	18	EH domain-containing protein 2	18	Fatty acid synthase
19	Complement C5	19	Calcium-activated chloride channel regulator 1	19	Tubulin beta-2B chain
20	Calcium-activated chloride channel regulator 1	20	T-complex protein 1 subunit beta	20	EH domain-containing protein 2
21	EH domain-containing protein 2	21	Pyruvate kinase PKM	21	Complement C5
22	Fatty acid synthase	22	Retinal dehydrogenase 1	22	Retinal dehydrogenase 1
23	Protein-glutamine gamma-glutamyltransferase	23	Fatty acid synthase	23	Myosin-14
24	Complement C3	24	Complement C3	24	Protein-glutamine gamma-glutamyltransferase 2
25	Pyruvate kinase PKM	25	Protein-glutamine gamma-glutamyltransferase 2	25	Myosin-7B
26	Myosin-7B	26	Tubulin beta-2B chain	26	Complement C3
27	Myosin-3	27	Myosin-14	27	Pyruvate kinase PKM
28	Ig alpha-1 chain C region	28	Aldehyde dehydrogenase, mitochondrial	28	Sodium-dependent phosphate transport protein 2B
29	Cathelicidin antimicrobial peptide	29	Calpain-1 catalytic subunit	29	Calpain-2 catalytic subunit
30	Calpain-1 catalytic subunit	30	Complement C5	30	Cathelicidin antimicrobial peptide

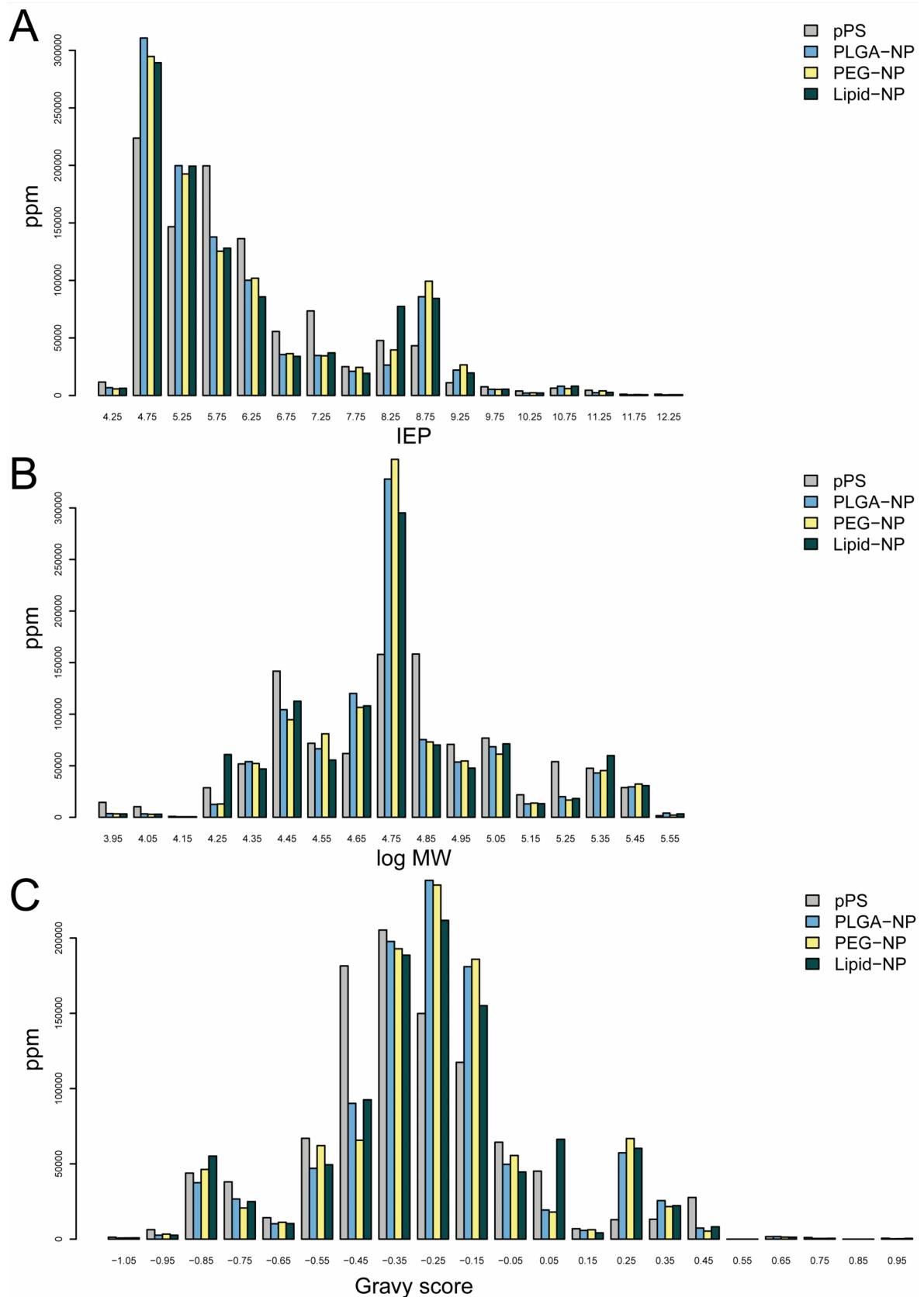


Figure 4-6: Relative distribution of the proteins found in the corona of PLGA-, PEG-, and Lipid-NPs by means of their isoelectric point (A), molecular weight (B), and hydrophobicity (Gravy score - C). Reproduced from [115].

Looking at individual proteins, there was however variation among the NPs. To find the significantly different proteins with respect to the various NPs, we deployed a pairwise comparison (limma) of all proteins identified in the NP coronas. In Figure 4-7, proteins with significant change are plotted in terms of fold change as a parameter, which allows for judgement of binding affinity and the relative change in concentration (Δppm), as a measure of possible surface coverage. By applying this method, it was expected that the proteins which are actually in contact with NP surfaces, driven by the affinity towards the respective material, and the proteins which are simply connected to the adherent lipid layers can be distinguished. Although up to 417 proteins were detected in the NP corona, only a small number of proteins stand out, due to a rather low Δppm or fold change. Table 4-4 shows a summary of the most interesting proteins, which can interestingly be largely connected to specific functions of the immune system. As there is no specific value which proves a certain degree of binding or importance, an arbitrary threshold of 2000 Δppm was chosen, together with a fold change threshold of ± 2 to exclude this statistically meaningless range. Using this limitation, all except for 6 proteins are excluded: SP-A (gene name: SFTPA1), SP-D (SFTPD), cathelicidin antimicrobial peptide (CAMP), myosin-3 (MYH3), apolipoprotein A-I (APOA1), and sodium-dependent phosphate transport protein 2B (SLC34A2). SP-A, as the most abundant protein in PS, was expected to be present in all three coronas. As mentioned above, it was decreased in comparison to amounts present in crude pPS, but showed increasing concentrations in the order PEG-<PLGA-<Lipid-NPs. The collectin SP-A, which was described in detail in the general introduction in Chapter 1, is a large protein of the host defense that binds via its CRD to pathogens and similar surfaces, including PL membranes (with its hydrophobic tail and the CRD), and also takes part in the organization of PS structures. Having these two binding options, the prevalence of which still needs to be clarified, it is entirely feasible that SP-A could directly bind to Lipid-NPs, to the quite hydrophobic PLGA-NPs, and even to PEG-NPs to a lesser extent. Adsorption of SP-A to PLGA-NPs could therefore already explain the subsequent lipid binding that was observed. The same could be true for the binding of second surfactant specific collectin SP-D to PEG-NPs. While the abundance of SP-D on PLGA- and Lipid-NPs (714 ppm and 2977 ppm) was rather low, in the corona of PEG-NPs it was greatly increased to 11757 ppm - twice as much as in the deployed crude pPS (5119 ppm), and exceeding even the abundant SP-A. The resulting fold change of 14.7 in comparison to PLGA-NPs and 4.0 to Lipid-NPs insinuates high affinity towards the hydrophilic polymer. SP-D also possesses the capability to interact with PL membranes by an unspecific binding, particularly to GPI_{no}, although with a weaker affinity than SP-A [164], which could explain the low-level lipid binding observed after the adsorption of SP-D to the

NP surface. The antibacterial peptide CAMP preferably bound to Lipid- and PLGA-NPs. It is known to readily interact with PL membranes and as part of the host defense [165], is the type of protein that is expected to be found on a pathogen invading the lungs. APOA1 is the only protein in this list which is typically found in the plasma corona of NPs with a high abundance [166-168] and was also found to adsorb together with lipids from high density lipoprotein complexes [168]. Surprisingly, the highest concentration of APOA1 was found on PLGA-NPs, the lowest on Lipid-NPs. SLC34A2, which is highly expressed in the lungs, is a phosphate transporter which might be involved in the genesis of PS vesicles. Although membranous, the reason for its adsorption to certain surfaces has however not been clarified. This is also unknown for MYH3, a protein which was until now not reported to be a relevant constituent of PS; nevertheless, another myosin (18A) is apparently functioning as a receptor for SP-A [169]. Beside the proteins which meet the two threshold criteria, there are others which only meet one of the limitations but are still of high interest for this study since they hold functions relevant to surface and/or lipid binding. “Deleted in malignant brain tumors 1 protein” (DMBT1), with the meaningful alternative name “Surfactant pulmonary-associated D-binding protein” is capable of binding not only SP-D [170] by protein-protein interactions at the CBR of SP-D, but is also able to directly bind to bacteria [171]. It is a membrane-bound scavenger receptor, expressed by macrophages and alveolar tissue, that showed in our experiments an adsorption behavior – in contrast to that of SP-D - in the order Lipid->PLGA->PEG-NPs. BPIFB1 belongs to the BPI fold-containing family that is expressed throughout the airways, putatively part of the host defense and even thought to be a new type of surfactant protein, though its functions remain unclear [172, 173]. The two ficolins 1 + 2 (or M-/L-ficolin) are secreted proteins with a collagen-like region and a fibrinogen-like domain, similar to collectins, allowing them to target pathogens such as bacteria and viruses [174-176]. They are furthermore involved in the activation of the lectin complement pathway. Table 4-4 reveals that each of the three particles has a unique adsorption pattern of the featured proteins. Apparently, the protein corona around Lipid- and PLGA-NPs is quite similar, with some exceptions: PEG-NPs tend to adsorb a completely distinct set of proteins, dominated by the increase in SP-D concentration. With regards to their occurrence, only four proteins are commonly measured in plasma: APOA1, CAMP, FCN1, and FCN2. The adsorption experiments with Alveofact® in the presence of FCS (Figure 4-5B) basically proved that plasma proteins – at least at this concentration – do not enhance the adsorption of lipids to NPs, leading to the conclusion that the remaining proteins might be involved in a protein-mediated lipid corona formation.

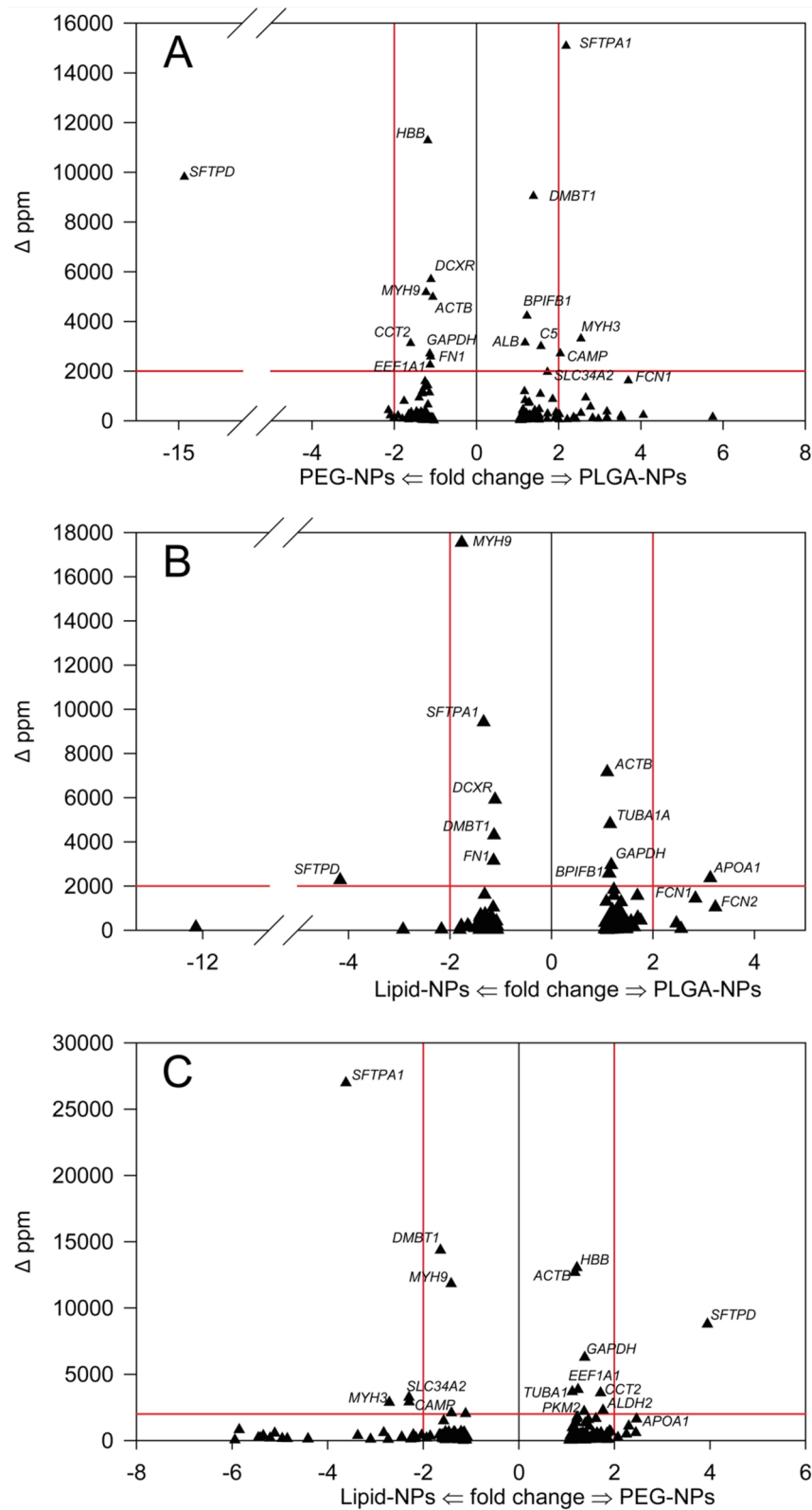


Figure 4-7: Direct comparison of relative protein amounts found in the corona of PLGA-, PEG-, and Lipid-NPs by means of relative change in abundance (Δ ppm) and fold change. An arbitrary threshold of 2000 Δ ppm and a threshold of ± 2 exclude all but 6 proteins, assumingly the proteins are directly binding to the NP surface and therewith show the highest affinity towards the material. Reproduced with permission from [115].

Table 4-4: Most prominent changes in abundance of proteins in the coronas of PLGA-, PEG-, and Lipid-NPs (* = no statistical difference).

	Protein		Nanoparticles			Abundance [ppm]	
	Name (gene symbol)	Relevant Annotations	PLGA	PEG	Lipid	pPS	Plasma (from [76])
fold change >2 / <= 2 AND Δppm > 2000	Surfactant Protein A (SFTPA1)	PL- binding and organization, carbohydrate binding, host defense	++	+	+++	101882,8	Not detected
	Surfactant Protein D (SFTPD)	Carbohydrate binding, interaction with PL, host defense	+	+++	++	5119,0	Not detected
	Cathelicidin antimicrobial peptide (CAMP)	Binds to bacteria, antibacterial, exosome associated	++	+	+++	1736,3	Not detected.
	Myosin-3 (MYH3)	-	+++	+	++	6689,6	Not detected
	Apolipoprotein A-I (APOA1)	PL and Cholesterol binding	+++	++	+	3805,1	32563
	Sodium-dependent phosphate transport protein 2B (SLC34A2)	Involved in surfactant synthesis, membrane-associated	+++*	+	+++*	23086,1	Not detected
fold change >2 / <= 2 OR Δppm > 2000	Deleted in malignant brain tumors 1 protein (DMBT1)	Interacts with SP-D, binds to bacteria, receptor activity, membrane associated	++	+	+++	19865,7	Not detected
	BPI fold-containing family B member 1 (BPIFB1)	Binds LPS, modulates cell response, binds PL	++	+	+++	8788,5	Not detected
	Ficolin 1/2 (FCN1, FCN2)	Binds pathogen-associated molecular patterns, membrane associated, excreted by macrophages	+++	+	++	2709,9 / 1426,7	Not detected

4.4 Summary and Conclusions

The results obtained from this study are the first showing the complete and detailed analysis of biomolecules as they occur in PS, *i.e.* proteins and lipids. pPS, as described in Chapter 2, allows for studying the composition of the NP corona for the first time on a larger scale. By the evaluation of different separation methods it could be shown that the access to isolated NP-corona complexes is unlikely more difficult than in plasma. Only magnetic separation showed an acceptable separation of the NPs from the non-binding supernatant. In this firmly bound corona, we found a highly conserved lipid mixture on all three NPs, which did not reflect the crude pPS composition. The amount of attached lipids differed among NPs, yet not in a manner which was related to particle mass or to particle surface area. One would assume a certain plateau of lipid concentration once the surface is saturated with hydrophobic lipids on all NPs directly interacting with PLs, since the dragging force during separation will remove additional PL layers. Lipids of a protein-depleted clinical surfactant did not adsorb to PEG- and PLGA-NPs, as obviously such a preparation is lacking specific proteins which promote the lipid binding, and furthermore, serum proteins did not change this outcome. Out of up to 417 detected proteins, we identified a number of proteins whose abundance in the coronas varied between NPs, leading to the conclusion that these proteins were in contact with the NP surface itself and either individually or by interplay of several proteins led to an increased hydrophobicity of the surfaces. These proteins were mostly connected to host defense and have been annotated to interact with lipids. Unique surfactant collectins, *i.e.* SP-A and SP-D, were two of these proteins, with SP-D especially seeming to selectively bind hydrophilic surfaces.

With regard to prospective studies, other techniques should be explored to separate the NP complexes, as magnetic separation is limited to NPs which can be magnetically loaded without changing the character of the NP itself. It is conceivable, that the corona in PS cannot as easily be classified into “hard” and “soft” components as it was shown in plasma, as there are no free single molecules in PS, but rather a complex membranous system which will always interact with hydrophobic surfaces. The dragging force will likely be the limiting factor of how many layers of proteins and lipids can be found on the NPs. By using single surfactant proteins in the presence of the lipid fraction of PS, future studies will hopefully reveal the kinetics of corona formation. A time-dependent analysis of corona evolution will show if there are affinity driven exchanges on the particle surface or if the PS layer adsorbs as such once the particle is hydrophobic enough. The lipid quantification of these studies could rely

on the determination of comparably few lipids, as about 90 wt% of lipids is made up of only ten lipid species; however, as we have omitted positively charged NPs, the lipid corona of such particles should be elucidated first. Lastly, for all aspects regarding NP toxicity and potential for drug delivery, it needs to be clarified what determines the cell-NP interaction in the lung: coronal proteins, lipids or both.

**5. IMPACT OF THE PULMONARY
SURFACTANT CORONA ON
NANOPARTICLE-MACROPHAGE
INTERACTIONS**

5.1 Introduction

For the sake of animal welfare, there is a strong tendency to search for ways to substitute experiments that involve experimenting with or sacrificing animals by, preferably, *in vitro* experiments [177]. To test drug penetration behavior, drug release and distribution of pharmaceuticals and new pharmaceutical carriers such as NPs in early stages of development, cell models based on either primary cells or cell lines are increasingly used. Depending on the effect that is tested, these *in vitro* models require a certain degree of complexity in order to adequately mirror the properties of the desired site of interaction. Therefore, single cell models are often replaced by co-culture models, which mimic the actual tissue more realistically [178]. In case of the interaction of NPs with cells of the alveoli, a typical cell co-culture would consist of epithelial cells and macrophages, the two dominant cell types present in such tissue [3], but could also be expanded to include fibroblasts, endothelial, or dendritic cells [179]. By using such a setup in simple submerged conditions one does not take into account however that the true situation in the lung is for several reasons considerably more complicated: The surface of the air-blood barrier is not a static system, but is expanding and contracting constantly due to breathing, resulting in a changing surface area and moving particles. The mode of deposition is also questionable in many studies, as the relevant deposition is an impaction of aerosol droplets or particles onto the thin lining fluid which covers the cells. Air-liquid conditions of cell models have emerged and bear a promising resemblance to the actual interface [180], furthermore they can be combined with depositing devices to simulate particulate delivery.

A major issue in modeling the alveolar epithelium is the lack of an established alveolar epithelial cell line which possesses the barrier function of a cell monolayer, in which cells are interconnected by tight junctions (AT-1), and that is concurrently capable of secreting pulmonary surfactant (AT-2). Primary epithelial cells and the recently established immortalized hAELVi cells have barrier properties of AT-1 cells and can be grown under air-liquid conditions [179, 181]. The most commonly used, adenocarcinoma cell line A549 is often used to test particle uptake. It secretes alveolar bodies, but is however not able to form tight junctions [182]. The uptake and penetration of NPs through epithelial cells however seems to be the rarer case anyway, as particles in the deep lung are very efficiently taken up by phagocytic cells [179]. For pharmaceutical NPs which aim to release drugs into the alveolar space in a sustained manner, or for targeted delivery to the macrophages (*i.e.* targeting intracellular pathogens such as *L. pneumophila* and *M. tuberculosis*), the uptake by AM is of

greater interest [183]. But if air-liquid conditions are desired, a co-culture with epithelial cells is necessary [178].

There is one factor which influences NP-cell interactions whose importance for *in vitro* experiments needs to be urgently evaluated: The influence of the formed PS corona at the surface of NPs on subsequent cell interactions [98]. In the preceding chapters, the presence of such a unique corona was proven. NPs interact with the membranous system of PS and adsorb lipids and proteins on their surface. *In vitro* uptake studies are commonly used for testing new formulations and drug delivery systems for lung delivery. It is generally valid to say that the mode of exposure for all studies needs to be standardized to allow inter-lab comparisons of uptake and cytotoxicity. Unfortunately, if looking into literature it can be seen that most experimenters choose to expose cells to NPs within the used cell medium, some within buffers, of which again some use FCS or other serums, without questioning the impact of the medium composition on NP surfaces and therewith cell interactions [98, 178]. When it comes to the lungs and the respective cell lines, it appears that even less emphasis is placed on simulating a realistic exposure. It has been clearly illustrated in the last chapters that none of the typically used dispersion liquids are a close match for the actual lung environment. The PS corona, with a composition as has been determined in chapter 4, cannot be expected to lead to the same modification of cell interactions as the protein corona of plasma. It has already been shown that single components of PS alter the uptake/association of NPs by cells. Kendall *et al.*, for instance, found that the extent to which polystyrene NPs are taken up by AM is dependent on SP-D, *in vivo* as well as *in vitro* [184]. In a similar study by Konduru *et al.*, GPSer had an uptake enhancing effect on single-walled carbon nanotubes [185]. The other lung collectin SP-A was found by Ruge *et al.* to increase the uptake of certain NPs by AM (PL-NPs in particular) [186], in the presence of an artificial mixture of PLs, however, this effect was moderated [101]. It can be concluded then, that only full surfactant - as used by Thorley *et al.*, who found an increased uptake of polystyrene NPs in the presence of concentrated BALF by an AT-1 like cell type [61] - will mimic the effects of the corona on cell interaction realistically, in a manner which is expected to be markedly different to the effects of a plasma corona. To prove this hypothesis, a cell line of AM from mice (MH-S) was used to test the change in nanotoxicity of several NPs in the presence and absence of pPS. Furthermore, the uptake or association of fluorescent polystyrene NPs after pre-incubation in media with different additives, *i.e.* pPS, protein depleted PS (Alveofact®) and FCS was probed.

5.2 Reagents and Methods

5.2.1 Reagents

Preparation of PLGA- and Eu-NPs was described in Chapter 3.3. The non-synthesized magnetite-containing nanoparticles that were used in cytotoxicity experiments were bought from the following suppliers: PEG-NP (nanomag®-D PEG 5000 250 nm) and ProtA-NP (nanomag®-D Protein-A 250 nm) were ordered from Micromod (Rostock, Germany), Lipid-NP (fluidMAG-Lipid 200 nm) and Starch-NP (fluidMAG-D 200 nm) were sourced from Chemicell GmbH (Berlin, Germany), and PS-NP (PS-MAG-COOH 350 nm) were obtained from microparticles GmbH (Berlin, Germany). All such NPs were used as received. For cell uptake experiments, fluorescent carboxylated polystyrene NPs (Fluoresbrite® COOH YG 0.05/0.2 μm and Fluoresbrite® multifluorescent 0.2 μm) were purchased from Polysciences Europe GmbH (Eppelheim, Germany). FCS was obtained from Lonza (Basel, Switzerland); all other reagents and solvents were bought from Sigma Aldrich (Munich, Germany). PS was isolated as described in Chapter 2, while Alveofact® was kindly provided by Lyomark Pharma GmbH.

5.2.2 MH-S Cultivation

MH-S macrophages (CRL-2019) were purchased from the American Type Culture Collection (Wesel, Germany) and grown in RPMI 1640 medium (Thermo Fisher Scientific), supplemented with 2 mM L-glutamine, 1% (v/v) HEPES, 25mM D-glucose, 18 mM sodium bicarbonate, 1 mM sodium pyruvate, 0.05 mM β -mercaptoethanol, and 10% (v/v) FCS in T75 flasks at 37 °C and 5% CO₂. For cytotoxicity and uptake experiments, cells were seeded in 96-well plates (Greiner Bio-One, Frickenhausen, Germany) at a density of 40,000 cells/well or in 24-well plates (Greiner Bio-One) at a density of 200,000 cells/well, respectively.

5.2.3 Pre-Incubation and Incubation of Nanoparticles

Before the addition of any NP dispersions, cells were washed with FCS-free MH-S medium and allowed to equilibrate for 1 h. If not stated otherwise, the ratio of nanoparticles to pPS or FCS was 1:2 (μg NPs to μg proteins). NPs were pre-incubated for 1 h at 37 °C and 5% CO₂ to form an equilibrated corona around NPs. For cell cytotoxicity measurements, NP dispersions were added to the cells and incubated for 4 h; untreated cells served as a control. Cell uptake was studied under various conditions for incubation and pre-incubation, as stated in the

specific descriptions of the experiments. In general, after the given incubation time in the dark, NP dispersions were discarded and the cells were washed three times with PBS.

5.2.4 Cell Viability Assay

The cytotoxic effect of NPs on lung macrophages was measured by means of metabolic activity, deploying the CellTiter-Blue® Cell Viability Assay (Promega, Mannheim, Germany) according to the manufacturer's manual. In brief, 400 µl of fresh medium was added after removal of the tested dispersion and subsequently 40 µl of CellTiter-Blue™ Reagent was added. Cells were incubated at 37 °C and 5% CO₂ for 30 min in the dark. The starting fluorescence intensity was measured in an Infinite 200 M microplate reader (Tecan GmbH, Crailsheim, Germany) at an excitation and emission wavelength of 560 and 590 nm respectively. Incubation was continued under the same conditions for 2 h and fluorescence intensity was read again. Cell viability was calculated according to Equation 5.1.

$$Viability \% = \frac{I_{2.5h\ sample} - I_{0.5h\ sample}}{I_{2.5h\ control} - I_{0.5h\ control}} * 100 \quad (5.1)$$

5.2.5 Nanoparticle Uptake / Association by Flow Cytometry

After incubation and washing, cells were detached from the plate by addition of Trypsin-EDTA (Thermo Fisher Scientific) and incubation at 37 °C for 5 min. Cells were redispersed in buffer (PBS + 2% FCS) and analyzed using flow cytometry (FACSCalibur™, BD Biosciences, San Jose, USA). Cell association/uptake of NPs was measured as mean fluorescence intensity in FL-1 channel (excitation 488 nm, emission 530 nm). For data acquisition, a minimum of 20,000 events was counted using BD CellQuest Pro™, which were subsequently processed in FlowJo vX.07 software (FlowJo LLC).

5.3 Results and Discussion

5.3.1 Nanoparticle Cytotoxicity is modified by Surfactant Adsorption

A set of various NPs was used to access the cytotoxic effect on the murine AM cell line MH-S. The particles were chosen based on differences in surface charge (PLGA, Eudragit), hydrophobicity (PEG, Lipid), and an expected surface-linked effect (Starch, Protein A). As professional phagocytes are somewhat resistant to cytotoxic effects, a larger decrease of viability was only observed for Eu-NPs (Figure 5-1A) and only at higher concentrations which are unlikely to occur in the lungs. The fact that positively charged NPs are more cytotoxic than negatively charged NPs was expected and caused by their ability to disrupt plasma membranes and to damage mitochondria and lysosomes [187].

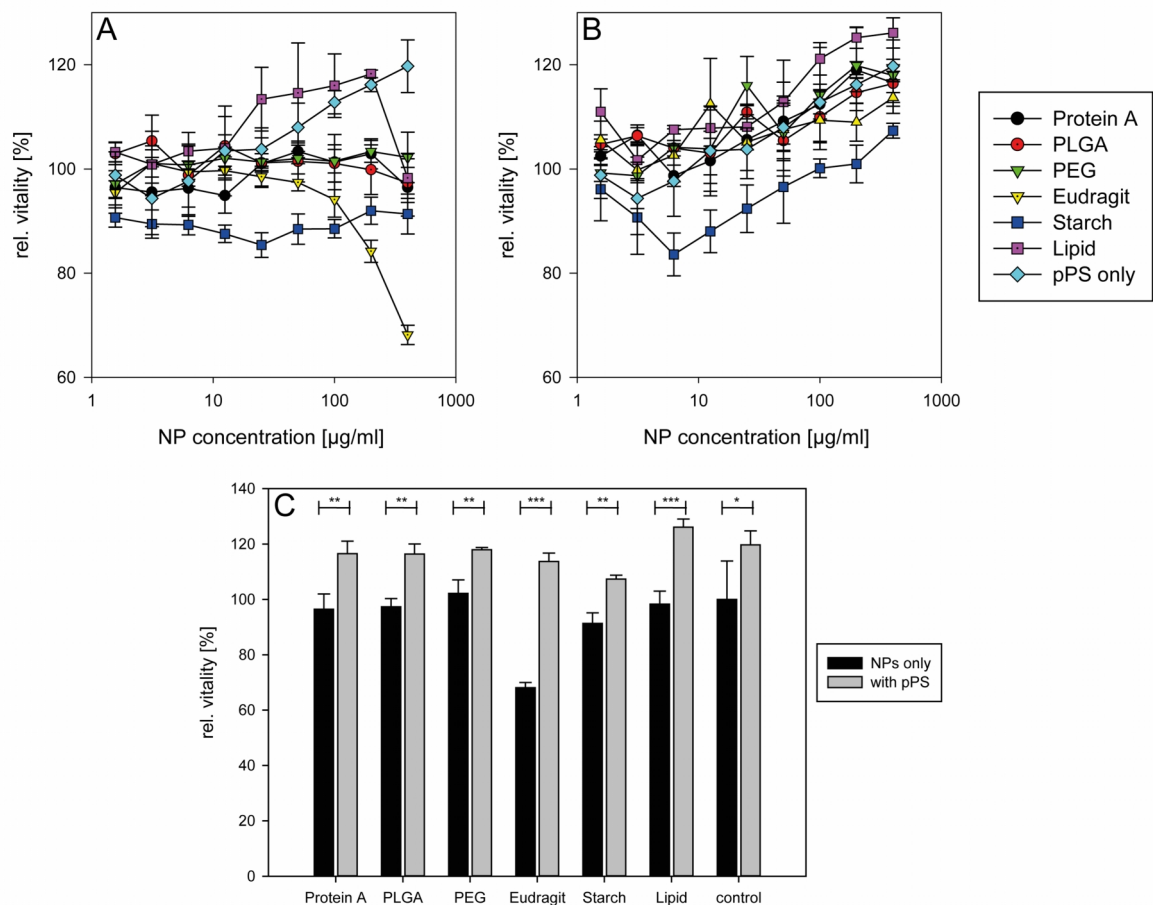


Figure 5-1: Influence of pPS on NP cytotoxicity. Relative vitality of MH-S alveolar macrophages after incubation with NPs in the absence (A) and presence of pPS (B). Cytotoxicity of all tested NPs is decreased with pPS (C – NP concentration = 400 µg/ml).

After pre-incubation of NPs with an increasing amount of pPS, all samples showed significantly higher viability rates (Figure 5-1B), equalizing the relative viability to about 120% in comparison to untreated cells at the highest NP and pPS concentration (Figure 5-1C). It would seem that the increase in viability is only related to the surfactant concentration as there is no longer a visible effect of NPs. The fact that AM do not show signs of stress or trauma in the presence of PS can be seen from AM grown under air-liquid conditions, which keep their original shape only if a surface tension lowering agent is added [188]. A possible explanation for the lack of a cytotoxic effect of the NPs might be that pPS either establishes a physical hindrance for the NPs, or more likely, if looking at the results in Chapter 4, it might equalize the surface charge (and other properties) of the NPs by formation of a PS corona.

5.3.2 Modification of Nanoparticle Uptake by Lung Macrophages after Corona Formation

By using flow cytometry and carboxylated polystyrene fluorescent NPs as model NPs, the association of NPs with cells can be easily assessed. An example of a typical distribution of MH-S cells in terms of forward and side scattering intensity is given in Figure 5-3A. The AM cell line showed high tolerance of incubation conditions and as apoptotic cells contributed a minor portion of the total cells, the data could be processed without the need for gating on subpopulations. Before the incubation of cells with the respective NP dispersion, NPs were pre-incubated in media with different additives to ensure a corona formation at equilibrium. Different concentrations of NPs were tested and it was found that 20 $\mu\text{g}/\text{ml}$ polystyrene NPs were most suitable to see changes within the detector range (Figure 5-2). As a typical medium additive which results in the formation of a plasma protein corona, the uptake in presence of 10% FCS was tested in comparison to a pPS concentration of 40 $\mu\text{g}/\text{ml}$, which was sufficient in earlier experiments to saturate corona formation. Although the overall mean fluorescence intensity was interestingly higher in samples with FCS, indicating a greater absolute uptake of particles, the distribution as shown in Figure 5-2 reveals that there are two fractions of cells in these samples; one fraction which takes up only few particles and one which takes up large amounts, while the uptake of pPS coated NPs appears more monodisperse. This behavior could be interpreted as a hint that there might not be the same uptake mechanism involved. This possibility deserves to be addressed further in later studies, as phagocytic cells feature a range of possibilities to interact with NPs [189], and searching for the exact mechanism would go beyond the scope of this thesis.

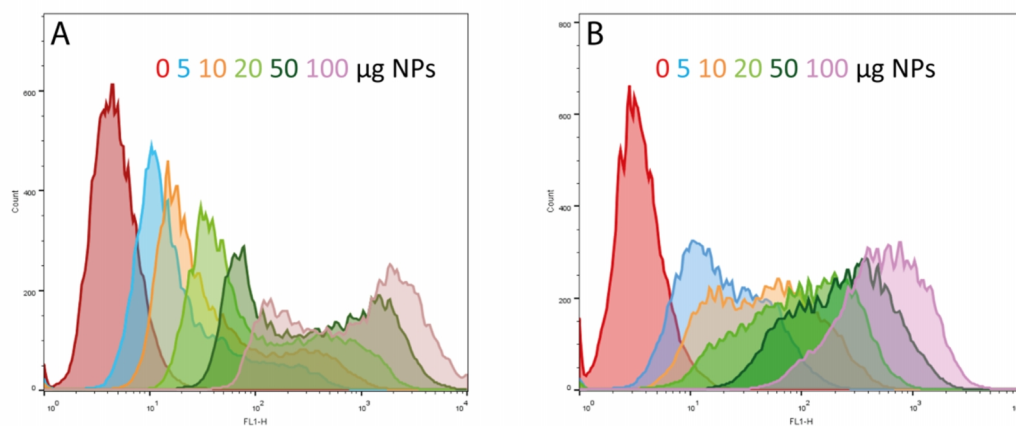


Figure 5-2: NP-cell association as a function of NP concentration. Although the overall mean fluorescence intensity (x-axis) of samples with 10% FCS (A) is higher than in samples with 40 µg/ml pPS (B), there are two fractions of cells visible in FCS samples which either show high or low fluorescence intensity.

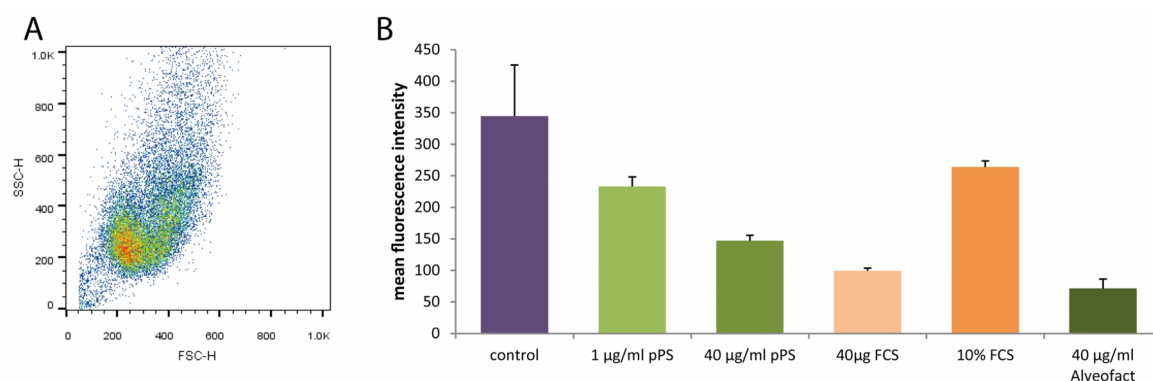


Figure 5-3: Distribution of cell counts shown for 20 µg/ml NPs + 40 µg/ml pPS (A). Uptake/association of 20 µg/ml polystyrene NPs by MH-S cells with different additives (B).

In general, it is difficult to relate and compare the direct effects of the investigated coronas on NP uptake, as plasma and PS represent two completely different systems. The first and most obvious question concerns which concentrations to compare at all. Here, all concentrations that are given for pPS relate to the concentration of proteins in the preparation; but, it needs to be considered that this also includes a tenfold amount of lipids. Nevertheless, a variation of additive concentrations has been tested. NPs without the presence of any PS preparation in RPMI always showed the highest association with macrophages, as reported earlier [72]. Very surprisingly, it became obvious (Figure 5-3B) that the uptake of NPs is decreased with increasing concentration of pPS. In contrast, very little amounts of serum proteins lead to a

minimal NP uptake, which was increasing with FCS concentration. A possible explanation for the latter could be the adsorption of low-expression but high affinity proteins on the surface of NPs, which efficiently mediate uptake, as opposed to the non-selective binding of abundant proteins in case of a low protein supply. Since the chosen pPS concentrations are sufficient to cover the whole NPs (see Chapter 4) and the surface is masked by a hydrophobic coating, it is unlikely that a further exchange of adsorbed molecules occurs. Higher concentrations of PS however increase the viscosity of the NP dispersions and add more multilamellar vesicles and membranes to the liquid, resulting in additional physical barriers which inhibit contact of NPs with the cells. This complies with the fact that the more rigid surfactant preparation Alveofact® inhibits NP uptake more than pPS at the same lipid concentration. With respect to bare carboxylated polystyrene NPs, a coating by pPS results in a diminished uptake. From this, the assertion that can be made that whenever the outcome of any uptake experiments in lung cells is unwittingly determined in an FCS containing media, the results certainly cannot be correlated with the actual *in vivo* behavior and surface modifications of NPs in the lungs, where no plasma proteins but rather PS is present.

5.3.3 NP Corona does Not form Instantaneously *In Situ*

In the all previous experiments NPs were pre-incubated to form an equilibrated corona. The protein corona around NPs in particular is thought to be established very quickly [81].

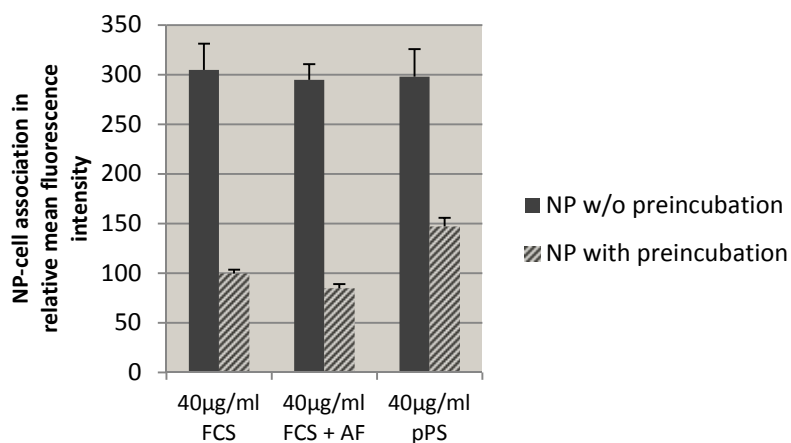


Figure 5-4: Difference of cell association with and without 1 h pre-incubation of NPs (20 µg/ml) with FCS, AF (Alveofact®) or pPS prior to incubation with cells. Cell association without pre-incubation appears to be faster than corona formation, regardless of the corona-forming additive.

By comparing the uptake of NPs with and without prior incubation for 1 h before adding the dispersion to the cells (Figure 5-4), it becomes clear that in this experimental set-up, the contact of the bare NPs with cells takes place faster than the formation of the corona. No significant difference in uptake could be observed when adding the NPs directly to the apical medium containing 40 $\mu\text{g}/\text{ml}$ pPS, 40 $\mu\text{g}/\text{ml}$ FCS, or 40 $\mu\text{g}/\text{ml}$ FCS + Alveofact®; samples with medium additives without pre-incubation in fact showed the same uptake as samples without any additives. Due to the limited availability of pPS, the precise incubation time needed to reach equilibrium could not be determined; however, preliminary experiments (data not shown) suggested that it lies between 15 and 30 min.

5.3.4 Cell Association vs. Uptake

To determine whether NPs are actively taken up by the AM or if they are only associated with the plasma membrane, the fluorescence intensity of cells after incubation of NPs at a physiologically relevant temperature of 37 °C, and at 4 °C was measured. At 4 °C mammalian cells do not proliferate, and as such it is possible to discriminate between active uptake and passive cell association.

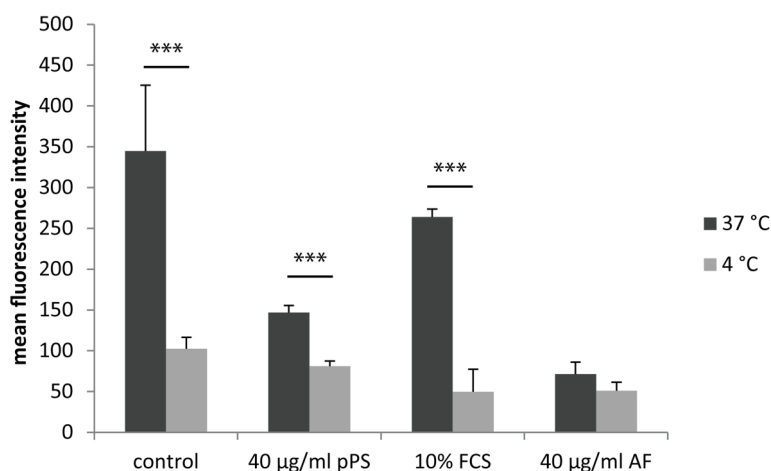


Figure 5-5: Cell association at 4 °C and uptake at 37 °C of 20 $\mu\text{g}/\text{ml}$ NPs. While the control without additives and the samples with FCS showed only minimal association at 4 °C, the proportion of NPs which interact with cells at 4 °C in presence of the pPS and Alveofact® corona is comparably high. (*) = $p < 0.001$)**

The extent to which the cellular interaction of NPs with different coronas is altered is shown in Figure 5-5. The results indicate that the uptake of NPs in the absence of any additives and of NPs coated with FCS is energy-dependent to a high degree: Without additives the association was reduced to 30% and with FCS to 19% of the active uptake. The association of

NPs with pPS and Alveofact® was decreased as well, although to a lesser extent (55% and 72% respectively). This suggests, that bare and FCS-coated particles are taken up by a specific pathway like clathrin- or calveolin-mediated endocytosis and phagocytosis, while NPs which are already coated by a lipid film, the PS, are able to coalesce with the plasma membranes of the cell more easily, meaning that no ATP is needed.

5.4 Summary and Conclusions

Macrophages, as one of the two most abundant cell types in the respiratory zone, and as professional phagocytes, are most likely to interact with inhaled NPs. This makes them most interesting from a viewpoint of pharmaceutical technology: Not only do they interfere with NP delivery to other cells due to their efficient clearance of such particulate matter, but they also present a target themselves. As complex *in vitro* systems are emerging, more attention needs to be paid to the actual NP properties *in situ*, which also includes the interaction with non-cellular barriers prior to cell contact, such as plasma proteins for particles intended for intravascular application. At this point it is clear that the simple principle of plasma protein corona formation cannot be transferred to the situation in the deep lung. By comparing the influence of the corona established after incubation of polystyrene NPs with PS, supplemented with the commonly used cell culture additive FCS in a relevant concentration, it became obvious that there are significant differences in how and to what degree NPs interact with AMs if they are pre-incubated with either of these additives. Not only does PS apparently protect AMs from the cytotoxic effects of NPs, we also found a significant difference in the uptake with the two, quite incomparable concentrations; though the contrasting trend in extent of uptake with the two additives at different concentrations showed that there are more effects in play than just the biochemical corona formation. Overall, it can be concluded that PS is indispensable if one aims to realistically mimic the interaction of NPs with cells of the deep lung, due to its unique nature. Neither the application of bare NPs nor the use of serum proteins as a substitute for the biological lung environment at the air-liquid interface is an option to simulate the *in vivo* behavior of NPs in *in vitro* models. In order to improve existing complex models, such as a primary cell model of epithelial cells and macrophages under air-liquid conditions, the presence of PS at the air-interface needs to be proven – although, this is not very likely, as the cells are usually not grown under air-liquid conditions for a long period. Furthermore, primary epithelial cells are sooner or later differentiating into AT-1 cells that do not produce PS. PS could therefore be used in the future as a standard medium supplement when culturing lung cells, in order to simulate the physical effects of PS by surface tension lowering on the cells and NPs, but most importantly in order to accurately simulate the biochemical composition of the PS corona as formed *in vivo*.

6. SUMMARY AND OUTLOOK

Corona formation on NPs in the deep lung is an emerging topic in nano-bio sciences. The processes that are involved in the adsorption of biomolecules on the surface of NPs are complex, even more so than the standard studied plasma corona, which has been far more thoroughly explored even though uptake of particles is more likely to occur via the lungs. The corona which evolves after contact with PS consists of proteins and lipids, and is therefore different in its biochemical composition to that of the plasma corona. The membranous/vesicular character of the PS in all its complexity also considerably modifies the colloidal behavior of inhaled NPs. By using and characterizing a porcine preparation of PS (pPS) which is, unlike the commercially available clinical preparations, not protein-depleted, it was possible to probe PS interactions with NPs. In particular, the influence of PS on NP colloidal stability, on the biochemical composition of the formed corona and its influence on cellular uptake were investigated, which is not feasible to undertake with rare human PS. The here used pPS has proven to be a suitable realistic surrogate and although clinical surfactant preparations, such as Curosurf[®], are more commonly used than any other model systems for surfactant, it became obvious that with lacking proteins the adsorption behavior changes. In this work it could be shown that all tested types of NPs (*i.e.* with different surface properties) – in whichever experimental set-up – interact with and are being influenced by PS. Especially PEGylated NPs which are usually considered rather “inert”, when it comes to adsorbing biomolecules, showed interaction with pPS. The biochemical analysis of the PS corona revealed that just a few lung-specific proteins may be responsible for mediating an interaction of highly hydrophobic phospholipid vesicles with hydrophilic NPs, which has never been observed in plasma.

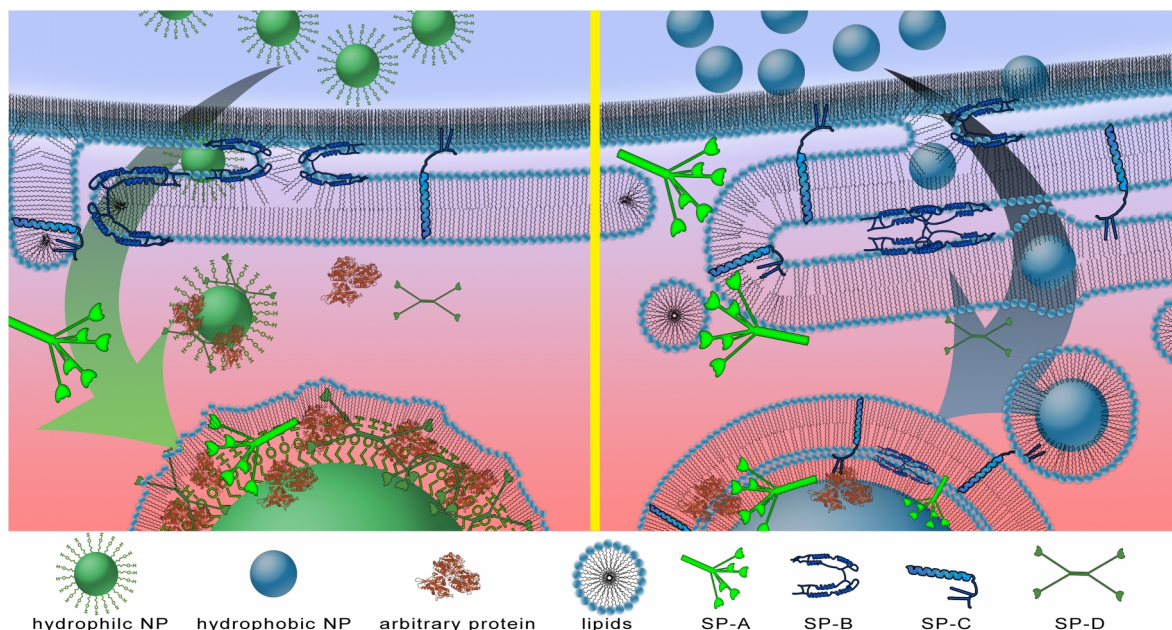


Figure 6-1: Scheme of a proposed corona formation mechanism. Reproduced with permission from [115].

This mediating effect of surfactant proteins (as schematically drawn in Figure 6-1) could lead to the observed corona formation on every particle. With such an assimilation of every surface, which will eventually result in a lipid corona, the lung has an efficient mechanism to protect the underlying cell layer from harm. It could be shown that even cytotoxic Eudragit NPs are well tolerated by macrophages and the mechanism by which the particles are taken up is most likely different to that which occurs in the absence of PS. The field of nano-bio interactions has evolved and drawn increasing attention in the last years; the idea that corona formation depends on the local environment and therefore needs to be adapted for each route of application is an emerging concept. This work has advanced the understanding of how NPs interact with the non-cellular barrier of the alveolar region in the lungs. PS, a very specific body fluid, cannot be replaced with any model such as plasma proteins, as the biochemical and biophysical properties of this mixture are unique. In future, the safety of nanopharmaceuticals intended for pulmonary delivery, together with cytotoxicity, efficiency, release, *etc.* as normally tested under *in vitro* conditions urgently needs to consider and include the effects that PS has on nanoparticulate delivery systems. PS might be the key to success or a significant barrier for targeted delivery to the lungs; either way, one can conclude in the words of Schleh *et al.*: “Pulmonary surfactant is indispensable in order to simulate the *in vivo* situation” [98].

7. BIBLIOGRAPHY

1. Patton, J.S., *Mechanisms of Macromolecule Absorption by the Lungs*. Advanced Drug Delivery Reviews, 1996. **19**(1): p. 3-36.
2. Ochs, M., et al., *The Number of Alveoli in the Human Lung*. Am J Respir Crit Care Med, 2004. **169**(1): p. 120-4.
3. Stone, K.C., et al., *Distribution of Lung Cell Numbers and Volumes between Alveolar and Nonalveolar Tissue*. Am Rev Respir Dis, 1992. **146**(2): p. 454-6.
4. Patton, J.S. and P.R. Byron, *Inhaling Medicines: Delivering Drugs to the Body through the Lungs*. Nat Rev Drug Discov, 2007. **6**(1): p. 67-74.
5. Sanders, N., et al., *Extracellular Barriers in Respiratory Gene Therapy*. Adv Drug Deliv Rev, 2009. **61**(2): p. 115-27.
6. Kirch, J., et al., *Optical Tweezers Reveal Relationship between Microstructure and Nanoparticle Penetration of Pulmonary Mucus*. Proc Natl Acad Sci U S A, 2012. **109**(45): p. 18355-60.
7. Bastacky, J., et al., *Alveolar Lining Layer Is Thin and Continuous - Low-Temperature Scanning Electron-Microscopy of Rat Lung*. Journal of Applied Physiology, 1995. **79**(5): p. 1615-1628.
8. Crapo, J.D., et al., *Cell Number and Cell Characteristics of the Normal Human Lung*. Am Rev Respir Dis, 1982. **126**(2): p. 332-7.
9. Weibel, E.R., *On the Tricks Alveolar Epithelial Cells Play to Make a Good Lung*. Am J Respir Crit Care Med, 2015. **191**(5): p. 504-13.
10. Wallace, W.A., M. Gillooly, and D. Lamb, *Intra-Alveolar Macrophage Numbers in Current Smokers and Non-Smokers: A Morphometric Study of Tissue Sections*. Thorax, 1992. **47**(6): p. 437-40.
11. Pérez-Gil, J. and T.E. Weaver, *Pulmonary Surfactant Pathophysiology: Current Models and Open Questions*. Physiology (Bethesda), 2010. **25**(3): p. 132-41.
12. Scanlon, V.C. and T. Sanders, *Essentials of Anatomy and Physiology*. 6th ed. 2014, Philadelphia: FA Davis.
13. Gehr, P., M. Bachofen, and E.R. Weibel, *The Normal Human Lung: Ultrastructure and Morphometric Estimation of Diffusion Capacity*. Respir Physiol, 1978. **32**(2): p. 121-40.
14. Lopez-Rodriguez, E. and J. Perez-Gil, *Structure-Function Relationships in Pulmonary Surfactant Membranes: From Biophysics to Therapy*. Biochim Biophys Acta, 2014. **1838**(6): p. 1568-85.
15. Veldhuizen, R., et al., *The Role of Lipids in Pulmonary Surfactant*. Biochim Biophys Acta, 1998. **1408**(2-3): p. 90-108.
16. Postle, A.D., E.L. Heeley, and D.C. Wilton, *A Comparison of the Molecular Species Compositions of Mammalian Lung Surfactant Phospholipids*. Comp Biochem Physiol A Mol Integr Physiol, 2001. **129**(1): p. 65-73.
17. Daniels, C.B. and S. Orgeig, *Pulmonary Surfactant: The Key to the Evolution of Air Breathing*. Physiology, 2003. **18**(4): p. 151-157.
18. Daniels, C.B., et al., *The Influence of Temperature, Phylogeny, and Lung Structure on the Lipid Composition of Reptilian Pulmonary Surfactant*. Exp Lung Res, 1996. **22**(3): p. 267-81.
19. Zuo, Y.Y., et al., *Current Perspectives in Pulmonary Surfactant--Inhibition, Enhancement and Evaluation*. Biochim Biophys Acta, 2008. **1778**(10): p. 1947-77.
20. Weaver, T.E., et al., *Intracellular and Oligomeric Forms of Surfactant-Associated Apolipoproteins(S) a in the Rat*. Biochimica et Biophysica Acta (BBA) - Protein Structure and Molecular Enzymology, 1985. **827**(3): p. 260-267.

21. Benne, C.A., et al., *Interactions of Surfactant Protein a with Influenza A Viruses: Binding and Neutralization*. Journal of Infectious Diseases, 1995. **171**(2): p. 335-341.
22. LeVine, A.M., et al., *Surfactant Protein-D Enhances Phagocytosis and Pulmonary Clearance of Respiratory Syncytial Virus*. Am J Respir Cell Mol Biol, 2004. **31**(2): p. 193-9.
23. LeVine, A.M., et al., *Distinct Effects of Surfactant Protein a or D Deficiency During Bacterial Infection on the Lung*. The Journal of Immunology, 2000. **165**(7): p. 3934-3940.
24. van Roozendaal, B.A., et al., *Role of Pulmonary Surfactant Protein D in Innate Defense against Candida Albicans*. J Infect Dis, 2000. **182**(3): p. 917-22.
25. Malhotra, R., et al., *Pollen Grains Bind to Lung Alveolar Type II Cells (A549) Via Lung Surfactant Protein a (Sp-a)*. Bioscience Reports, 1993. **13**(2): p. 79-90.
26. Stuart, L.M., P.M. Henson, and R.W. Vandivier, *Collectins: Opsonins for Apoptotic Cells and Regulators of Inflammation*. Curr Dir Autoimmun, 2006. **9**: p. 143-61.
27. Ogasawara, Y., Y. Kuroki, and T. Akino, *Pulmonary Surfactant Protein D Specifically Binds to Phosphatidylinositol*. Journal of Biological Chemistry, 1992. **267**(29): p. 21244-21249.
28. Pérez-Gil, J., *Structure of Pulmonary Surfactant Membranes and Films: The Role of Proteins and Lipid-Protein Interactions*. Biochim Biophys Acta, 2008. **1778**(7-8): p. 1676-95.
29. Wu, H., et al., *Surfactant Proteins a and D Inhibit the Growth of Gram-Negative Bacteria by Increasing Membrane Permeability*. J Clin Invest, 2003. **111**(10): p. 1589-602.
30. Mason, R.J. and D.R. Voelker, *Regulatory Mechanisms of Surfactant Secretion*. Biochim Biophys Acta, 1998. **1408**(2-3): p. 226-40.
31. Serrano, A.G. and J. Pérez-Gil, *Protein-Lipid Interactions and Surface Activity in the Pulmonary Surfactant System*. Chem Phys Lipids, 2006. **141**(1-2): p. 105-18.
32. Perez-Gil, J., A. Cruz, and C. Casals, *Solubility of Hydrophobic Surfactant Proteins in Organic Solvent/Water Mixtures. Structural Studies on Sp-B and Sp-C in Aqueous Organic Solvents and Lipids*. Biochim Biophys Acta, 1993. **1168**(3): p. 261-70.
33. Noguee, L.M., *Genetics of the Hydrophobic Surfactant Proteins*. Biochim Biophys Acta, 1998. **1408**(2-3): p. 323-33.
34. Johansson, J., H. Jörnvall, and T. Curstedt, *Human Surfactant Polypeptide Sp-B Disulfide Bridges, C-Terminal End, and Peptide Analysis of the Airway Form*. FEBS Letters, 1992. **301**(2): p. 165-167.
35. Wert, S.E., J.A. Whitsett, and L.M. Noguee, *Genetic Disorders of Surfactant Dysfunction*. Pediatr Dev Pathol, 2009. **12**(4): p. 253-74.
36. Chang, R., S. Nir, and F.R. Poulain, *Analysis of Binding and Membrane Destabilization of Phospholipid Membranes by Surfactant Apoprotein B*. Biochimica et Biophysica Acta (BBA) - Biomembranes, 1998. **1371**(2): p. 254-264.
37. Olmeda, B., B. Garcia-Alvarez, and J. Perez-Gil, *Structure-Function Correlations of Pulmonary Surfactant Protein Sp-B and the Saposin-Like Family of Proteins*. Eur Biophys J, 2013. **42**(2-3): p. 209-22.
38. Schurch, D., et al., *Combined and Independent Action of Proteins Sp-B and Sp-C in the Surface Behavior and Mechanical Stability of Pulmonary Surfactant Films*. Biophys J, 2010. **99**(10): p. 3290-9.
39. Weaver, T.E. and J.J. Conkright, *Function of Surfactant Proteins B and C*. Annu Rev Physiol, 2001. **63**: p. 555-78.
40. Johansson, J., *Structure and Properties of Surfactant Protein C*. Biochim Biophys Acta, 1998. **1408**(2-3): p. 161-72.

41. Casals, C. and O. Canadas, *Role of Lipid Ordered/Disordered Phase Coexistence in Pulmonary Surfactant Function*. Biochim Biophys Acta, 2012. **1818**(11): p. 2550-62.
42. Bernardino de la Serna, J., et al., *Segregated Phases in Pulmonary Surfactant Membranes Do Not Show Coexistence of Lipid Populations with Differentiated Dynamic Properties*. Biophys J, 2009. **97**(5): p. 1381-9.
43. Parra, E. and J. Pérez-Gil, *Composition, Structure and Mechanical Properties Define Performance of Pulmonary Surfactant Membranes and Films*. Chem Phys Lipids, 2014.
44. Williams, M.C., *Conversion of Lamellar Body Membranes into Tubular Myelin in Alveoli of Fetal Rat Lungs*. The Journal of Cell Biology, 1977. **72**(2): p. 260-277.
45. Polin, R.A., et al., *Surfactant Replacement Therapy for Preterm and Term Neonates with Respiratory Distress*. Pediatrics, 2014. **133**(1): p. 156-63.
46. Kuroki, Y., et al., *Surfactant Proteins a and D: Disease Markers*. Biochim Biophys Acta, 1998. **1408**(2-3): p. 334-45.
47. Ohlmeier, S., et al., *Proteomics of Human Lung Tissue Identifies Surfactant Protein a as a Marker of Chronic Obstructive Pulmonary Disease*. J Proteome Res, 2008. **7**(12): p. 5125-32.
48. Cheng, G., et al., *Increased Levels of Surfactant Protein a and D in Bronchoalveolar Lavage Fluids in Patients with Bronchial Asthma*. Eur Respir J, 2000. **16**(5): p. 831-5.
49. Kerr, M.H. and J.Y. Paton, *Surfactant Protein Levels in Severe Respiratory Syncytial Virus Infection*. Am J Respir Crit Care Med, 1999. **159**(4 Pt 1): p. 1115-8.
50. Eisner, M.D., *Plasma Surfactant Protein Levels and Clinical Outcomes in Patients with Acute Lung Injury*. Thorax, 2003. **58**(11): p. 983-988.
51. Bailey, M.M. and C.J. Berkland, *Nanoparticle Formulations in Pulmonary Drug Delivery*. Med Res Rev, 2009. **29**(1): p. 196-212.
52. European Commission, *Commission Recommendation of 18 October 2011 on the Definition of Nanomaterial*. Official J Eur Union, 2011. **50**: p. 38-40.
53. European Science Foundation, *Scientific Forward Look on Nanomedicine*, in *European Science Foundation Policy Briefing*. 2005.
54. Duncan, R. and R. Gaspar, *Nanomedicine(S) under the Microscope*. Mol Pharm, 2011. **8**(6): p. 2101-41.
55. Carvalho, T.C., J.I. Peters, and R.O. Williams, 3rd, *Influence of Particle Size on Regional Lung Deposition--What Evidence Is There?* Int J Pharm, 2011. **406**(1-2): p. 1-10.
56. Traini, D., *Inhalation Drug Delivery*, in *Inhalation Drug Delivery*. 2013, John Wiley & Sons, Ltd. p. 1-14.
57. Geiser, M., *Update on Macrophage Clearance of Inhaled Micro- and Nanoparticles*. J Aerosol Med Pulm Drug Deliv, 2010. **23**(4): p. 207-17.
58. Stone, K.C., et al., *Allometric Relationships of Cell Numbers and Size in the Mammalian Lung*. Am J Respir Cell Mol Biol, 1992. **6**(2): p. 235-43.
59. Tscheka, C., et al., *Macrophage Uptake of Cylindrical Microparticles Investigated with Correlative Microscopy*. Eur J Pharm Biopharm, 2015. **95**(Pt A): p. 151-5.
60. Chono, S., et al., *Influence of Particle Size on Drug Delivery to Rat Alveolar Macrophages Following Pulmonary Administration of Ciprofloxacin Incorporated into Liposomes*. J Drug Target, 2006. **14**(8): p. 557-66.

61. Thorley, A.J., et al., *Critical Determinants of Uptake and Translocation of Nanoparticles by the Human Pulmonary Alveolar Epithelium*. ACS Nano, 2014. **8**(11): p. 11778-89.
62. Choi, H.S., et al., *Rapid Translocation of Nanoparticles from the Lung Airspaces to the Body*. Nat Biotechnol, 2010. **28**(12): p. 1300-3.
63. Nel, A.E., et al., *Understanding Biophysicochemical Interactions at the Nano-Bio Interface*. Nat Mater, 2009. **8**(7): p. 543-57.
64. Walczyk, D., et al., *What the Cell "Sees" in Bionanoscience*. Journal of the American Chemical Society, 2010. **132**(16): p. 5761-5768.
65. Gref, R., et al., *'Stealth' Corona-Core Nanoparticles Surface Modified by Polyethylene Glycol (Peg): Influences of the Corona (Peg Chain Length and Surface Density) and of the Core Composition on Phagocytic Uptake and Plasma Protein Adsorption*. Colloids and Surfaces B: Biointerfaces, 2000. **18**(3-4): p. 301-313.
66. Cedervall, T., et al., *Understanding the Nanoparticle-Protein Corona Using Methods to Quantify Exchange Rates and Affinities of Proteins for Nanoparticles*. Proc Natl Acad Sci U S A, 2007. **104**(7): p. 2050-5.
67. Jenkin, C.R., *The Role of Opsonins in the Clearance of Living and Inert Particles by Cells of the Reticuloendothelial System*. Journal of Experimental Medicine, 1961. **114**(3): p. 363-374.
68. Vroman, L., et al., *Interaction of High Molecular Weight Kininogen, Factor XII, and Fibrinogen in Plasma at Interfaces*. Blood, 1980. **55**(1): p. 156-159.
69. Docter, D., et al., *No King without a Crown--Impact of the Nanomaterial-Protein Corona on Nanobiomedicine*. Nanomedicine (Lond), 2015. **10**(3): p. 503-19.
70. Docter, D., et al., *The Nanoparticle Biomolecule Corona: Lessons Learned - Challenge Accepted?* Chem Soc Rev, 2015. **44**(17): p. 6094-121.
71. Monopoli, M.P., et al., *Biomolecular Coronas Provide the Biological Identity of Nanosized Materials*. Nat Nanotechnol, 2012. **7**(12): p. 779-86.
72. Lesniak, A., et al., *Effects of the Presence or Absence of a Protein Corona on Silica Nanoparticle Uptake and Impact on Cells*. ACS Nano, 2012. **6**(7): p. 5845-57.
73. Gebauer, J.S., et al., *Impact of the Nanoparticle-Protein Corona on Colloidal Stability and Protein Structure*. Langmuir, 2012. **28**(25): p. 9673-9.
74. Walkey, C.D., et al., *Protein Corona Fingerprinting Predicts the Cellular Interaction of Gold and Silver Nanoparticles*. ACS Nano, 2014. **8**(3): p. 2439-55.
75. Monopoli, M.P., et al., *Comparisons of Nanoparticle Protein Corona Complexes Isolated with Different Methods*. Nano LIFE, 2013. **03**(04): p. 1343004.
76. Tenzer, S., et al., *Nanoparticle Size Is a Critical Physicochemical Determinant of the Human Blood Plasma Corona: A Comprehensive Quantitative Proteomic Analysis*. ACS Nano, 2011. **5**(9): p. 7155-7167.
77. Lundqvist, M., et al., *Nanoparticle Size and Surface Properties Determine the Protein Corona with Possible Implications for Biological Impacts*. Proc Natl Acad Sci U S A, 2008. **105**(38): p. 14265-70.
78. Gessner, A., et al., *Influence of Surface Charge Density on Protein Adsorption on Polymeric Nanoparticles: Analysis by Two-Dimensional Electrophoresis*. European Journal of Pharmaceutics and Biopharmaceutics, 2002. **54**(2): p. 165-170.
79. Monopoli, M.P., et al., *Physical-Chemical Aspects of Protein Corona: Relevance to in Vitro and in Vivo Biological Impacts of Nanoparticles*. J Am Chem Soc, 2011. **133**(8): p. 2525-34.

80. Gagner, J.E., et al., *Effect of Gold Nanoparticle Morphology on Adsorbed Protein Structure and Function*. *Biomaterials*, 2011. **32**(29): p. 7241-52.
81. Tenzer, S., et al., *Rapid Formation of Plasma Protein Corona Critically Affects Nanoparticle Pathophysiology*. *Nat Nanotechnol*, 2013. **8**(10): p. 772-81.
82. Mahmoudi, M., et al., *Temperature: The "Ignored" Factor at the Nanobio Interface*. *ACS Nano*, 2013. **7**(8): p. 6555-62.
83. Caracciolo, G., et al., *Evolution of the Protein Corona of Lipid Gene Vectors as a Function of Plasma Concentration*. *Langmuir*, 2011. **27**(24): p. 15048-53.
84. Alexis, F., et al., *Factors Affecting the Clearance and Biodistribution of Polymeric Nanoparticles*. *Mol Pharm*, 2008. **5**(4): p. 505-15.
85. Ge, C., et al., *Binding of Blood Proteins to Carbon Nanotubes Reduces Cytotoxicity*. *Proc Natl Acad Sci U S A*, 2011. **108**(41): p. 16968-73.
86. Behzadi, S., et al., *Protein Corona Change the Drug Release Profile of Nanocarriers: The "Overlooked" Factor at the Nanobio Interface*. *Colloids and Surfaces, B: Biointerfaces*, 2014. **123**: p. 143-9.
87. Ritz, S., et al., *Protein Corona of Nanoparticles: Distinct Proteins Regulate the Cellular Uptake*. *Biomacromolecules*, 2015. **16**(4): p. 1311-21.
88. Hadjidemetriou, M., et al., *In Vivo Biomolecule Corona around Blood-Circulating, Clinically Used and Antibody-Targeted Lipid Bilayer Nanoscale Vesicles*. *ACS Nano*, 2015. **9**(8): p. 8142-56.
89. Wan, S., et al., *The "Sweet" Side of the Protein Corona: Effects of Glycosylation on Nanoparticle-Cell Interactions*. *ACS Nano*, 2015.
90. Mirshafiee, V., et al., *Impact of Protein Pre-Coating on the Protein Corona Composition and Nanoparticle Cellular Uptake*. *Biomaterials*, 2016. **75**: p. 295-304.
91. Luby, A.O., E.K. Breitner, and K.K. Comfort, *Preliminary Protein Corona Formation Stabilizes Gold Nanoparticles and Improves Deposition Efficiency*. *Applied Nanoscience*, 2015.
92. Hu, C.M., et al., *Nanoparticle Biointerfacing by Platelet Membrane Cloaking*. *Nature*, 2015. **526**(7571): p. 118-21.
93. Yin, H., et al., *Reducing the Cytotoxicity of ZnO Nanoparticles by a Pre-Formed Protein Corona in a Supplemented Cell Culture Medium*. *RSC Adv*, 2015. **5**(90): p. 73963-73973.
94. Peng, Q., et al., *Enhanced Biostability of Nanoparticle-Based Drug Delivery Systems by Albumin Corona*. *Nanomedicine (Lond)*, 2015. **10**(2): p. 205-14.
95. Dai, Q., et al., *Monoclonal Antibody-Functionalized Multilayered Particles: Targeting Cancer Cells in the Presence of Protein Coronas*. *ACS Nano*, 2015. **9**(3): p. 2876-85.
96. Caracciolo, G., et al., *Stealth Effect of Biomolecular Corona on Nanoparticle Uptake by Immune Cells*. *Langmuir*, 2015. **31**(39): p. 10764-73.
97. Mahmoud, N.N., et al., *Colloidal Stability of Gold Nanorod Solution Upon Exposure to Excised Human Skin: Effect of Surface Chemistry and Protein Adsorption*. *Int J Biochem Cell Biol*, 2016.
98. Schleh, C., W.G. Kreyling, and C.M. Lehr, *Pulmonary Surfactant Is Indispensable in Order to Simulate the in Vivo Situation*. *Particle and Fibre Toxicology*, 2013. **10**.
99. Kumar, A., et al., *What Are the Biological and Therapeutic Implications of Biomolecule Corona Formation on the Surface of Inhaled Nanomedicines?* *Nanomedicine*, 2015. **10**(3): p. 343-345.

100. Beck-Broichsitter, M., et al., *Biophysical Investigation of Pulmonary Surfactant Surface Properties Upon Contact with Polymeric Nanoparticles in Vitro*. *Nanomedicine*, 2011. **7**(3): p. 341-50.
101. Ruge, C.A., et al., *The Interplay of Lung Surfactant Proteins and Lipids Assimilates the Macrophage Clearance of Nanoparticles*. *PLoS One*, 2012. **7**(7): p. e40775.
102. Kuroki, Y., et al., *Elevated Levels of Lung Surfactant Protein a in Sera from Patients with Idiopathic Pulmonary Fibrosis and Pulmonary Alveolar Proteinosis*. *Am Rev Respir Dis*, 1993. **147**(3): p. 723-9.
103. Noguee, L.M., et al., *Brief Report: Deficiency of Pulmonary Surfactant Protein B in Congenital Alveolar Proteinosis*. *N Engl J Med*, 1993. **328**(6): p. 406-10.
104. Landsiedel, R., et al., *Pulmonary Toxicity of Nanomaterials: A Critical Comparison of Published in Vitro Assays and in Vivo Inhalation or Instillation Studies*. *Nanomedicine (Lond)*, 2014. **9**(16): p. 2557-85.
105. Jones, M.C., et al., *Quantitative Assessment of Nanoparticle Surface Hydrophobicity and Its Influence on Pulmonary Biocompatibility*. *J Control Release*, 2014. **183**: p. 94-104.
106. Fox, G.F. and U. Sothnathan, *The Choice of Surfactant for Treatment of Respiratory Distress Syndrome in Preterm Infants : A Review of the Evidence*. *Infant*, 2005. **1**(1): p. 8-12.
107. Pohlmann, G., et al., *A Novel Continuous Powder Aerosolizer (Cpa) for Inhalative Administration of Highly Concentrated Recombinant Surfactant Protein-C (Rsp-C) Surfactant to Preterm Neonates*. *Journal of Aerosol Medicine and Pulmonary Drug Delivery*, 2013. **26**(6): p. 370-379.
108. Walther, F.J., J.M. Hernandez-Juviel, and A.J. Waring, *Aerosol Delivery of Synthetic Lung Surfactant*. *PeerJ*, 2014. **2**: p. e403.
109. Moya, F., et al., *One-Year Follow-up of Very Preterm Infants Who Received Lucinactant for Prevention of Respiratory Distress Syndrome: Results from 2 Multicenter Randomized, Controlled Trials*. *Pediatrics*, 2007. **119**(6): p. e1361-70.
110. Beck-Broichsitter, M., et al., *Biophysical Inhibition of Synthetic Vs. Naturally-Derived Pulmonary Surfactant Preparations by Polymeric Nanoparticles*. *Biochim Biophys Acta*, 2014. **1838**(1 Pt B): p. 474-81.
111. Blanco, O., et al., *Interfacial Behavior and Structural Properties of a Clinical Lung Surfactant from Porcine Source*. *Biochim Biophys Acta*, 2012. **1818**(11): p. 2756-66.
112. Shelley, S.A., J.E. Paciga, and J.U. Balis, *Purification of Surfactant from Lung Washings and Washings Contaminated with Blood Constituents*. *Lipids*, 1977. **12**(6): p. 505-10.
113. Bernhard, W., et al., *Commercial Versus Native Surfactants. Surface Activity, Molecular Components, and the Effect of Calcium*. *Am J Respir Crit Care Med*, 2000. **162**(4 Pt 1): p. 1524-33.
114. Taesch, H.W., et al., *Inactivation of Pulmonary Surfactant Due to Serum-Inhibited Adsorption and Reversal by Hydrophilic Polymers: Experimental*. *Biophys J*, 2005. **89**(3): p. 1769-79.
115. Raesch, S.S., et al., *Proteomic and Lipidomic Analysis of Nanoparticle Corona Upon Contact with Lung Surfactant Reveals Differences in Protein, but Not Lipid Composition*. *ACS Nano*, 2015. **9**(12): p. 11872-85.
116. Barenholz, Y. and S. Amselem, *Quality Control Assays in the Development and Clinical Use of Liposome-Based Formulations*, in *Liposome Technology*, G. Gregoriadis, Editor. 1993, CRC Press: Boca Raton, FL. . p. 527-616.
117. Docter, D., et al., *Quantitative Profiling of the Protein Coronas That Form around Nanoparticles*. *Nat Protoc*, 2014. **9**(9): p. 2030-44.
118. Bhatia, V.N., et al., *Software Tool for Researching Annotations of Proteins: Open-Source Protein Annotation Software with Data Visualization*. *Anal Chem*, 2009. **81**(23): p. 9819-23.

119. Kyte, J. and R.F. Doolittle, *A Simple Method for Displaying the Hydrophobic Character of a Protein*. Journal of Molecular Biology, 1982. **157**(1): p. 105-132.
120. *The Lipid Maps Lipidomics Gateway*. Available from: <http://www.lipidmaps.org/>.
121. Bligh, E.G. and W.J. Dyer, *A Rapid Method of Total Lipid Extraction and Purification*. Canadian journal of biochemistry and physiology, 1959. **37**(8): p. 911-917.
122. Pluskal, T., et al., *Mzmine 2: Modular Framework for Processing, Visualizing, and Analyzing Mass Spectrometry-Based Molecular Profile Data*. BMC Bioinformatics, 2010. **11**: p. 395.
123. Fahy, E., et al., *Lipid Maps Online Tools for Lipid Research*. Nucleic Acids Res, 2007. **35**(Web Server issue): p. W606-12.
124. Guideline, I.H.T., *Validation of Analytical Procedures: Text and Methodology*. Q2 (R1), 2005. **1**.
125. Griese, M., *Pulmonary Surfactant in Health and Human Lung Diseases: State of the Art*. European Respiratory Journal, 1999. **13**(6): p. 1455.
126. Newton, D.A., et al., *Hemoglobin Is Expressed by Alveolar Epithelial Cells*. J Biol Chem, 2006. **281**(9): p. 5668-76.
127. Olmeda, B., et al., *Effect of Hypoxia on Lung Gene Expression and Proteomic Profile: Insights into the Pulmonary Surfactant Response*. J Proteomics, 2014. **101**: p. 179-91.
128. Bernhard, W., et al., *Conductive Airway Surfactant: Surface-Tension Function, Biochemical Composition, and Possible Alveolar Origin*. Am J Respir Cell Mol Biol, 1997. **17**(1): p. 41-50.
129. Zuo, Y.Y. and F. Possmayer, *How Does Pulmonary Surfactant Reduce Surface Tension to Very Low Values?* J Appl Physiol (1985), 2007. **102**(5): p. 1733-4.
130. Jiang, J., G. Oberdörster, and P. Biswas, *Characterization of Size, Surface Charge, and Agglomeration State of Nanoparticle Dispersions for Toxicological Studies*. Journal of Nanoparticle Research, 2008. **11**(1): p. 77-89.
131. Zhang, S., H. Gao, and G. Bao, *Physical Principles of Nanoparticle Cellular Endocytosis*. ACS Nano, 2015. **9**(9): p. 8655-71.
132. Sauer, U.G., et al., *Influence of Dispersive Agent on Nanomaterial Agglomeration and Implications for Biological Effects in Vivo or in Vitro*. Toxicol In Vitro, 2014. **29**(1): p. 182-186.
133. Kelly, P.M., et al., *Mapping Protein Binding Sites on the Biomolecular Corona of Nanoparticles*. Nat Nanotechnol, 2015. **10**(5): p. 472-9.
134. Aubin-Tam, M.E. and K. Hamad-Schifferli, *Structure and Function of Nanoparticle-Protein Conjugates*. Biomed Mater, 2008. **3**(3): p. 034001.
135. Walkey, C.D., et al., *Nanoparticle Size and Surface Chemistry Determine Serum Protein Adsorption and Macrophage Uptake*. J Am Chem Soc, 2012. **134**(4): p. 2139-47.
136. Jedlovszky-Hajdu, A., et al., *Surface Coatings Shape the Protein Corona of Spions with Relevance to Their Application in Vivo*. Langmuir, 2012. **28**(42): p. 14983-91.
137. Monopoli, M.P., et al., *Formation and Characterization of the Nanoparticle-Protein Corona*. Methods Mol Biol, 2013. **1025**: p. 137-55.
138. Casals, E., et al., *Time Evolution of the Nanoparticle Protein Corona*. ACS Nano, 2010. **4**(7): p. 3623-32.
139. Dunlop, D.J., *Superparamagnetic and Single-Domain Threshold Sizes in Magnetite*. Journal of Geophysical Research, 1973. **78**(11): p. 1780-1793.

140. Laurent, S., et al., *Magnetic Iron Oxide Nanoparticles: Synthesis, Stabilization, Vectorization, Physicochemical Characterizations, and Biological Applications*. Chem Rev, 2008. **108**(6): p. 2064-110.
141. Ravi Kumar, M.N.V., U. Bakowsky, and C.M. Lehr, *Preparation and Characterization of Cationic Plga Nanospheres as DNA Carriers*. Biomaterials, 2004. **25**(10): p. 1771-1777.
142. Leonenko, Z.V., et al., *Investigation of Temperature-Induced Phase Transitions in Dopc and Dppc Phospholipid Bilayers Using Temperature-Controlled Scanning Force Microscopy*. Biophys J, 2004. **86**(6): p. 3783-93.
143. Seeger, W., et al., *Surfactant Inhibition by Plasma Proteins: Differential Sensitivity of Various Surfactant Preparations*. European Respiratory Journal, 1993. **6**(7): p. 971-977.
144. Holm, B.A., G. Enhorning, and R.H. Notter, *A Biophysical Mechanism by Which Plasma Proteins Inhibit Lung Surfactant Activity*. Chemistry and Physics of Lipids, 1988. **49**(1-2): p. 49-55.
145. Hupfeld, S., D. Ausbacher, and M. Brandl, *Asymmetric Flow Field-Flow Fractionation of Liposomes: Optimization of Fractionation Variables*. J Sep Sci, 2009. **32**(9): p. 1465-70.
146. Kammer, F.v.d., et al., *Separation and Characterization of Nanoparticles in Complex Food and Environmental Samples by Field-Flow Fractionation*. TrAC Trends in Analytical Chemistry, 2011. **30**(3): p. 425-436.
147. Runyon, J.R., M. Ulmius, and L. Nilsson, *A Perspective on the Characterization of Colloids and Macromolecules Using Asymmetrical Flow Field-Flow Fractionation*. Colloids and Surfaces A: Physicochemical and Engineering Aspects, 2014. **442**: p. 25-33.
148. Pino, P.d., et al., *Protein Corona Formation around Nanoparticles – from the Past to the Future*. Materials Horizons, 2014. **1**(3): p. 301.
149. Casals, C., *Role of Surfactant Protein a (Sp-a)/Lipid Interactions for Sp-a Functions in the Lung*. Fetal and Pediatric Pathology, 2001. **20**(4): p. 249-268.
150. Rodríguez Patino, J.M. and M.R.R. Niño, *Protein Adsorption and Protein-Lipid Interactions at the Air-Aqueous Solution Interface*. Colloids and Surfaces A: Physicochemical and Engineering Aspects, 1995. **103**(1-2): p. 91-103.
151. Kapralov, A.A., et al., *Adsorption of Surfactant Lipids by Single-Walled Carbon Nanotubes in Mouse Lung Upon Pharyngeal Aspiration*. ACS Nano, 2012. **6**(5): p. 4147-56.
152. Tyurina, Y.Y., et al., *Global Phospholipidomics Analysis Reveals Selective Pulmonary Peroxidation Profiles Upon Inhalation of Single-Walled Carbon Nanotubes*. ACS Nano, 2011. **5**(9): p. 7342-53.
153. Jahn, O., S. Tenzer, and H.B. Werner, *Myelin Proteomics: Molecular Anatomy of an Insulating Sheath*. Mol Neurobiol, 2009. **40**(1): p. 55-72.
154. Hu, G., et al., *Physicochemical Properties of Nanoparticles Regulate Translocation across Pulmonary Surfactant Monolayer and Formation of Lipoprotein Corona*. ACS Nano, 2013. **7**(12): p. 10525-33.
155. Wohlleben, W., et al., *Influence of Agglomeration and Specific Lung Lining Lipid/Protein Interaction on Short-Term Inhalation Toxicity*. Nanotoxicology, 2016: p. 1-11.
156. Smyth, G.K., *Linear Models and Empirical Bayes Methods for Assessing Differential Expression in Microarray Experiments*. Stat Appl Genet Mol Biol, 2004. **3**: p. Article3.
157. Kammers, K., et al., *Detecting Significant Changes in Protein Abundance*. EuPA Open Proteomics, 2015. **7**: p. 11-19.
158. R Core Team, R: *A Language and Environment for Statistical Computing*. R Foundation for Statistical Computing. 2014: Vienna, Austria.

159. Ritchie, M.E., et al., *Limma Powers Differential Expression Analyses for Rna-Sequencing and Microarray Studies*. Nucleic Acids Res, 2015. **43**(7): p. e47.
160. Gentleman, R.C., et al., *Bioconductor: Open Software Development for Computational Biology and Bioinformatics*. Genome Biol, 2004. **5**(10): p. R80.
161. Benjamini, Y. and Y. Hochberg, *Controlling the False Discovery Rate - a Practical and Powerful Approach to Multiple Testing*. Journal of the Royal Statistical Society: Series B (Statistical Methodology), 1995. **57**(1): p. 289-300.
162. Grek, C.L., et al., *Hypoxia up-Regulates Expression of Hemoglobin in Alveolar Epithelial Cells*. Am J Respir Cell Mol Biol, 2011. **44**(4): p. 439-47.
163. Klausner, R.D., et al., *Interaction of Tubulin with Phospholipid Vesicles. I. Association with Vesicles at the Phase Transition*. Journal of Biological Chemistry, 1981. **256**(11): p. 5879-5885.
164. Crouch, E. and J.R. Wright, *Surfactant Proteins a and D and Pulmonary Host Defense*. Annu Rev Physiol, 2001. **63**: p. 521-54.
165. Bals, R., et al., *The Peptide Antibiotic LL-37/Hcap-18 Is Expressed in Epithelia of the Human Lung Where It Has Broad Antimicrobial Activity at the Airway Surface*. Proceedings of the National Academy of Sciences, 1998. **95**(16): p. 9541-9546.
166. Cedervall, T., et al., *Detailed Identification of Plasma Proteins Adsorbed on Copolymer Nanoparticles*. Angew Chem Int Ed Engl, 2007. **46**(30): p. 5754-6.
167. Meerasa, A., J.G. Huang, and F.X. Gu, *Human Serum Lipoproteins Influence Protein Deposition Patterns on Nanoparticle Surfaces*. ACS Appl Mater Interfaces, 2013. **5**(3): p. 489-93.
168. Hellstrand, E., et al., *Complete High-Density Lipoproteins in Nanoparticle Corona*. FEBS J, 2009. **276**(12): p. 3372-81.
169. Yang, C.H., et al., *Identification of the Surfactant Protein a Receptor 210 as the Unconventional Myosin 18a*. J Biol Chem, 2005. **280**(41): p. 34447-57.
170. Holmskov, U., *Isolation and Characterization of a New Member of the Scavenger Receptor Superfamily, Glycoprotein-340 (Gp-340), as a Lung Surfactant Protein-D Binding Molecule*. Journal of Biological Chemistry, 1997. **272**(21): p. 13743-13749.
171. Madsen, J., et al., *Crp-Ductin, the Mouse Homologue of Gp-340/ Deleted in Malignant Brain Tumors 1 (Dmbt1), Binds Gram-Positive and Gram-Negative Bacteria and Interacts with Lung Surfactant Protein D*. Eur J Immunol, 2003. **33**(8): p. 2327-36.
172. Bingle, C.D., *Plunc: A Novel Family of Candidate Host Defence Proteins Expressed in the Upper Airways and Nasopharynx*. Human Molecular Genetics, 2002. **11**(8): p. 937-943.
173. Bingle, L., et al., *Bpijb1 (Lplunc1) Is Upregulated in Cystic Fibrosis Lung Disease*. Histochem Cell Biol, 2012. **138**(5): p. 749-58.
174. Liu, Y., et al., *Human M-Ficolin Is a Secretory Protein That Activates the Lectin Complement Pathway*. The Journal of Immunology, 2005. **175**(5): p. 3150-3156.
175. Hoppe, H.J. and K.B.M. Reid, *Collectins - Soluble-Proteins Containing Collagenous Regions and Lectin Domains - and Their Roles in Innate Immunity*. Protein Science, 1994. **3**(8): p. 1143-1158.
176. Pan, Q., et al., *L-Ficolin Binds to the Glycoproteins Hemagglutinin and Neuraminidase and Inhibits Influenza a Virus Infection Both in Vitro and in Vivo*. J Innate Immun, 2012. **4**(3): p. 312-24.
177. Russell, W.M.S. and R.L. Burch, *The Principles of Humane Experimental Technique*. 1959, London: Methuen.

-
178. Braakhuis, H.M., et al., *Progress and Future of in Vitro Models to Study Translocation of Nanoparticles*. Arch Toxicol, 2015. **89**(9): p. 1469-95.
179. Hittinger, M., et al., *Preclinical Safety and Efficacy Models for Pulmonary Drug Delivery of Antimicrobials with Focus on in Vitro Models*. Adv Drug Deliv Rev, 2015. **85**: p. 44-56.
180. Lin, H., et al., *Air-Liquid Interface (Ali) Culture of Human Bronchial Epithelial Cell Monolayers as an in Vitro Model for Airway Drug Transport Studies*. J Pharm Sci, 2007. **96**(2): p. 341-50.
181. Kuehn, A., et al., *Human Alveolar Epithelial Cells Expressing Tight Junctions to Model the Air-Blood Barrier*. ALTEX, 2016.
182. Elbert, K.J., et al., *Monolayers of Human Alveolar Epithelial Cells in Primary Culture for Pulmonary Absorption and Transport Studies*. Pharmaceutical Research, 1999. **16**(5): p. 601-608.
183. Lee, W.H., et al., *Nano- and Micro-Based Inhaled Drug Delivery Systems for Targeting Alveolar Macrophages*. Expert Opin Drug Deliv, 2015. **12**(6): p. 1009-26.
184. Kendall, M., et al., *Surfactant Protein D (Sp-D) Alters Cellular Uptake of Particles and Nanoparticles*. Nanotoxicology, 2013. **7**(5): p. 963-73.
185. Konduru, N.V., et al., *Phosphatidylserine Targets Single-Walled Carbon Nanotubes to Professional Phagocytes in Vitro and in Vivo*. PLoS One, 2009. **4**(2): p. e4398.
186. Ruge, C.A., et al., *Uptake of Nanoparticles by Alveolar Macrophages Is Triggered by Surfactant Protein A*. Nanomedicine, 2011. **7**(6): p. 690-3.
187. Frohlich, E., *The Role of Surface Charge in Cellular Uptake and Cytotoxicity of Medical Nanoparticles*. Int J Nanomedicine, 2012. **7**: p. 5577-91.
188. Akei, H., et al., *Surface Tension Influences Cell Shape and Phagocytosis in Alveolar Macrophages*. Am J Physiol Lung Cell Mol Physiol, 2006. **291**(4): p. L572-9.
189. Oh, N. and J.H. Park, *Endocytosis and Exocytosis of Nanoparticles in Mammalian Cells*. Int J Nanomedicine, 2014. **9 Suppl 1**: p. 51-63.

8. LIST OF

8.1 Abbreviations

ALF	alveolar lining fluid
AM	alveolar macrophages
API	active pharmaceutical ingredient
AT-1	type 1 alveolar epithelial cells
AT-2	type 2 alveolar epithelial cells
AUC	area under the curve
(p)BAL(F)	(porcine) bronchoalveolar lavage (fluid)
BCA	bicinchoninic acid assay
CHAPS	3-[(3-cholamidopropyl)dimethylammonio]-1-propanesulfonate
CRD	carbohydrate recognition domain
DCS	differential centrifugal sedimentation
DLS	dynamic light scattering
DPPC	dipalmitoylphosphatidylcholine
FASP	filter-aided sample preparation
FCS	fetal calve serum
GPChol	phosphatidylcholine
GPEth	phosphatidylethanolamine
GPGlyc	phosphatidylglycerol
GPI _{no}	phosphatidylinositol
GPSer	phosphatidylserine
(U)HPLC-MS	ultra high performance liquid chromatography – mass spectrometry
IRDS	infant respiratory distress syndrome
LB	lamellar body
MMAD	mass median aerodynamic diameter
NP(s)	nanoparticle(s)
NTA	nanoparticle tracking analysis
PAP	pulmonary alveolar proteinosis
PBS	phosphate-buffered saline
PDI	polydispersity index
PEG	polyethylene glycol
PL(s)	phospholipid(s)
PLGA	poly(lactic-co-glycolic acid)
POPG	1-palmitoyl-2-oleoylphosphatidylcholine
pPS	porcine pulmonary surfactant
PS	pulmonary surfactant
QP	quadrupole
RP	reversed phase
RPMI	Roswell Park Memorial Institute (cell culture medium)
RT	room temperature
SD	standard deviation
SDS-PAGE	sodium dodecyl sulfate polyacrylamide gel electrophoresis
SEM	scanning electron microscopy
SM	sphingomyelin
SP-X	pulmonary surfactant-associated protein X
SRM	single reaction mode
SWCNT	single-walled carbon nanotubes
TBS	tris-buffered saline
TEM	transmission electron microscopy
TLC	thin layer chromatography
TM	tubular myelin

8.2 Figures

Figure 1-1: Generations of the respiratory tree.....	2
Figure 1-2: Structure of the alveolus (A) and transmission electron microscopy image of the alveolar space (B) with visible erythrocytes (ER).....	4
Figure 1-3: General structure of phospholipids.....	6
Figure 1-4: Structure of pulmonary surfactant-associated proteins A, B, C, and D.....	7
Figure 1-5: Structural organization of pulmonary surfactant at the air-liquid interface.....	10
Figure 1-6: Deposition of inhaled particles in the lung as a function of their MMAD.....	13
Figure 1-7: Corona evolution over time.....	15
Figure 1-8: Schematic of the discrimination between "hard" and "soft" corona at equilibrium.....	16
Figure 2-1: Schematic representation of the pPS isolation process.....	25
Figure 2-2: Scheme of sample preparation procedure (A), and TLC as control of exhaustive extraction (B).....	30
Figure 2-3: Principle of PL detection in an LC- triple quadrupole set-up (A). Example breakdown curve of a DPPC standard during direct injection (B).....	31
Figure 2-4: Final gradient, allowing separation of all PL classes.....	33
Figure 2-5: Typical separation of all standards injected.....	34
Figure 2-6: Data processing workflow of the established phospholipid analysis.....	35
Figure 2-7: Example images of the pPS preparation steps.....	38
Figure 2-8: Temperature ramp of pPS.....	39
Figure 2-9: Influence of temperature on pPS vesicle size.....	40
Figure 2-10: Separation of pPS lipids by normal phase TLC.....	41
Figure 2-11: Relative distribution of lipids found in pulmonary surfactant by means of lipid classes and overall chain length of phospholipids by wt%.....	42
Figure 2-12: Comparison of chloroform/methanol and acetone protein precipitation by SDS-PAGE.....	42
Figure 2-13: "2-Dimensional"-separation of pPS proteins.....	43
Figure 2-14: Western blotting of pPS after SDS-PAGE proved the presence of SP-B and SP-C in the preparation.....	44
Figure 2-15: Comparison of the relative cumulated gene ontology terms of the entity of proteins found in crude plasma.....	47
Figure 3-1: Schematic of the nanoparticle preparation process.....	55

Figure 3-2: magPLGA-NPs are attracted by a permanent neodymium magnet within minutes.	56
Figure 3-3: DLS measurements of 200 nm PS-COOH NPs during titration with pPS.	58
Figure 3-4: Influence of fluorescence filter on nanoparticle tracking analysis in presence of pPS.	59
Figure 3-5: NTA measurements of 200 nm multifluorescent PS-COOH NPs with different incubation additives.....	60
Figure 3-6: Surfactant-NPs interactions as observed by AF4.	62
Figure 3-7: Analysis of magPLGA-NPs in the presence of pPS, by DCS.	63
Figure 3-8: DCS measurements of different NPs in a 24-48% sucrose gradient.....	63
Figure 3-9: Mode of detection in differential centrifugal sedimentation.	64
Figure 3-10: Apparent size increase in nm of different NPs after incubation with pPS.	65
Figure 4-1: Characterization of NPs used in Chapter 4.....	72
Figure 4-2: Comparison of separation methods to access the PS corona.	76
Figure 4-3: Absolute amounts of lipids determined in the corona of PLGA-, PEG-, and Lipid-NPs.....	77
Figure 4-4: Relative comparison of the lipids found in the corona of PLGA-, PEG-, and Lipid-NPs in comparison to crude pPS.....	78
Figure 4-5: Incubation of PLGA-, PEG-, and Lipid-NPs with Alveofact®.....	80
Figure 4-6: Relative distribution of the proteins found in the corona of PLGA-, PEG-, and Lipid-NPs.....	83
Figure 4-7: Direct comparison of relative protein amounts found in the corona of PLGA-, PEG-, and Lipid-NPs by means of relative change in abundance (Δ ppm) and fold change.	86
Figure 5-1: Influence of pPS on NP cytotoxicity.....	95
Figure 5-2: NP-cell association as a function of NP concentration.	97
Figure 5-3: Distribution of cell counts.....	97
Figure 5-4: Difference of cell association with and without 1 h pre-incubation of NPs (20 μ g/ml) with FCS, AF (Alveofact®) or pPS prior to incubation with cells.	98
Figure 5-5: Cell association at 4 °C and uptake at 37 °C of 20 μ g/ml NPs.	99
Figure 6-1: Scheme of a proposed corona formation mechanism.....	104

8.3 Tables

Table 1-1: Lipid composition of pulmonary surfactant according to [14] and [19].....	6
Table 1-2: Summary of some of the most recent findings regarding the plasma protein corona.	17

Table 2-1: Structures of the measured phospholipid classes shown together with the monitored fragment (in brackets).....	32
Table 2-2: Limit of Detection (L_D), limit of quantification (L_Q) and total number of species measured.....	36
Table 2-3: Detailed lipid composition of pPS	41
Table 2-4: Top 30 most abundant proteins in pulmonary Surfactant and plasma (data taken from Tenzer <i>et al.</i> , proteins occurring in both lists in bold).....	45
Table 2-5: Comparison of the determined concentrations of lipids in the used surfactant preparation to values found in the literature.	46
Table 3-1: Average properties of the produced magPLGA- and magEu-NPs.....	56
Table 3-2: Average peak maxima of the measured PS-COOH NPs after incubation with different additives.....	61
Table 4-1: Characterization of the used NPs.	71
Table 4-2: Top 10 most abundant lipid species found in crude pPS and in the corona of PLGA-, PEG-, and Lipid-NPs.....	79
Table 4-3: Top 30 most abundant proteins in the corona of PLGA-, PEG-, and Lipid-NPs.	82
Table 4-4: Most prominent changes in abundance of proteins in the coronas of PLGA-, PEG-, and Lipid-NPs	87

9. DANKSAGUNG / ACKNOWLEDGMENTS

“Finis coronat opus” – “Das Ende krönt das Werk” (Ovid, *Heroides* 2, 85)

Weder das Werk, also die Arbeit im Labor sowie die dazugehörige Planung und Auswertung, noch das Ende – diese Dissertation – wären ohne die Mithilfe einer großen Anzahl von Menschen möglich gewesen. Sei es direkt durch Experimente und Ratschläge oder indirekt durch ihre Unterstützung bei dem nervenaufreibenden Unterfangen ‚Doktorarbeit‘. In den zurückliegenden fast vier Jahren gab es zwar oft Momente des Erfolgs, aber auch nicht selten Zeiten der Ahnungslosigkeit, der Frustration oder sogar der Verzweiflung, und so manche dieser Hürden wäre ohne die Ermutigung durch andere für mich nur sehr schwer zu überwinden gewesen.

An erster Stelle muss hier selbstverständlich mein Doktorvater Claus-Michael Lehr genannt werden, der mir kurz nachdem ich mich schon mit dem Gedanken vertraut gemacht hatte, im Ausland zu promovieren, die Möglichkeit gab, in seiner Arbeitsgruppe zu forschen. Gerade nach der eigentlichen Arbeit im Labor fingen seine Betreuung und die Vorbereitung auf das Leben nach der Promotion an. Ich habe viel von dir gelernt, was ich auf meinen zukünftigen Lebensweg mitnehmen werde.

Des Weiteren bedanke ich mich bei Christian Arnold Ruge, dessen wissenschaftliche Arbeit die Grundlage meiner war. Er nahm mich zu Beginn meiner Promotion (wenn auch leider zu kurz) als seinen „Padawan“ an die Hand, um mich in das Doktorandenleben einzuführen. Unvergessen wird mir unsere Dienstreise nach Madrid bleiben; bei Gin & Tonic lässt sich einfach besser über Wissenschaft sprechen. Einen seiner ersten Tipps „Work smarter, not harder!“ konnte ich leider nicht immer befolgen.

Sarah Gordon, my most favourite Kiwi to the days, proofread this dissertation. Chur bro for making heaps of sweet as corrections and suggestions. However, she didn't correct this strange-sounding paragraph.

There are two main aspects in this work: pulmonary surfactant and the nanoparticle corona. The first one I got to know during a stay in the lab of Jesús Pérez-Gil at the Complutense University of Madrid and I thank all the people who cordially welcomed me and introduced me to the world of lipids and proteins in the lungs, above all Jesús himself and Elena Lopez Rodriguez. Without you I wouldn't have known what this strange stuff actually is that I was working with.

A closer look to the professional community working on the nanoparticle corona did I get during a stay in Dublin in the lab of Kenneth Dawson. I won't forget the twelve pubs of Christmas with you guys (oh wait, I already forgot pretty much every single one of them), as well as what I've learned in this impressive group. Thank all of you, you're doing a fantastic job.

Auf dem Weg bis zur Abgabe begleiteten mich so einige ‚Leidensgenossen‘, denen ich für ihre Unterstützung und die tolle Kollegialität danken möchte. Allen voran Chrissi Mathes, der es nur zu oft ging wie mir, Florian Gräf, der vermutlich gerade ‚off-season‘ hat, meinen langjährigen Bürogenossen Sarah Barthold und Stephanie Kletting genauso wie meinen nicht ganz so langjährigen Bürokollegen Branko Vukosavljevic und Khiet Duy Ho. Emad Malaeksefat sei gedankt für die langen, aber unterhaltsamen Nächte zwischen und unter Schweineinnereien, Xabi Murgia nicht nur für den entspannten Aufenthalt in der Dresdner Neustadt und Sandra Sapich für die Abende mit Durchflusszytometrie und Rosé. Dank auch an Arianna Castoldi, die gleichzeitig quirlig und müde sein kann (beides ansteckend), an meine Lieblingsniederländerin Remi Hendrix, ebenso an Birthe Kann, Anna Kühn, Nico Mell, Hanzey Yasar, Jenny Juntke, Nathalie Jung, Marius Hittinger, Christina Draheim, Salem Seif, Ana Melero und Lutz Franzen. Euch und allen anderen die ich vergessen habe danke ich für die tolle Zeit im und außerhalb des Labors.

Stefan Tenzer danke ich für die ergiebige Zusammenarbeit, Dominik Selzer und Alexander Rurainki für ihre Hilfe bei Fragen mathematischer Natur und Pavel Pšenica für seine hilfreiche Arbeit an der AF4.

Ohne die wichtige und fantastische Arbeit unsere Techniker wäre jeder Doktorand völlig verloren. Deshalb ist es mir wichtig, mich vor allem bei Chiara de Rossi zu bedanken, die einfach jedes Gerät bedienen kann und bei Petra König, ohne die keine Zelle überleben würde. Auch Jana Westhues, Peter Meiers und Marijas Jurisic haben mir tatkräftig unter die Arme gegriffen. Gleichfalls danke ich unserem Office-Team, das dafür gesorgt hat, dass ‚der Laden läuft‘: Karin Groß, Sarah Müller, Stephanie Kallenborn und Isabelle Conrad-Kehl.

Marc Schneider und Brigitta Loretz hatten immer ein offenes Ohr für jegliche Art von Problemen und meistens auch die passenden Lösungen parat. Danke dafür.

Ganz besonders wichtig war mir auch die Unterstützung durch die Person, die mir nicht nur auf der Arbeit, sondern auch privat vieles einfacher und angenehmer gemacht hat und mich so manchmal davor bewahrt hat, den Kopf zu verlieren. Vielen Dank Julia!

Meiner Familie ist nicht genug zu danken. Allen voran meinen Eltern Maria und Albert, meinen Geschwistern Sarah und Jonas und meiner Großmutter Elisabeth. Es tut mir leid, dass ihr wohl erst mit dieser Arbeit erfahrt, was ich in den letzten fast vier Jahren überhaupt „so getrieben habe“. Auf die Frage: „Wie sieht es mit deiner Doktorarbeit aus?“ gibt es oft leider keine für beide Seiten befriedigende Antwort. Gleiches gilt für alle Freunde, für die ich leider viel zu wenig Zeit hatte.

Bewusst an das Ende setze ich den Dank an denjenigen, von dem ich die wichtigste Hilfe erfahren habe. Für Ulrich Schäfer gilt fast alles zuvor Gesagte und mehr. Ohne deine Bereitschaft, Uli aus dem Ruhestand heraus dafür zu sorgen, dass „aus mir ein Doktor wird“, wäre diese Arbeit nicht machbar gewesen, und ich wäre elendig zwischen Papern und unnötigen Versuchen verendet. Auch wenn unsere Fachgespräche manchmal sehr kurzfristig stattfanden, nämlich dann wenn du unerwartet in der Tür auftauchtest, wäre ich ohne sie auf der Strecke geblieben. Als einer der letzten von dir betreuten Doktoranden (zum Unglück für viele angehende) schließe ich mit einem besonders herzlichen Dankeschön für deine Korrekturen und Ratschläge.

„I refuse to join any club that would have me as a member.“

Groucho Marx